Dark matter signals in cosmic accelerators

Marina Cermeño Gavilán

Centre for Cosmology, Particle Physics and Phenomenology (CP3),
Université Catholique de Louvain, Belgium.

June 21, 2022

UCLouvain

MultiDark
Multimessenger Approach
for Dark Matter Detection

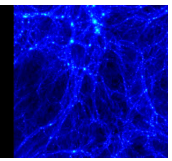

Current DM constraints and limitations

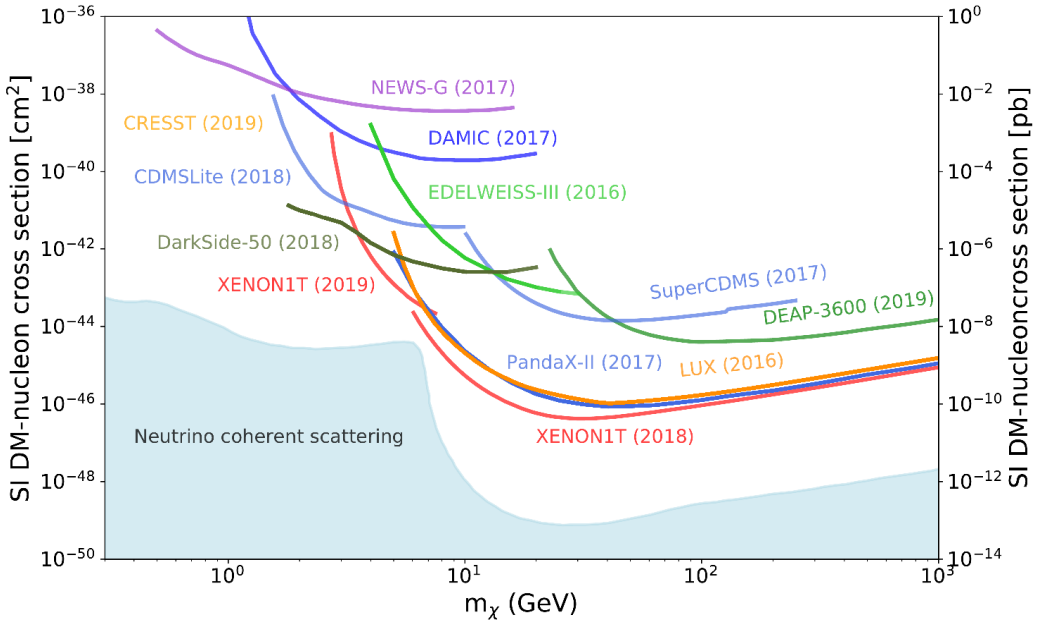

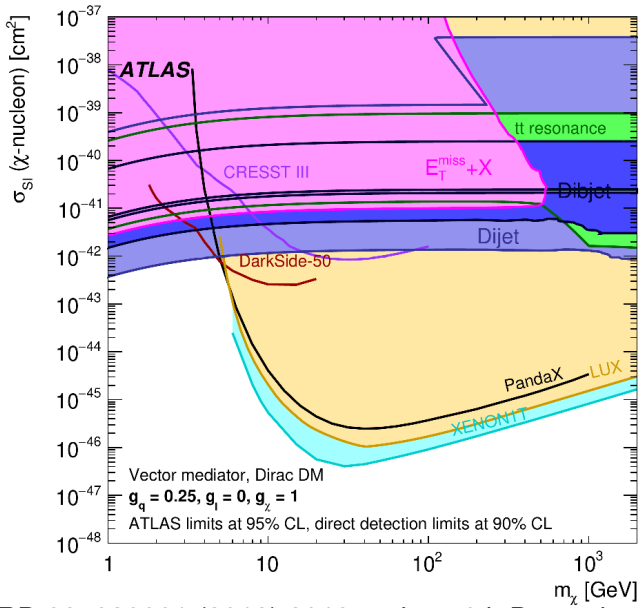

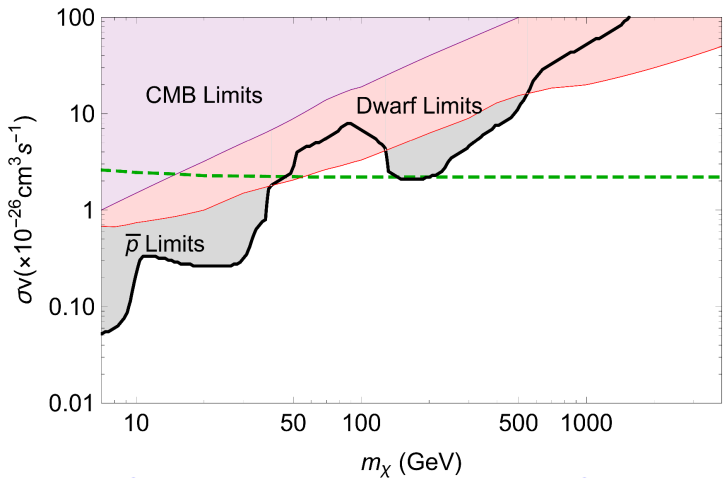

M. Tanabashi et al., PRD 98, 030001 (2018) 2019 update, 6th December, The Atlas Collaboration, JHEP05 (2019) 142, Cholis et al., PRD 99 (2019) 103026

Limitations of conventional experiments

- Direct detection (DD) experiments are close to reaching the neutrino floor
- Light DM (LDM), $m_\chi \lesssim 1$ GeV, provides nuclear recoil energies, $E_r \sim \frac{q^2}{2m_N} \sim 1$ eV, below the energy threshold of current conventional terrestial searches $E_r \sim 1$ keV
- Momemtum suppressed interactions, $\sigma_{\chi,N} \sim \mathcal{O}(q^4)$, in DD experiments ($q \to 0$)
- Velocity suppressed anihilation channels, $\langle \sigma v \rangle \sim \mathcal{O}(v^2)$, in the solar vicinity $v \sim 10^{-3}$
- Secluded DM, almost negligible rate for DD and collider production due to the reduction of its couplings to SM particles by this intermediate state (mediator)

Astrophysical scenarios: Compact objects

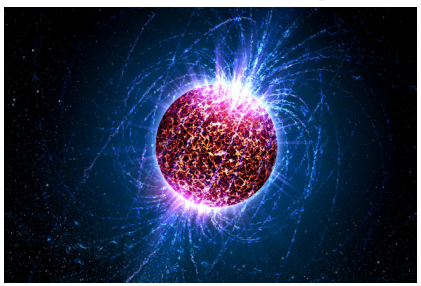
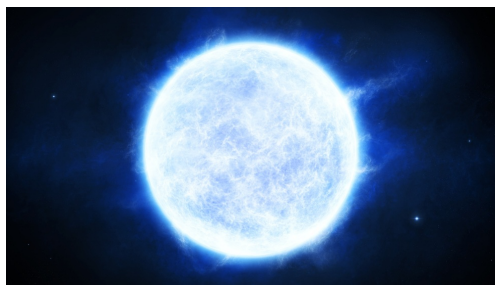
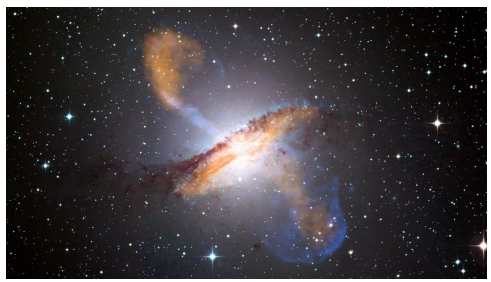

Dark matter in compact stars

- Neutron stars (NSs) born with $T \sim 30$ MeV, after $t \sim 10^6$ yrs $T \sim 1$ keV, surface temperatures $T_s \sim 10^{-3} - 10^{-1}$ keV
- White dwarfs (WDs) born with $T \sim 10$ keV, cool down to $T \sim 0.1 - 1$ keV, surface temperatures $T_s \sim 10^{-4} - 10^{-3}$ keV
- High compactness, $M_{NS}/R_{NS} \sim 0.1$, $M_{WD}/R_{WD} \sim 10^{-5}$, $M_\odot/R_\odot \sim 10^{-6}$
  $R_{NS} \sim 10$ km, $M_{NS} \sim 1.45$ M$_\odot$, $R_{WD} \sim 0.12 R_\odot$, $M_{WD} \sim 0.6$ M$_\odot$
- High baryonic density, $\rho_{NS} \sim 10^{14}$ g/cm^3, $\rho_{WD} \sim 10^5 - 10^7$ g/cm^3, $\rho_\odot \sim 1.6\ 10^2$ g/cm^3

White Dwarf

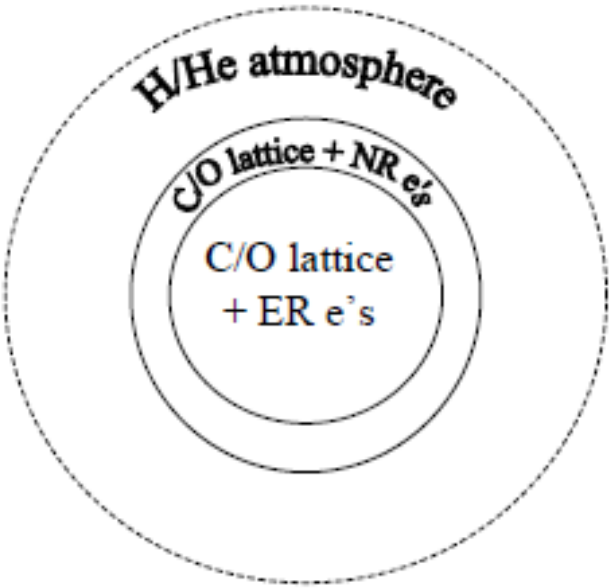

Neutron Star

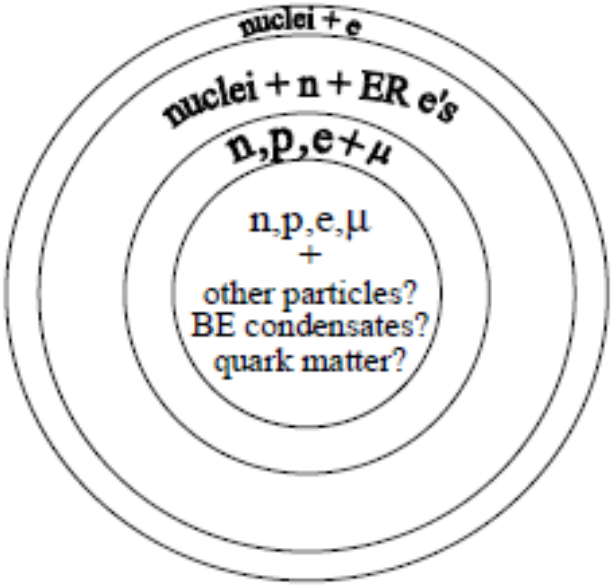

Dark matter in compact stars

- The distribution of NSs in the MW peaks at $\langle r \rangle \lesssim 4$ kpc, where $\rho_\chi \sim 30\ \rho_{\chi,0}^{ambient}$, some GCs with a core DM density $\rho_\chi \sim 100\ \mathrm{GeV/cm^3} \Rightarrow$ **high DM density around them**
- Gravitational boost $\beta_{NS} \sim 0.6$, $\beta_{WD} \sim 10^{-2} \Rightarrow$ **No negligible momentum transferred**
- Capture rate, *Gould, ApJ 321 (1987) 571, Güver et al., JCAP 05 (2014) 03*

$$\Gamma_{\rm capt} = \frac{8}{3}\pi^2 \frac{\rho_\chi}{m_\chi} \frac{GMR}{1-\frac{2GM}{R}} \bar{v}^2 \left(\frac{3}{2\pi\bar{v}^2}\right)^{\frac{3}{2}} f$$

- $\bar{v}$ the average χ velocity in the existing DM distribution at the star location
- $f \sim 1$ for $\sigma_{\chi,i} \gtrsim \sigma_0$, with $\sigma_{\chi,i}$ the DM-i-th type SM particle cross section, $\sigma_0 = \frac{\pi m_i R^2}{M}$, $f \sim \frac{\sigma_{\chi,i}}{\sigma_0}$ otherwise
- **Very good DM accretors**

  Efficient capture $\sigma_{\chi,N}^{NS} \gtrsim 10^{-45}\mathrm{cm}^2$, $\sigma_{\chi,N}^{WD} \gtrsim 10^{-39}\ \mathrm{cm}^2$, $\sigma_{\chi,N}^{Sun} \gtrsim 5\ 10^{-36}\mathrm{cm}^2$
- After thermalising $v \sim \sqrt{\frac{T}{m_\chi}}$, spherical cloud in the core $r_{th} = \sqrt{\frac{9T}{8\pi G\rho_c mx}}$, $r_{th} \ll R_*$
- **Annihilations more likely to happen than in the interestellar medium**

Signatures of DM in compact stars

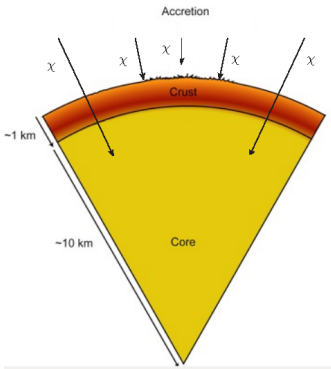

- Opacities in stellar nuclear scenarios after DM accretion considering medium effects, *i.e., Pauli blocking, nucleon effective masses, momemtum dependent form factors, etc*

  ***Cermeño**, Peréz-García, Silk, PRD 94 (2016) 023509, Bell et al., JCAP 09 (2020) 028*

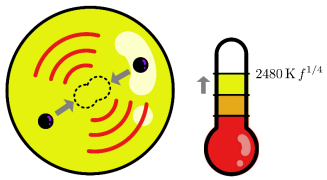

- Heating from annihilation

  *Kouvaris, Tinyakov, PRD 82 (2010) 063531, **Cermeño**, Peréz-García, Lineros, ApJ. 863 (2018) 157, McCullough, Fairbairn, PRD 81 (2010) 083520, **Cermeño**, Peréz-García, PRD 98 (2018) 063002*

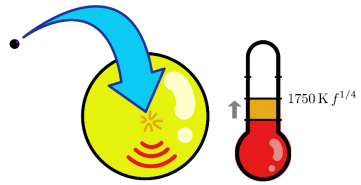

- Kinetic heating

  Baryakhtar et al., PRL 119 (2017) 131801, Raj, Tanedo, Yu PRD 97 (2018) 043006, Bell, Busoni, Robles, JCAP 09 (2018) 018, Acevedo et al., JCAP 03 (2020) 038, Joglekar et al., PRD 102 (2020) 123002

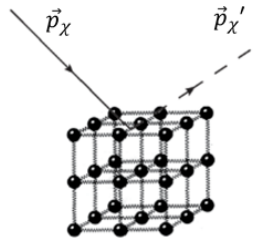

- Phonon excitation in the NS outer crust ⇒ impact on the thermal conductivity ⇒ isotropization of the temperature profile

  ***Cermeño**, Peréz-García, Silk, PRD 94 (2016) 6, 063001*

- BH formation and star destruction

  Kouvaris, Tinyakov, PRD 83 (2011) 083512, Janish, Narayan, Riggins, PRD 100 (2019) 035008, Garani, Genolili, Hambye, JCAP 05 (2019) 035

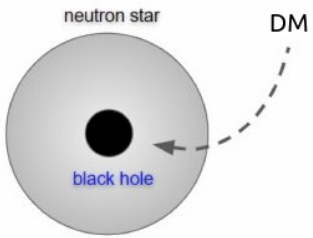

NS heating

Baryakhtar et al., PRL 119 (2017) 131801, Raj, Tanedo, Yu PRD 97 (2018) 043006

Blackbody emission $T_{\rm kin} = 1750 f^{1/4}$ K, $T_{\rm ann} = 2480 f^{1/4}$ K

Without DM a NS would cool down below $T_{\rm ann}$ in $t \sim 2\ 10^7$ yr

The coldest NS observed (PSRJ2144-3933) $\log_{10}(T_s[K]) \sim 4.6$
Guillot et al., ApJ 874 (2019) 175

Detectable temperatures by the James Webb Space Telescope (launched in Dec 2021) *Chatterjee et al., arXiv:2205.05048*

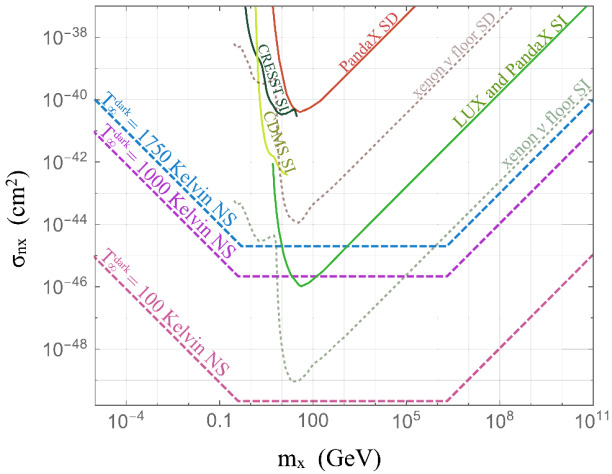

***Cermeño**, Pérez-García and Lineros, ApJ 863 (2018) 157*

$$Q_E = 4 \int d\Phi(p_1,p_2,p_3,p_4)\,(2\pi)^4 \delta^4(p_1+p_2-p_3-p_4)(E_1+E_2)\,|\overline{\mathcal{M}}|^2 f(f_1,f_2,f_3,f_4)$$

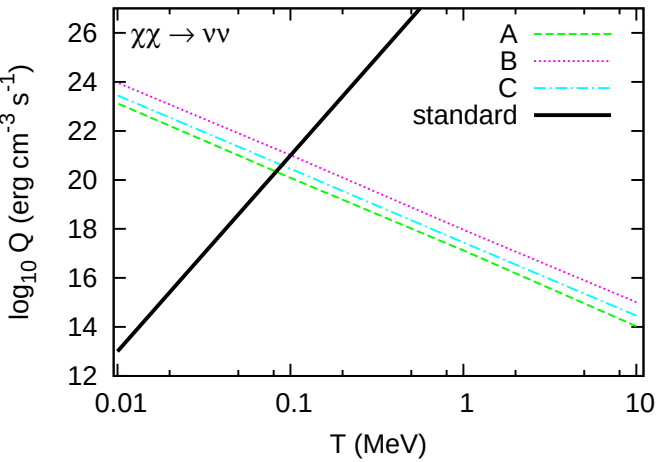

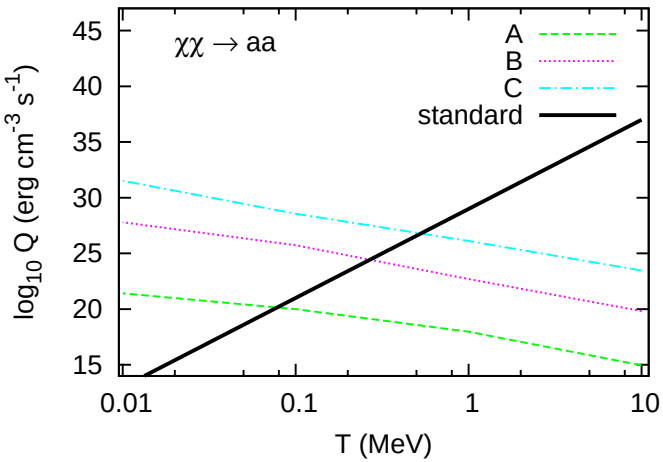

$$Q_E(T, N_\chi) = Q_0 \left(\frac{N_\chi}{N_{0,\chi}}\right)^2 \left(\frac{T}{1\,\text{MeV}}\right)^{-3}$$

$$N_{\chi,0} = 1.5\times10^{39} \left(\frac{\rho_\chi}{\rho_{\chi,0}^{ambient}}\right)\left(\frac{1\ \text{GeV}}{m_\chi}\right)\left(\frac{\sigma_{\chi,N}}{10^{-43}\ \text{cm}^2}\right)$$

Emission in $\lesssim 7\,\%$ of the stellar volume

$Q_E(T, N_\chi) > Q_{MURCA}$ for $T \in [0.01, 0.1]$ MeV during the NS entire lifetime for model C

NS heating $\rightarrow$ simulation needed to study the effect on the T profile

NS heating

Pérez-García et al., PLB 827 (2022) 136937

$$\frac{e^{-\lambda-2\Phi}}{4\pi r^2}\frac{\partial}{\partial r}\left(e^{2\Phi}L\right) = -Q + Q_\chi - \frac{c_V}{e^{\Phi}}\frac{\partial T}{\partial t}$$

$$\frac{L}{4\pi\kappa r^2} = e^{-\lambda-\Phi}\frac{\partial}{\partial r}\left(Te^{\Phi}\right)$$

Q standard neutrino emissivity,
$Q_\chi \equiv Q_E(T, N_\chi)$ neutrino emissivity from self-annihilating DM,
c_V heat capacity per unit volume, κ thermal conductivity,
L the local luminosity, $\Phi(r)$ and $\lambda(r)$ the metric functions,
$e^{-\lambda} = \sqrt{1-2Gm(r)/r}$, $m(r)$ is the gravitational mass enclosed within a sphere of radius r, $\Phi(R) = -\lambda(R)$

$m_\chi = 0.1$ GeV, $m_a = 0.05$ GeV, coupling fixed providing the correct relic abundance

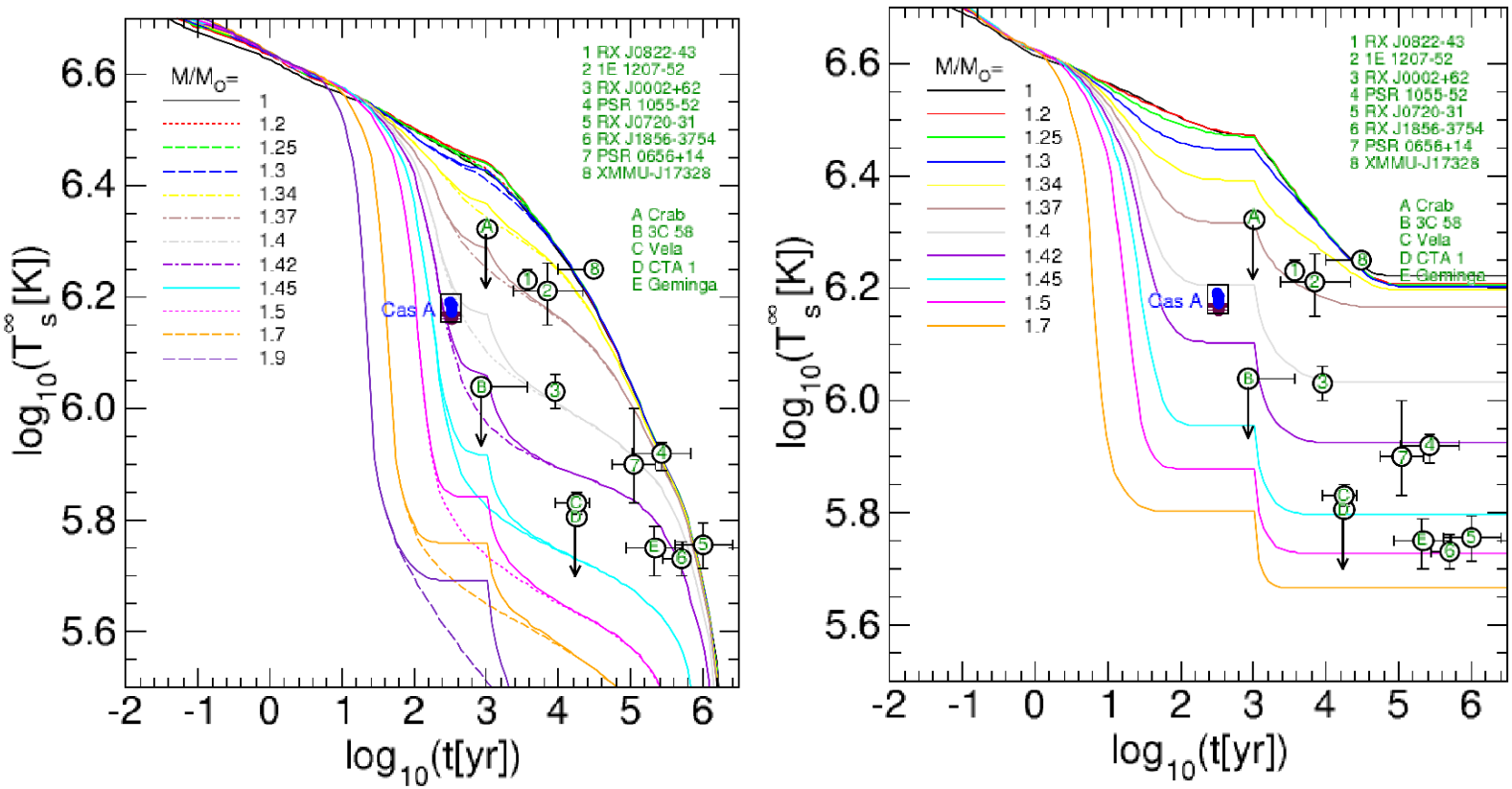

WD heating

Cermeño *and Pérez-García, PRD 98 (2018) 063002*

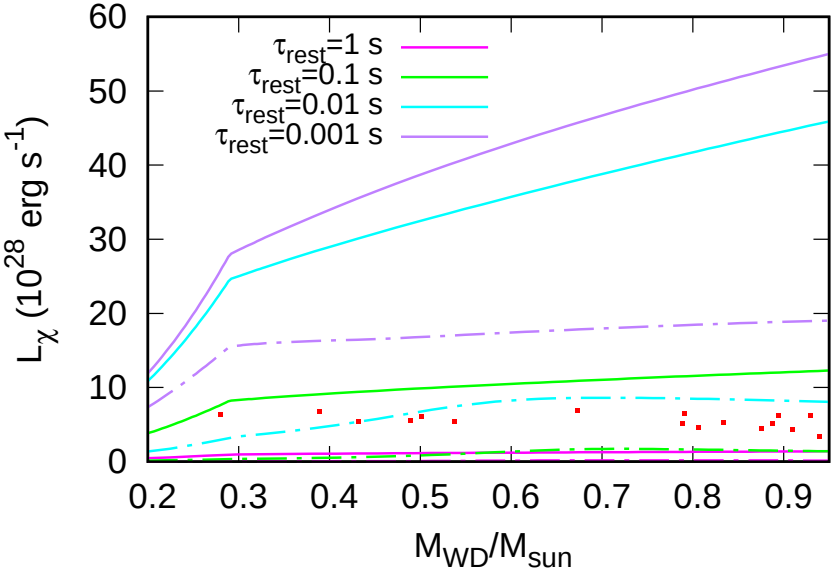

Luminosity effects for WDs in the M4 GC

$$L_\chi = \Gamma_{\rm ann} \int_0^R N\, e^{-\int_0^r \frac{m_Y dr'}{\tau_{\rm rest} E_Y(r')}} \int_{E_-(r)}^{E_+(r)} E_\gamma \frac{dN_\gamma(r)}{dE_\gamma} dE_\gamma dr$$

$\chi\bar{\chi} \to YY,\ Y \to \gamma\gamma$

$m_\chi = 0.5$ GeV, $\sigma_{\chi,N} = \sigma_{Y,N} = 10^{-39}$ cm^2

solid lines $m_Y = 0.375$ GeV, dashed lines $m_Y = 0.01$ GeV

red points L_{exp} in the M4 GC from

M. McCullough and M. Fairbairn, PRD 81 (2010) 083520

If $L_\chi > 1.5 L_{exp}$ (50 % of tolerance) $\Rightarrow$ excluded points of the parameter space

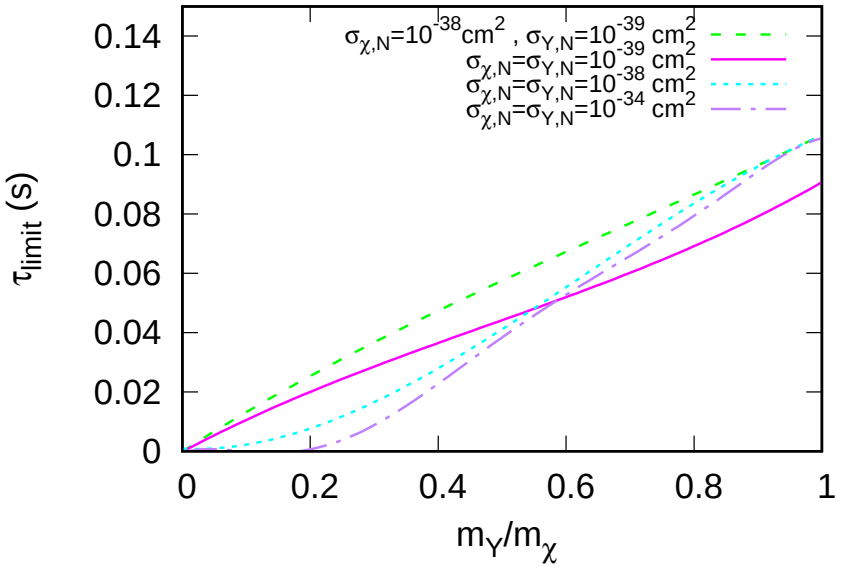

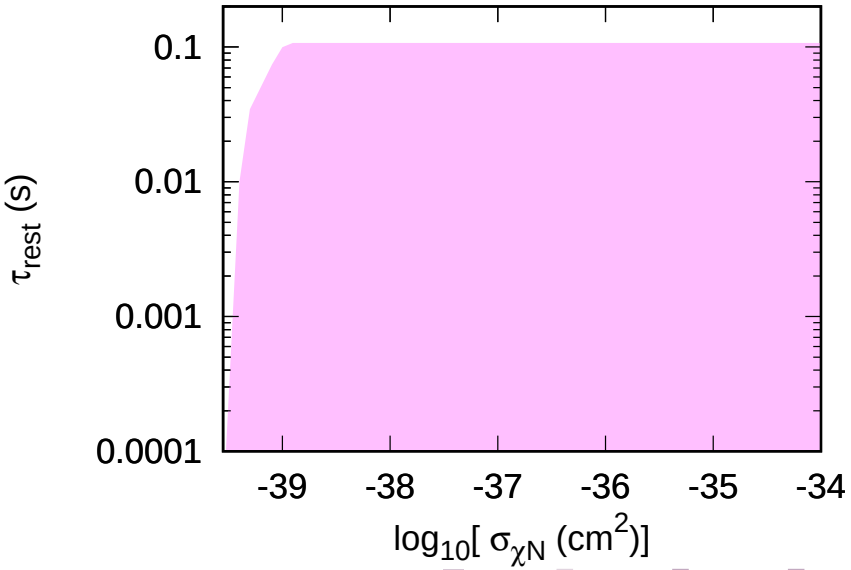

WD heating

Bell, Busoni, Ramirez-Quezada, Robles, Virgato, JCAP 10 (2021) 083

Dirac DM, no long-lived mediators

Contraints on the SI proton cross-section ⇒ stronger than DD for $m_\chi \lesssim 1$ GeV

Capture by electron scattering only relevant for leptophilic DM ⇒ improving DD constraints for $\sigma_{e\chi}$

Name	Operator	Coupling
D1	$\bar{\chi}\chi\,\bar{f}f$	y_f/Λ_f^2
D2	$\bar{\chi}\gamma^5\chi\,\bar{f}f$	iy_f/Λ_f^2
D3	$\bar{\chi}\chi\,\bar{f}\gamma^5 f$	iy_f/Λ_f^2
D4	$\bar{\chi}\gamma^5\chi\,\bar{f}\gamma^5 f$	y_f/Λ_f^2
D5	$\bar{\chi}\gamma_\mu\chi\,\bar{f}\gamma^\mu f$	$1/\Lambda_f^2$

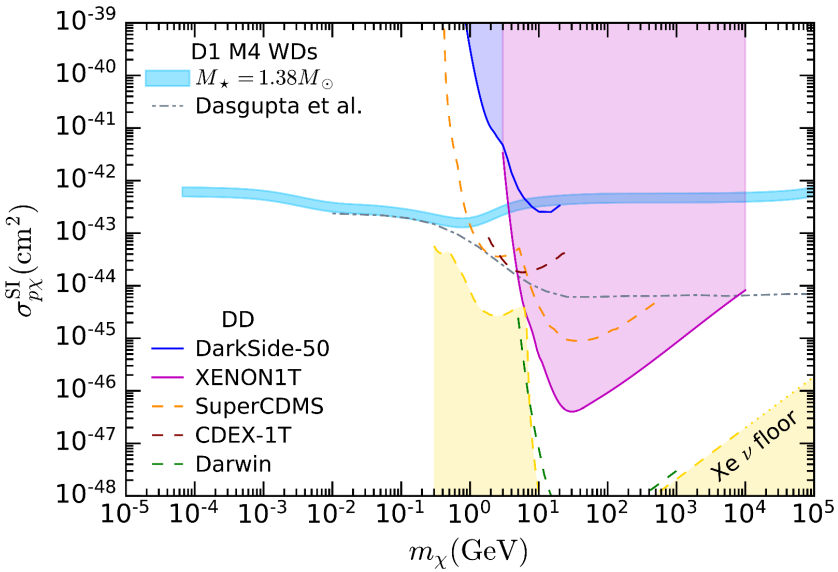

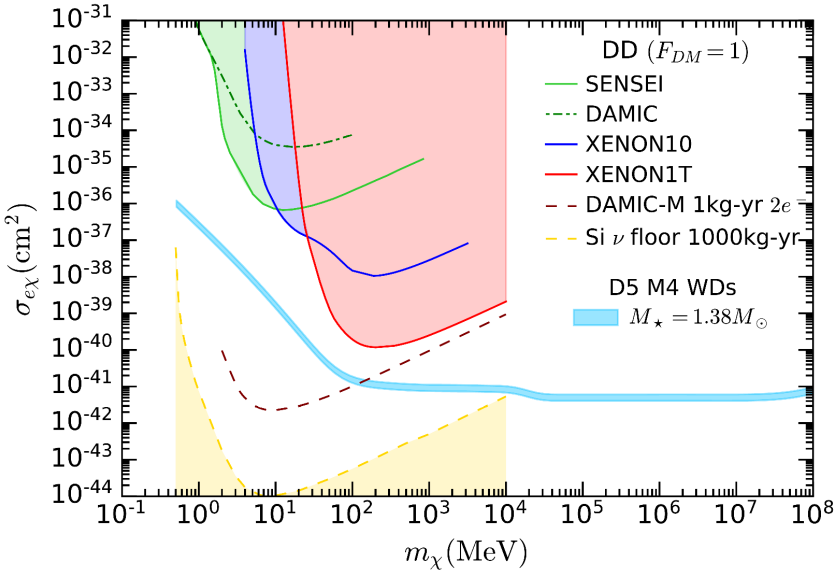

Beyond stardard indirect photon searches of DM in the center of galaxies

The differential flux of photons from the self-annihilation of DM particles in a region of the sky characterised by a solid angle of observation $\Omega_{\rm obs}$

$$\frac{d\Phi}{dE_\gamma}(E_\gamma, \Delta\Omega_{\rm obs}) = \frac{\langle\sigma v\rangle}{8\pi m_\chi^2}\frac{dN}{dE_\gamma}(E_\gamma)\int_{\Delta\Omega_{\rm obs}} {\rm d}\Omega \int_{\rm l.o.s} {\rm d}s\ \rho^2_{DM}(r(s,\theta))$$

- $\langle\sigma v\rangle$ averaged annihilation cross section of DM particles of mass m_χ
- $\frac{dN}{dE_\gamma}(E_\gamma)$ energy spectrum per annihilation event, E_γ photon energy
- $\rho_{DM}(r)$ DM density profile,
  $r^2 = s^2 + r_0^2 - 2r_0 s\ \cos\theta$, r_0 radial distance from the observer to the target

The center of large galaxies are expected to possess **supermassive black holes**

Some young galaxies possess **active galactic nuclei (AGN)** and are expected to gather a higher DM component than the center of our Galaxy

DM density in Centaurus A

Adiabatic growth of a super-massive black hole in a region with an initial DM distribution $\rho^0_{\rm DM}(r) \propto \rho_0\,(r/r_0)^{-\gamma}$ (we take $\gamma = 1$) $\Rightarrow$ **DM spike formation** *Gondolo, Silk, PRL 83 (1999) 1719*

$$\rho_{DM}(r) = \begin{cases} 0 & r < 4R_{\rm S} \\ \frac{\rho_{\rm sp}(r)\rho_{\rm sat}}{\rho_{\rm sp}(r)+\rho_{\rm sat}} & 4R_{\rm S} \le r < R_{\rm sp} \\ \rho_0 \left(\frac{r}{r_0}\right)^{-1} \left(1+\frac{r}{r_0}\right)^{-2} & r \ge R_{\rm sp} \end{cases},$$

$$\rho_{\rm sp}(r) = \rho_0 \left(\frac{R_{\rm sp}}{r_0}\right)^{-1} \left(1 - \frac{4R_S}{r}\right)^3 \left(\frac{R_{\rm sp}}{r}\right)^{7/3},$$

$$\rho_{\rm sat} \simeq \frac{m_\chi}{\langle\sigma v\rangle t_{BH}}$$

$R_S = 5 \times 10^{-6}$ pc, $R_{sp} = 10^8 R_{\rm S}$
$r_0 = 20$ kpc, $\rho_0 \sim 1$ GeV/cm^3

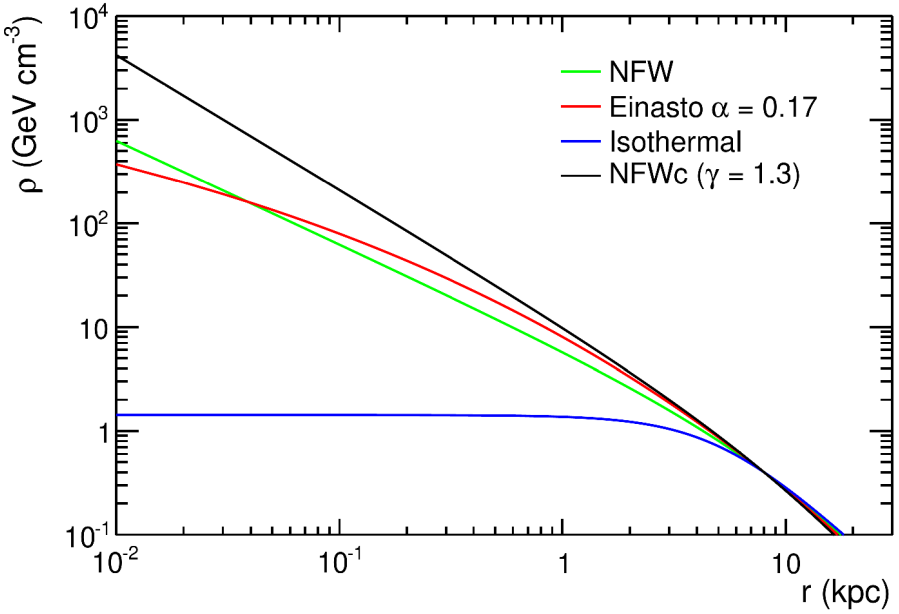

The Fermi-LAT Collaboration PRD 91 (2015) 122002

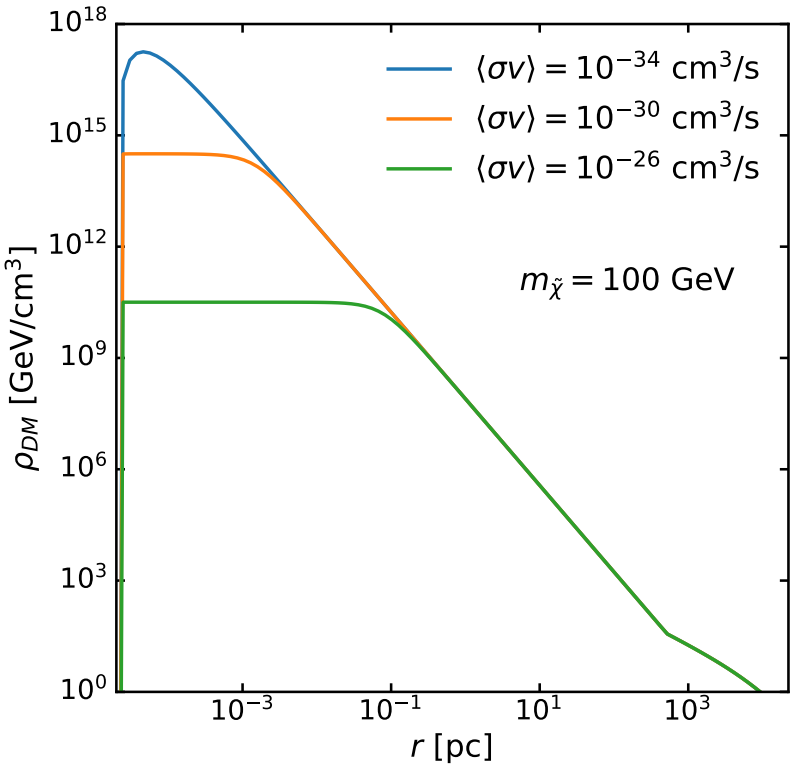

***Cermeño**, Degrande, Mantani, PRD 105 (2022) 8*

Active galactic nuclei as high energy electron sources

- Active galactic nuclei, such as Cen A, are well-known sources of high-energy particles (electrons and protons)
- Photon signatures expected both from self-annihilations and DM scattering
- The gamma-ray photons coming from the Cen A core can be explained by synchrotron radiation and synchrotron self-Compton radiation from two emitting zones (both located at 30° with respect to the line of sight) *Abdalla et al., A & A 619 (2018) A71*

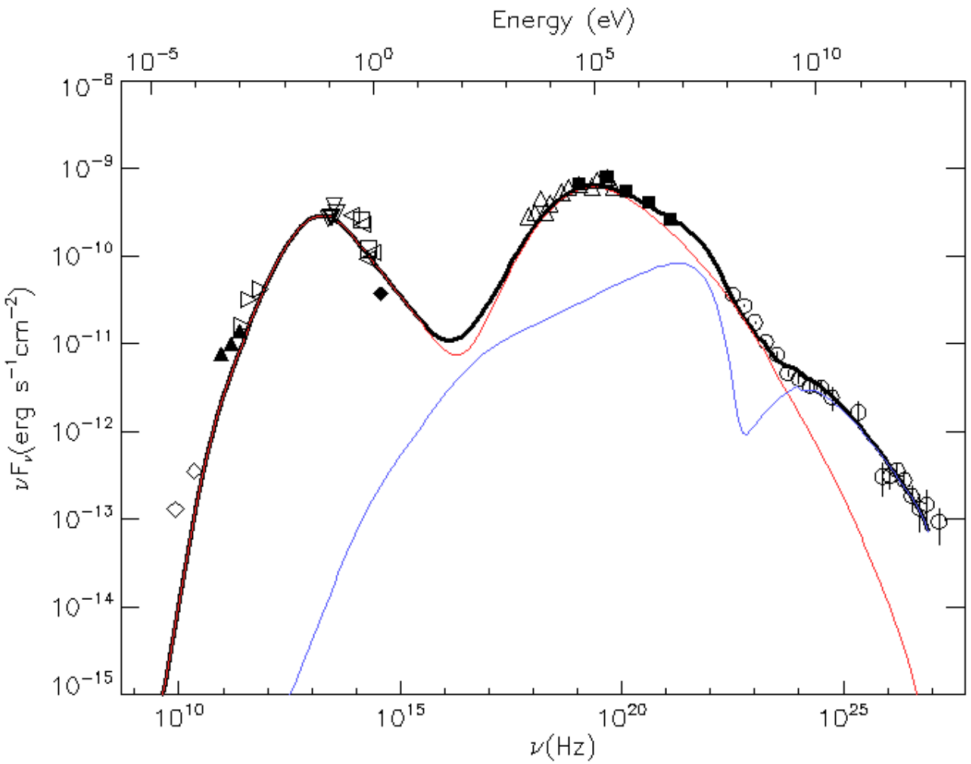

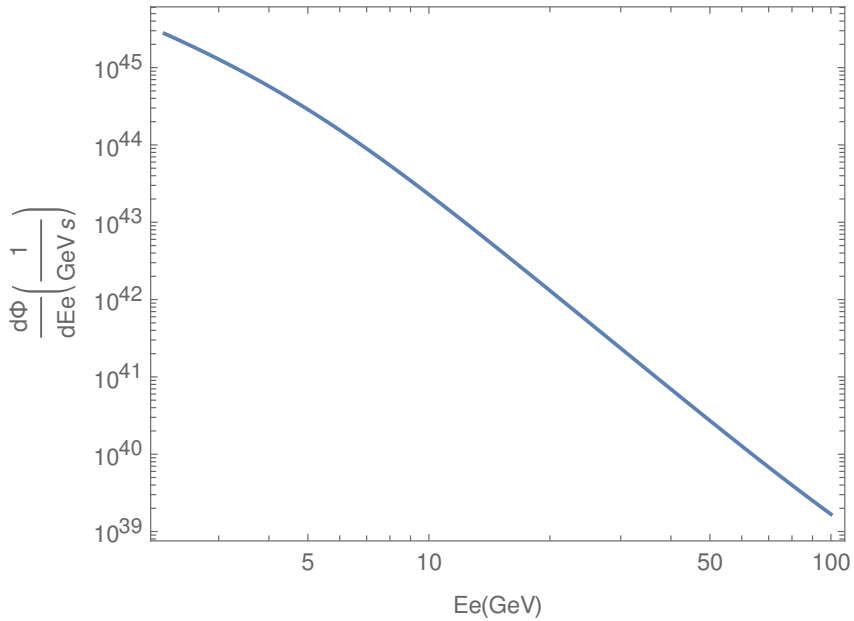

Testing models difficult to probe in conventional sites

- $\mathcal{L}_{DM} = i\bar{\psi}_{\tilde{\chi}}(\not{D} - m_{\tilde{\chi}})\psi_{\tilde{\chi}} + D_\mu\varphi^\dagger D^\mu\varphi - m_\varphi\varphi^\dagger\varphi + (a_R\,\bar{e}_R\,\psi_{\tilde{\chi}}\,\varphi + h.c.)\,,\ m_\varphi \gtrsim m_{\tilde{\chi}}$
- Relevant photon production $\tilde{\chi}\tilde{\chi} \to \gamma\gamma, \tilde{\chi}\tilde{\chi} \to e^-e^+\gamma, \tilde{\chi}e^- \to \tilde{\chi}e^-\gamma$
- Circular polarisation asymmetries $\sim 100\,\%$ from photons produced by $\tilde{\chi}e^- \to \tilde{\chi}e^-\gamma$
  Cermeño, *Degrande, Mantani, PRD 105 (2022) 8*

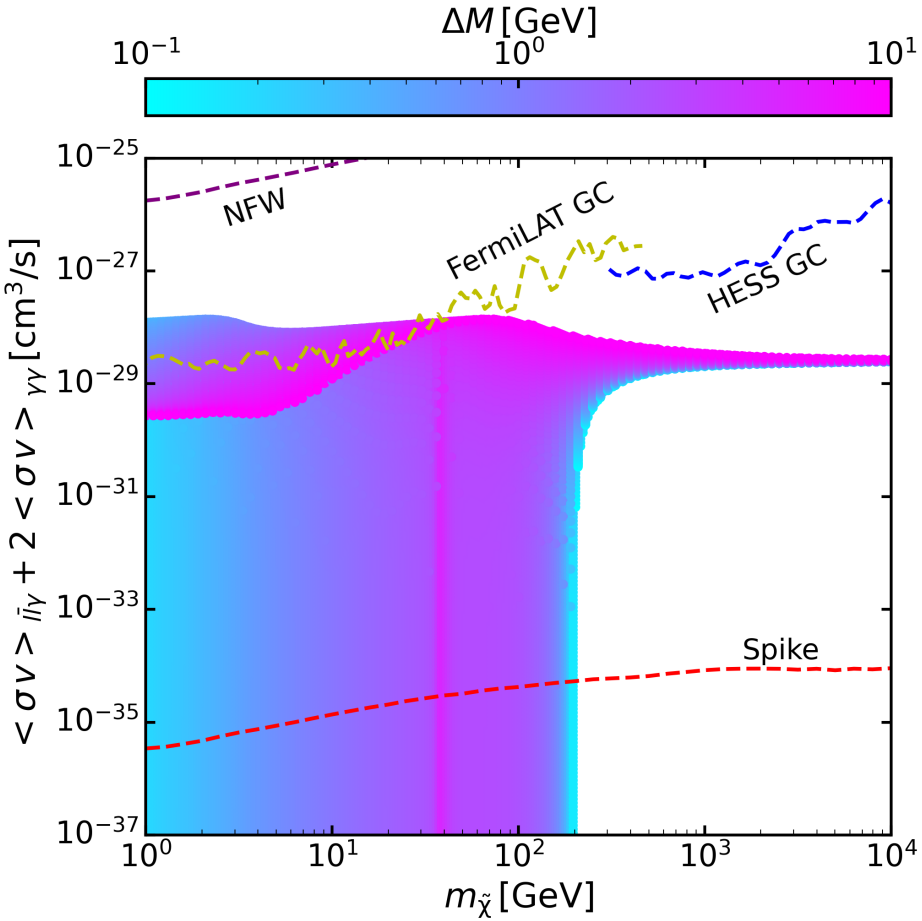

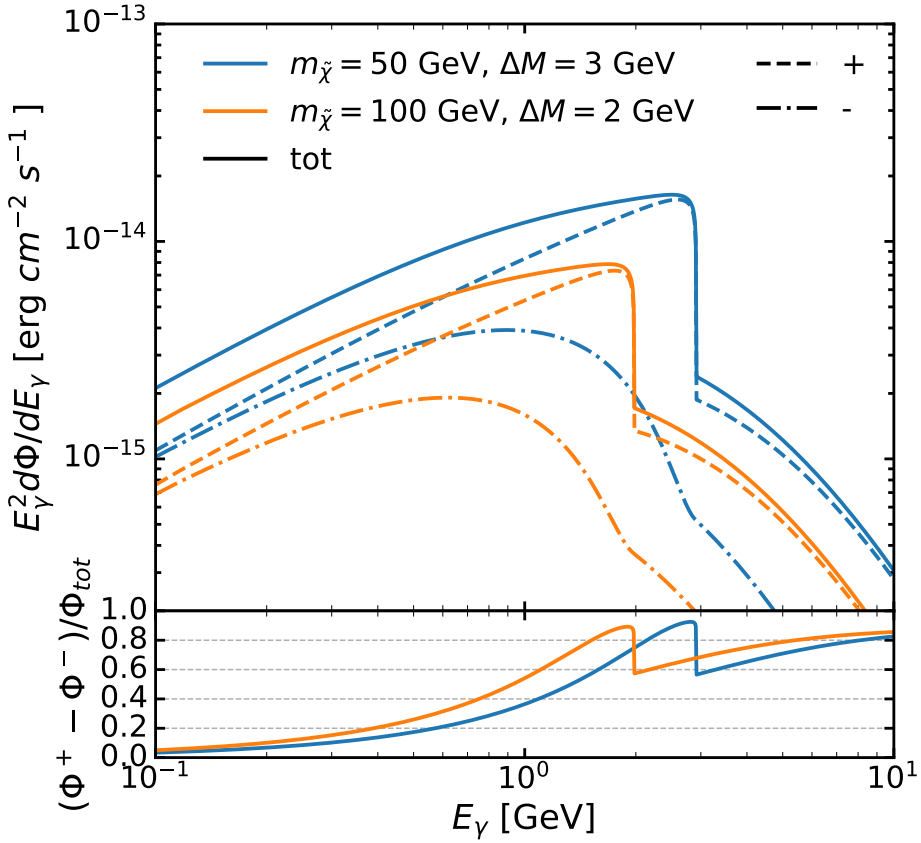

Sensitivity of Fermi-LAT to measure flux from $\tilde{\chi}e^- \to \tilde{\chi}e^-\gamma$ around $5\ 10^{13}$ erg cm^{-2} s^{-1}

Conclusions

- Some popular DM candidates that evade conventional experiments may be well suited to be studied indirectly in astrophysical scenarios
- The extreme conditions of compact objects (NSs, WDs, AGN), namely high density and compactness, make them suitable to gravitationally accrete a sizable DM component
- In the interior of compact stars, once captured, DM thermalise creating a small and dense DM core in the center
- Different indirect signals can arise from NS and WD which can help us to find or constrain DM: heating, phonon excitation, BH formation and star destruction
- Some AGN, such as Centaurus A, are expected to possess a DM density spike in their interior which would have survive to date contrary to the case of our Galaxy
- The study of indirect DM signals coming from self-annihilation or DM scattering with the baryonic matter of the AGN can test models difficult to test by searches in conventional sites

Backup slides

Candidates

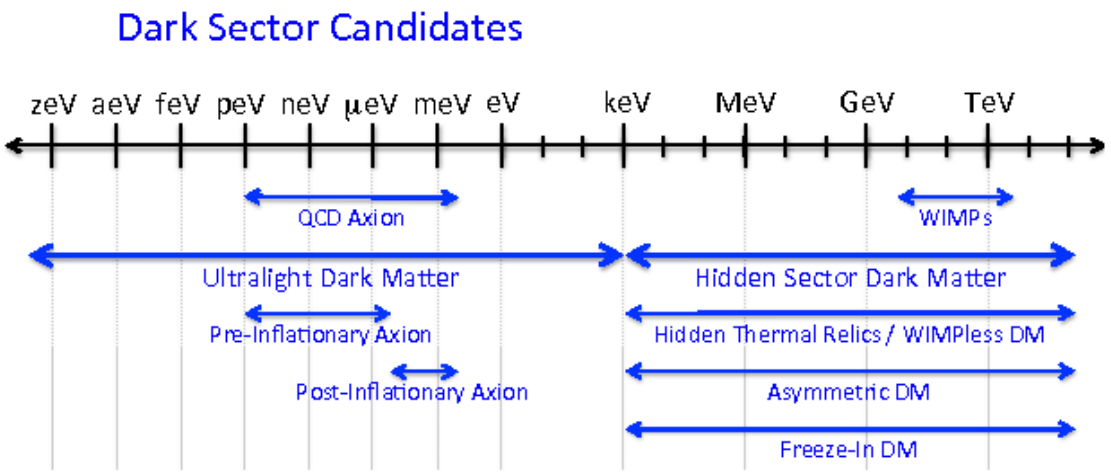

Battaglieri et al., 1707.04591

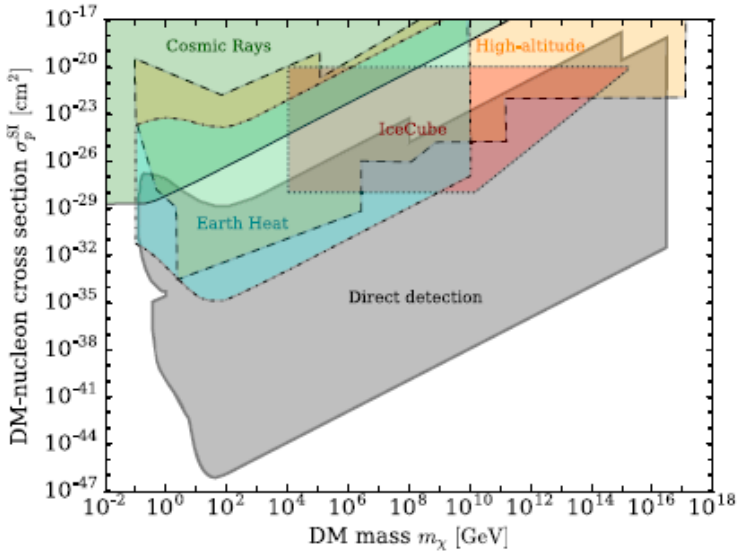

Kavanagh, PRD 97 (2018) 123013

We focus on

- Hidden Sector DM
- $5\ 10^{-3}\ \mathrm{GeV} \lesssim m_\chi \lesssim 10\ \mathrm{GeV}$, with χ the DM particle
- WIMPs (Weakly Interacting Massive Particles), DM-nucleon cross-sections $10^{-47}\ \mathrm{cm}^2 \lesssim \sigma_{\chi,N} \lesssim 10^{-40}\ \mathrm{cm}^2$
- SIMPs (Strongly Interacting Massive Particles), $10^{-40}\ \mathrm{cm}^2 \lesssim \sigma_{\chi,N} \lesssim 10^{-32}\mathrm{cm}^2\,\frac{m_\chi}{\mathrm{GeV}}$ in order to not exceed the Earth heat flux *Mack et al., PRD 76 (2007) 043523*

DM mass ranges probed in compact objects

Baryakhtar et al., 2022 Snowmass Contribution, arXiv: 2203.07984

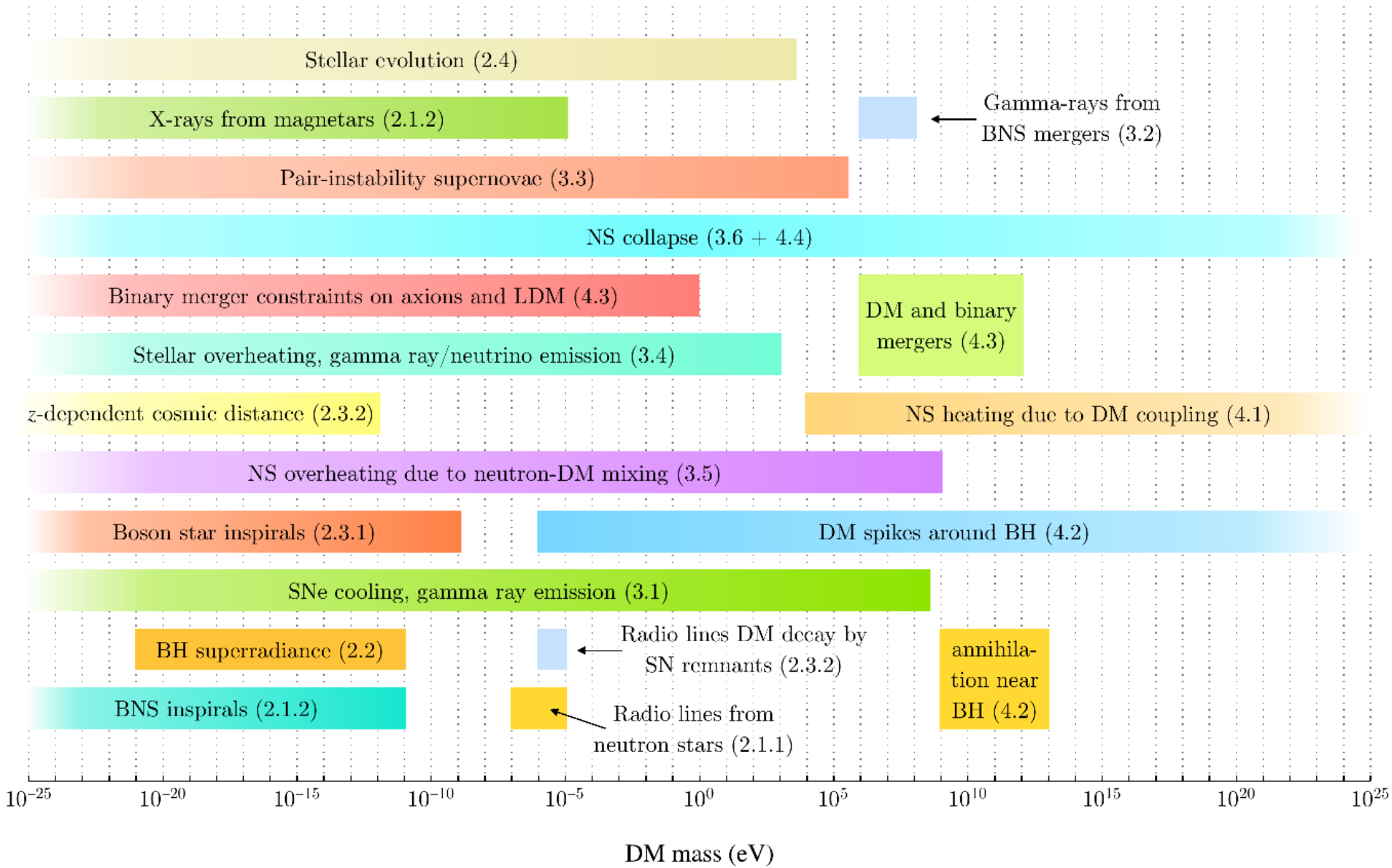

DM accretion in dense stars

- For a WD: $\Gamma_{\rm capt} \simeq 6\times10^{27}\left(\frac{M}{0.6M_\odot}\right)\left(\frac{R}{0.01R_\odot}\right)\left(\frac{1\,\rm GeV}{m_\chi}\right)\left(\frac{\rho_\chi^{ambient}}{0.3\,\frac{\rm GeV}{\rm cm^3}}\right) f\ \rm s^{-1},\ Y_\chi = N_\chi/N_B < 10^{-10}$
- For NSs: $\Gamma_{\rm capt} \simeq 6\times10^{25}\left(\frac{M}{1.5M_\odot}\right)\left(\frac{R}{12\,\rm km}\right)\left(\frac{1\,\rm GeV}{m_\chi}\right)\left(\frac{\rho_\chi^{ambient}}{0.3\,\frac{\rm GeV}{\rm cm^3}}\right) f\ \rm s^{-1},\ Y_\chi = N_\chi/N_B < 10^{-20}$

Improved treatments *Bell et al., JCAP 09 (2020) 028, JCAP 03 (2021) 086, JCAP 11 (2021) 056, JCAP 10 (2021) 083* internal structure, Pauli blocking, relativistic kinematics, gravitational focusing, multiple scattering effects,momentum-dependent form factors, baryon strong interactions...

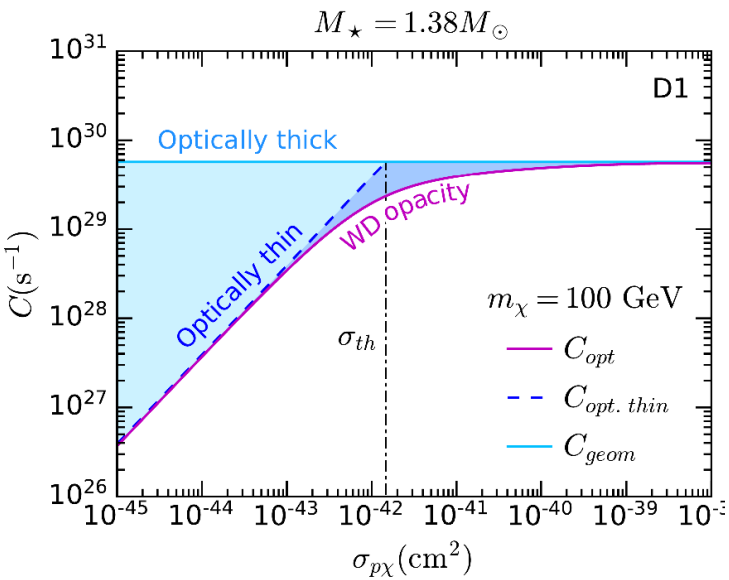

Bell et al., JCAP 10 (2021) 083

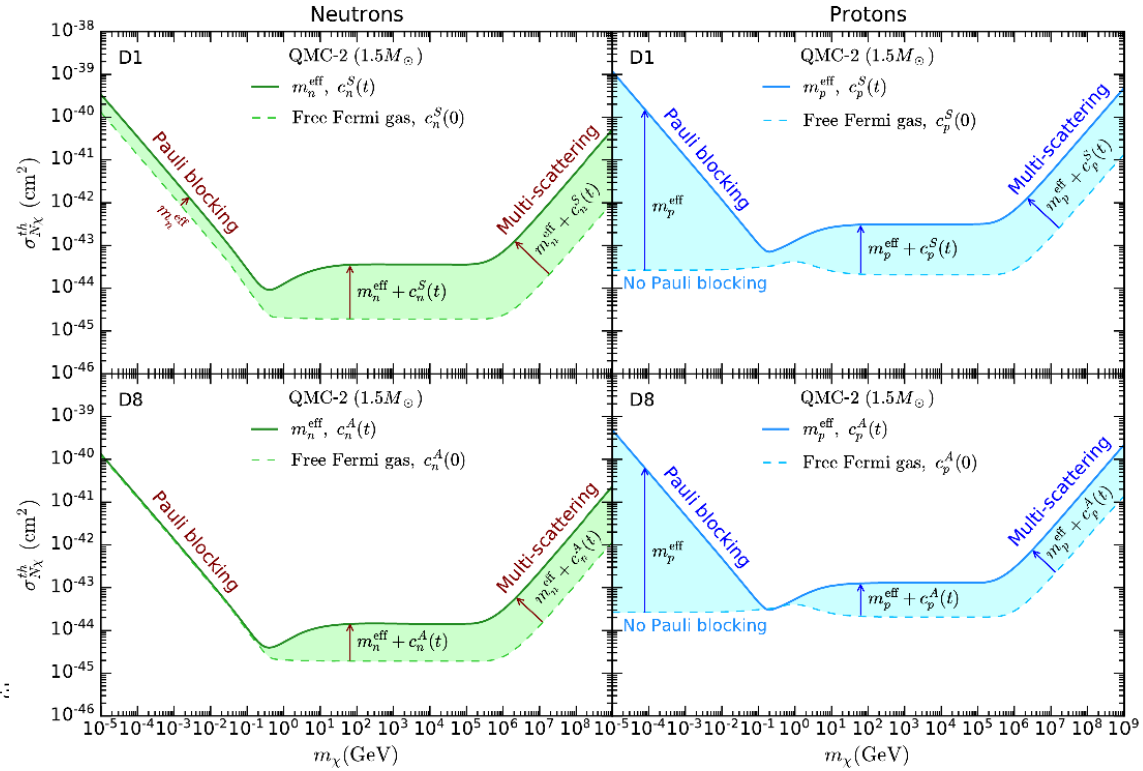

Bell et al., JCAP 11 (2021) 056

BH formation and star destruction

Asymmetric DM in the compact star core ⇒ collapse into a BH

Garani, Genolili, Hambye, JCAP 05 (2019) 035, Janish, Narayan, Riggins, PRD 100 (2019) 035008

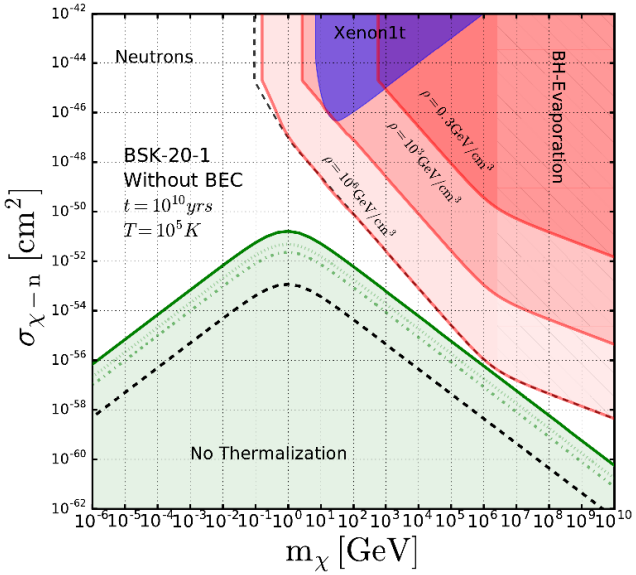

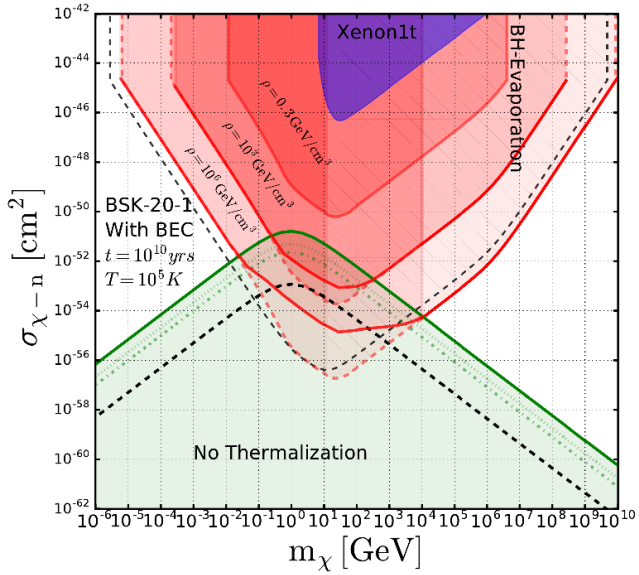

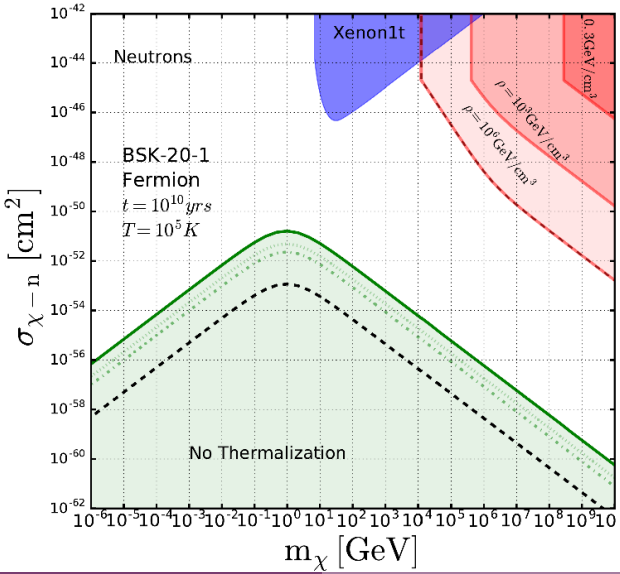

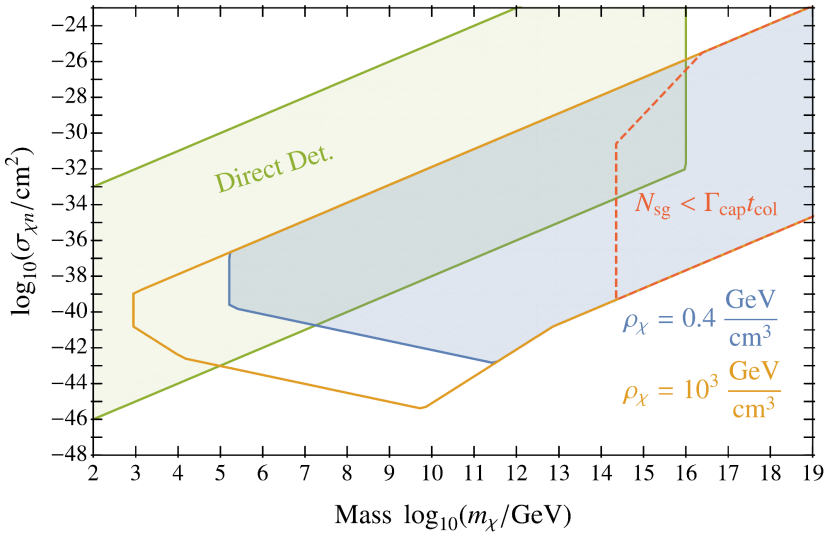

BH formation and WD destruction

Janish, Narayan, Riggins, PRD 100 (2019) 035008

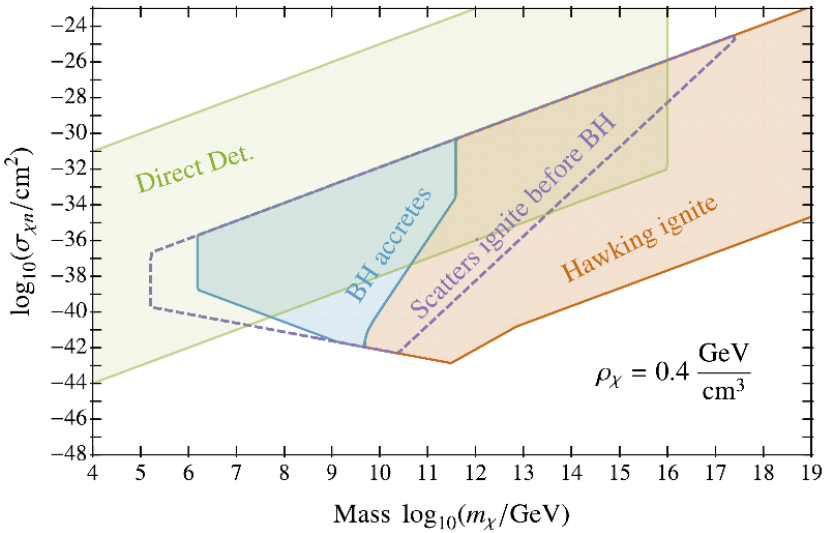

FIG. 4. Constraints on fermionic asymmetric DM whic forms a DM core and collapses to a mini black hole in a WI The black hole either ignites a supernova via Hawking emis sion (red) or accretes and eats the star (or possibly ignites supernova) (blue). Also shown (purple) are the constraints o DM-nuclei scatters igniting a supernova during core collaps before formation of a black hole.

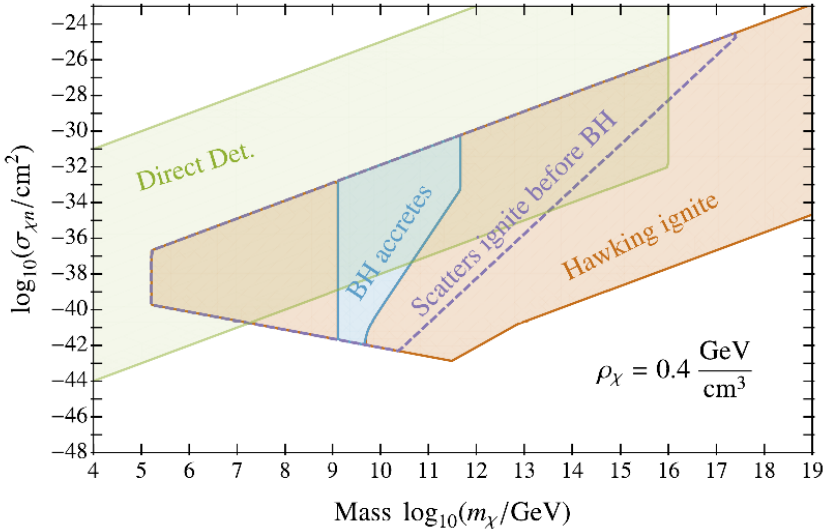

FIG. 5. Constraints on bosonic asymmetric DM which forms a DM core and collapses to a mini black hole in a WD. The black hole either ignites a supernova via Hawking emission (red) or accretes and eats the star (or possibly ignites a supernova) (blue). Also shown (purple) are the constraints on DM-nuclei scatters igniting a supernova during core collapse before formation of a black hole.

Cooling secuence NS

Grigorian, Kolomeitsev, Maslov, Voskresensky, Universe 4 (2018) 2, 29

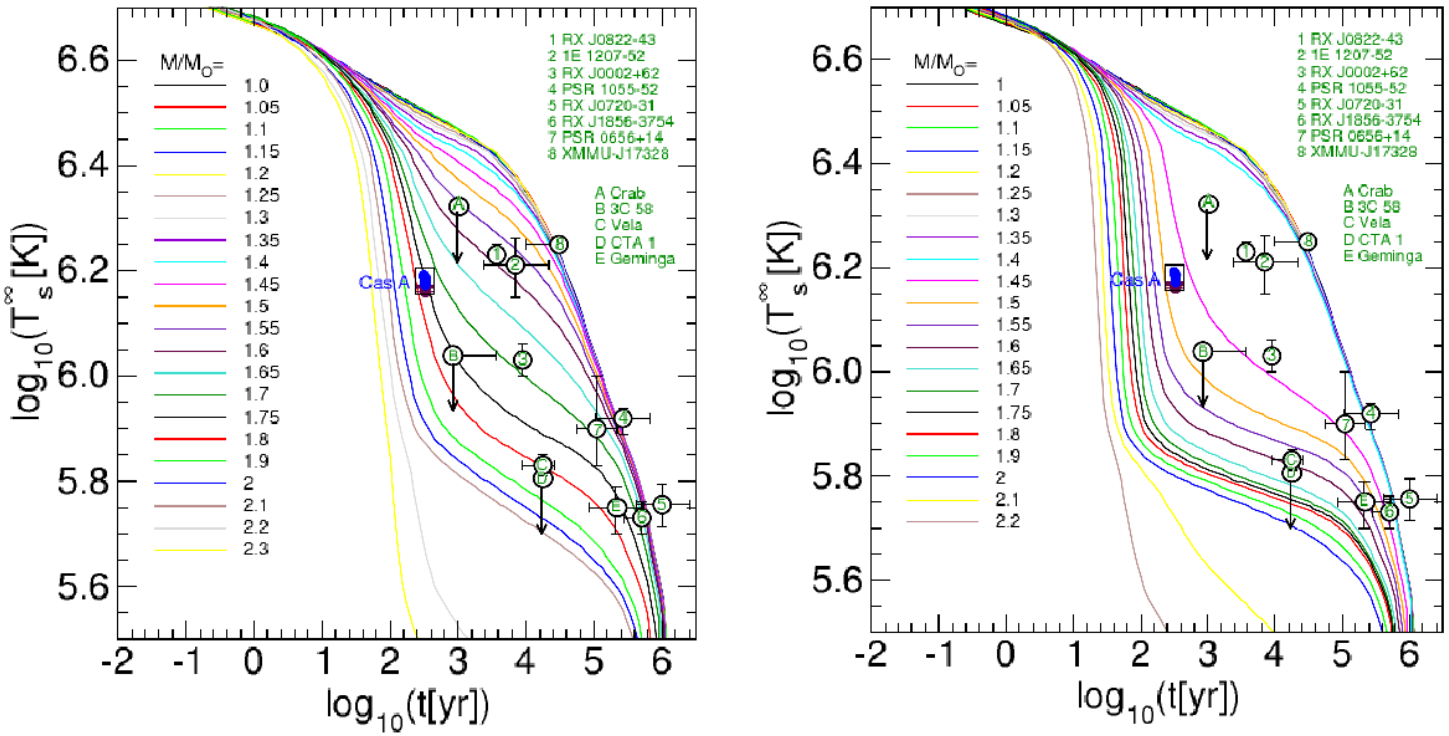

FIG. 4: Redshifted surface temperature as a function of the neutron star age for various neutron star masses and choice of the EoS. Left panel: MKVOR model without the inclusion of hyperons. Right panel: MKVORHϕ model with hyperons included with the gaps following from the TN-FGA parameter choice. Proton gaps for both calculations without and with hyperons are taken following EEHO model.

Constraints for long-lived mediators

Leane, Linden, Mukhopadhyay, Toro, PRD 103 (2021) 075030

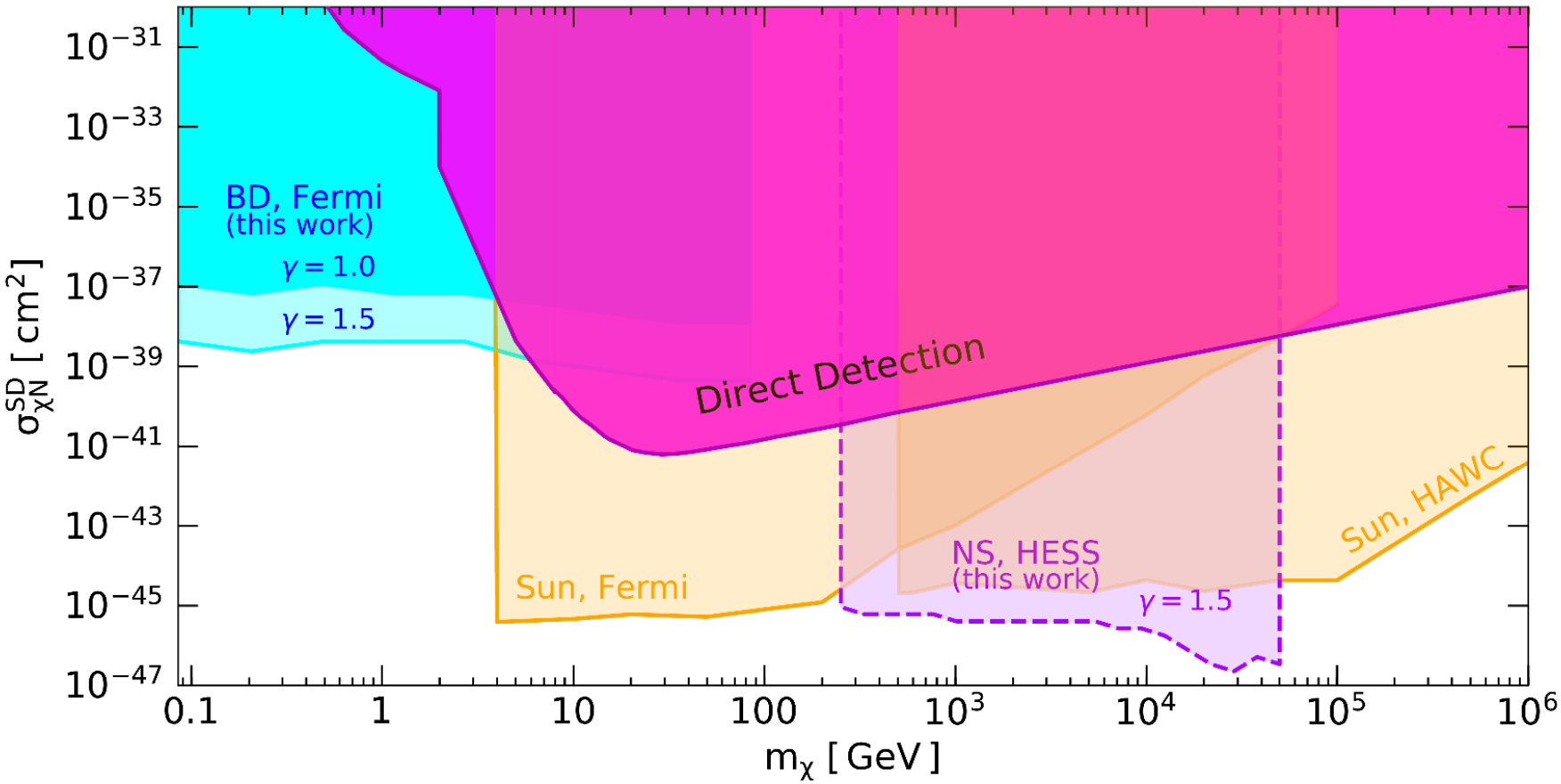

FIG. 5. Scattering cross section limits for DM annihilation to long-lived mediators decaying to $\gamma\gamma$ in Brown Dwarfs (using *Fermi*), the Sun (using *Fermi* and HAWC [45, 47]), and Neutron Stars (using H.E.S.S.). The BD and NS limits are new calculations in this work, calculated using the full Galactic Center population of BDs or NSs. The $\gamma = 1.0, 1.5$ values correspond to the inner slope of the DM density profile. Our limits have some assumptions; see text for details.

De Broglie wavelenghts for DM boosted by NSs

- $E_\chi = \gamma m_\chi \simeq 1.26 m_\chi \Rightarrow |\vec{p}_\chi| = \sqrt{E_\chi^2 - m_\chi^2} = \sqrt{\gamma^2 - 1} m_\chi \simeq 0.77 m_\chi$
- $\lambda\!\!\!^{-} = \frac{\hbar}{|\vec{p_\chi}|} \simeq \frac{197.33\ \text{MeV fm}}{0.77 m_\chi}$
- De Broglie wavelenght $\lambda = 2\pi\lambda\!\!\!^{-}$, provides information about the internal structure that DM particles will see when colliding

m_χ (GeV)	λ (fm)
0.5	3.2204
0.8	2.0128
1	1.6102
5	0.3220

- $m_\chi = 500\ \text{MeV}, 800\ \text{MeV}, 1\ \text{GeV} \Rightarrow \lambda \lesssim \text{R}_{\text{Nucleus}}$, sees nuclear inner structure, but not quark structure. $m_\chi = 5\ \text{GeV}$ sees quark structure

$\chi - N$ differential cross section

$$d\sigma = \frac{|\overline{\mathcal{M}}_N|^2}{4\sqrt{(pk)^2 - m_N^{*2} m_\chi^2}} f_N(E)(1 - f_N(E'))(2\pi)^4 \delta^{(4)}(p + k - p' - k') \frac{d^3\vec{p'}}{(2\pi)^3 2E'} \frac{d^3\vec{k'}}{(2\pi)^3 2\omega'}$$

- As DM inside the star remains tiny at all times, $\frac{N_\chi}{N_B} < 2\ 10^{-13}$, all outgoing states are allowed, $f_\chi(\omega') \approx 0$
- $m_N^*/m_N = 0.4, 0.7, 0.85$ for $n/n_{sat} = 2, 1, 0.5$

$\chi - N$ differential cross section per unit volume

$$\frac{1}{V}\frac{d\sigma}{d\Omega dq_0} = \int_{|\vec{p}_-|}^{\infty} \frac{d|\vec{p}||\vec{p}|}{4(2\pi)^4 E'} \frac{m_N|\vec{k}'|}{|\vec{q}|} \delta(cos\ \theta - cos\ \theta_0)\Theta(|\vec{p}|^2 - |\vec{p}_-|^2) \frac{|\overline{\mathcal{M}}_N|^2 f_N(E)(1 - f_N(E'))}{4\sqrt{E^2\omega^2 - m_N^{*2}m_\chi^2}}$$

$$-\infty < q_0 \leqslant \omega - m_\chi$$

- $\cos\theta_0 = \frac{m_N^*}{|\vec{p}||\vec{q}|}\left(q_0 - \frac{|\vec{q}|^2}{2m_N^*}\right)$ and $|\cos\theta_0| \leqslant 1 \Rightarrow q_0 \leqslant \frac{|\vec{q}|}{2m_N^*}(|\vec{q}| + 2|\vec{p_F}|)$
- $q_0 \leq \omega - m_\chi$
- $|\vec{q}| < 2|\vec{k}|$

Differential cross section per unit volume for $T = 0$

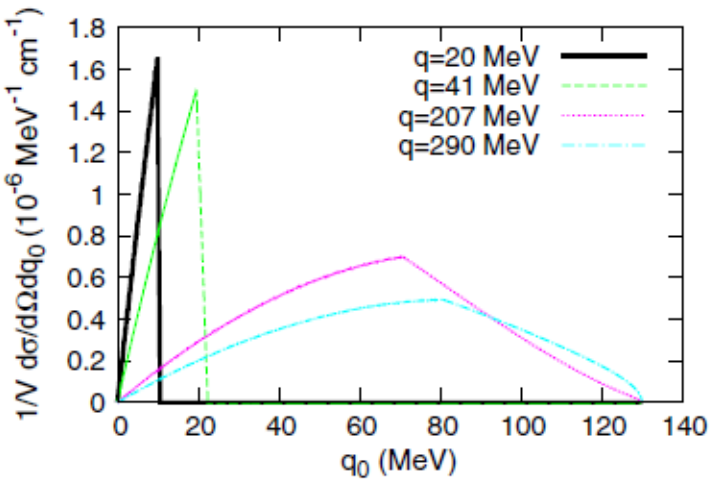

FIG. 1. Differential cross section per unit volume as a function of the energy transfer q_0 for values of $|\vec{q}| = 20$, 41, 207, and 290 MeV. The DM particle mass is $m_\chi = 0.5$ GeV, and $T = 0$ at $n = n_0$.

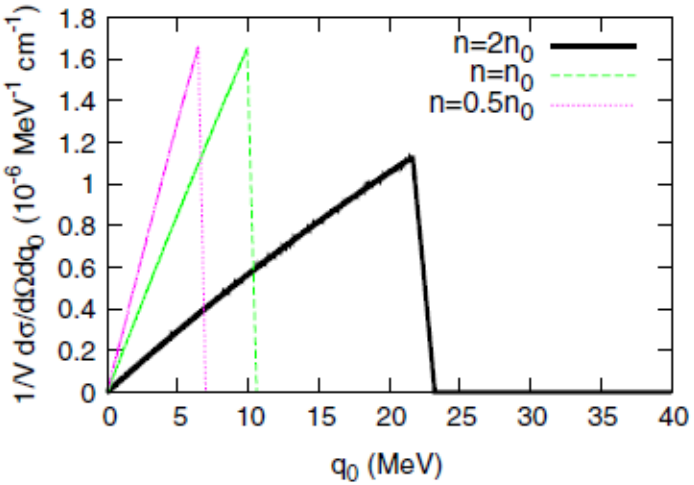

FIG. 2. Differential cross section per unit volume as a function of the energy transfer q_0 for nucleon densities $n = (0.5, 1, 2)n_0$. We set $|\vec{q}| = 20$ MeV and $m_\chi = 0.5$ GeV at $T = 0$.

Differential cross section per unit volume at $T \neq 0$ and mean free path at $T = 0$

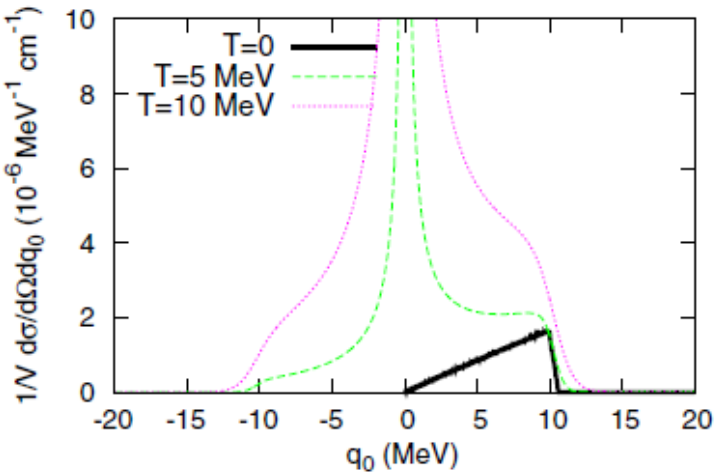

FIG. 4. Differential cross section per unit volume as a function of the energy transfer q_0 at $T = 0$, 5, 10 MeV for a nucleon density $n = n_0$. We set $|\vec{q}| = 20$ MeV and $m_\chi = 0.5$ GeV.

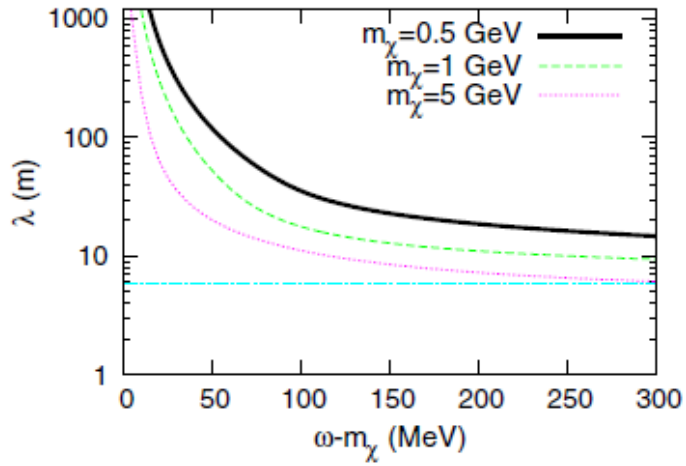

FIG. 5. Dark matter mean free path as a function of kinetic energy for $m_\chi = 0.5$, 1, and 5 GeV at $T = 0$ and $n = n_{\rm sat}$. Dot-dashed line shows that the simplified estimate yields a constant value $\lambda_\chi \simeq 1/\sigma_{\chi N} n \sim 5.9$ m, assuming current experimental sensitivities $\sigma_{\chi N} \sim 10^{-41}$ cm^2. See text for details.

Maximum values for the differential cross section per unit volume at $T = 0$

- $|\vec{p}_-| = \frac{m_N^*}{|\vec{q}|}\left(q_0 - \frac{|\vec{q}|^2}{2m_N^*}\right)$
- $|\vec{p}| \leq |\vec{p_F}| \Rightarrow f_N(E) = 1, |\vec{p}| > |\vec{p_F}| \Rightarrow f_N(E) = 0$
- $E_4 = E_2 + q_0 \Rightarrow |\vec{p'}| = \sqrt{(E + q_0)^2 - m_N^{*2}}$
- $(1 - f_N(E')) = 1$ for $|\vec{p'}| \geq |\vec{p_F}| \Rightarrow |\vec{p}| \geq \tilde{p} = \sqrt{(E_F - q_0)^2 - m_N^{*2}}$
- Area of $f_N(E)(1 - f_N(E'))$ will reach its maximum value when $|\vec{p}_-| = \tilde{p}$
- If $|\vec{p}_-| < \tilde{p}$ area $|\vec{p_F}| - \tilde{p}$
- If $|\vec{p}_-| > \tilde{p}$ area $|\vec{p_F}| - |\vec{p}_-|$

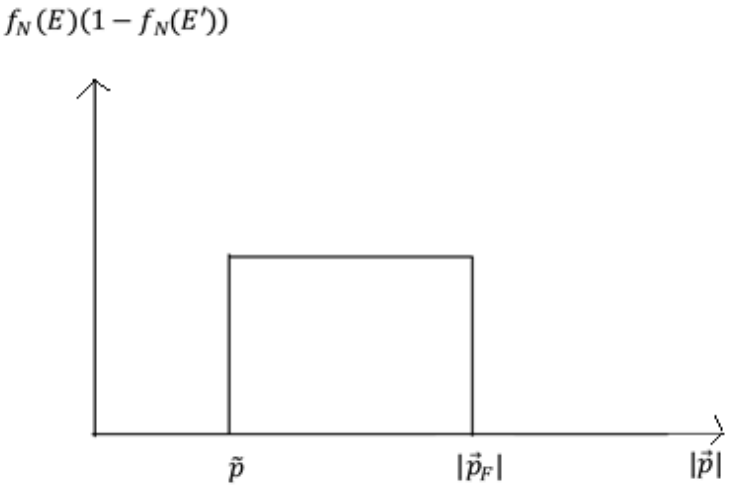

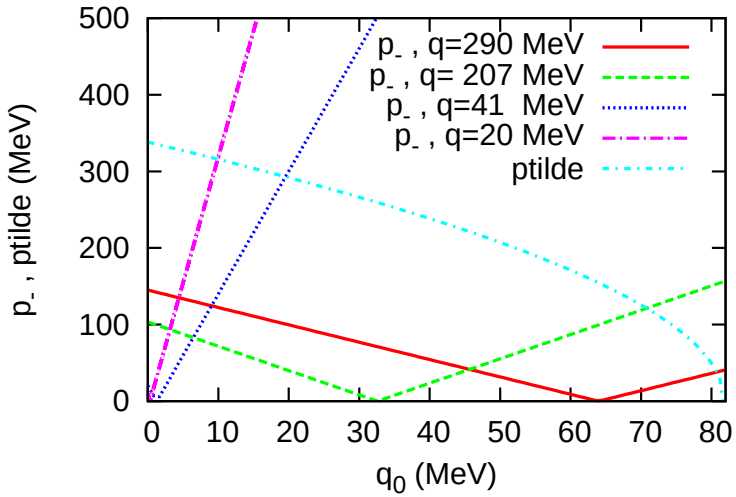

Feynman amplitude for the χ–N scalar-vector interaction

- $\mathcal{L} = \sum_{N=n,p} g_{Ns} \chi \bar{\chi} N \bar{N}$

$$|\overline{\mathcal{M}_{Ns}}|^2 = 4g_{Ns}^2(p'p + m_N^2)(k'k + m_\chi^2) = 4g_{Ns}^2(E'E - \vec{p}\vec{p'} + m_N^2)(\omega'\omega - \vec{k}\vec{k'} + m_\chi^2) \simeq$$

$$4g_{Ns}^2(E'E + m_N^2)(\omega'\omega + m_\chi^2)$$

- $\mathcal{L} = \sum_{N=n,p} g_{Nv} \chi \gamma^\mu \bar{\chi} N \gamma_\mu \bar{N}$

$$|\overline{\mathcal{M}_{Nv}}|^2 = 8g_{Nv}^2[2m_N^2 m_\chi^2 - m_N^2 k'k - m_\chi^2 p'p + (p'k')(pk) + (p'k)(pk')] =$$

$$8g_{Nv}^2[2m_N^2 m_\chi^2 - m_N^2(\omega\omega' - \vec{k'}\vec{k}) - m_\chi^2(E'E - \vec{p'}\vec{p}) + (E'\omega' - \vec{p'}\vec{k'})(E\omega - \vec{p}\vec{k}) + (E'\omega - \vec{p'}\vec{k})(E\omega' - \vec{p}\vec{k'})] \simeq$$

$$8g_{NV}^2(2m_N^2 m_\chi^2 - m_N^2 \omega\omega' - m_\chi^2 E'E + 2E'\omega' E\omega)$$

- $$|\overline{\mathcal{M}_N}|^2 \simeq 4g_{Ns}^2(E'E + m_N^2)(\omega'\omega + m_\chi^2) + 8g_{Nv}^2(2m_N^2 m_\chi^2 - m_N^2\omega\omega' - m_\chi^2 E'E + 2E'\omega' E\omega) +$$

$$8g_{Ns}g_{Nv}m_N m_\chi(E + E')(\omega + \omega')$$

Feynman amplitudes for the $\chi\chi \to \nu\nu$ and $\chi\chi \to aa$ annihilations

- For $\chi\chi \to \nu\nu$

$$|\overline{\mathcal{M}}_{f\bar{f}}|^2 = \frac{g_\chi^2 g_f^2}{4} \frac{s^2}{(s-m_a^2)^2 + E_{\vec{q}}^2 \Gamma^2}$$

$s = (p_1 + p_2)^2 = (p_3 + p_4)^2$, $E_{\vec{q}} = \sqrt{|\vec{q}|^2 + m_a^2}$ and Γ the a decay width via $a \to f\bar{f}$

- For $\chi\chi \to aa$

$$|\overline{\mathcal{M}}_{aa}|^2 = \frac{-g_\chi^4}{2}\left(\mathcal{M}_T\mathcal{M}_T^* + \mathcal{M}_U\mathcal{M}_U^* + \mathcal{M}_{mixing}\mathcal{M}_{mixing}^*\right)$$

$$\mathcal{M}_T\mathcal{M}_T^* = \frac{(t-m_a)^2 - m_\chi^2(m_\chi^2+2m_a^2)}{(t-m_\chi^2)^2} \qquad \mathcal{M}_U\mathcal{M}_U^* = \frac{(u-m_a)^2 - m_\chi^2(m_\chi^2+2m_a^2)}{(u-m_\chi^2)^2}$$

$$\mathcal{M}_{mixing}\mathcal{M}_{mixing}^* = \frac{(s-2m_\chi^2)(2m_a^2-s)+2m_\chi^2(m_\chi^2+2m_a^2-2s)}{(t-m_\chi^2)(u-m_\chi^2)} - \frac{2(t-m_a^2)^2}{(t-m_\chi^2)(u-m_\chi^2)} + 2\frac{2m_\chi^2-s}{(u-m_\chi^2)}$$

$s = (p_1 + p_2)^2$, $t = (p_1 - p_3)^2$ and $u = 2m_\chi^2 + 2m_a^2 - s - t$ Mandelstam variables

Photon energy flux outside the WD

The photon energy flux at a distance d from the WD center

$$E_\gamma^2 \frac{d\Phi}{dE_\gamma} = \frac{\Gamma_{\rm ann}}{4\pi d^2} E_\gamma^2 \frac{dN_\gamma}{dE_\gamma}(R) \frac{N \tau_{rest} E_Y(R)}{m_Y} e^{-\frac{m_Y R}{\tau_{rest} E_Y(R)}} \left(1 - e^{-\frac{m_Y (d-R)}{\tau_{rest} E_Y(R)}}\right)$$

$m_\chi = 0.8$ GeV, $m_Y = 0.1$ GeV, $\sigma_{\chi,N} = \sigma_{Y,N}$, $\rho_c = 3.3\ 10^5$ g/cm^3, $d = 2R = 5.4\ 10^9$ cm

Solid lines $\tau_{rest} = 0.1$ s $\leftrightarrow \lambda_{\rm D} = 2.4\ 10^{10}$ cm > 2R

Dashed lines $\tau_{rest} = 0.8$ s $\leftrightarrow \lambda_{\rm D} = 2\ 10^{11}$ cm > 2R

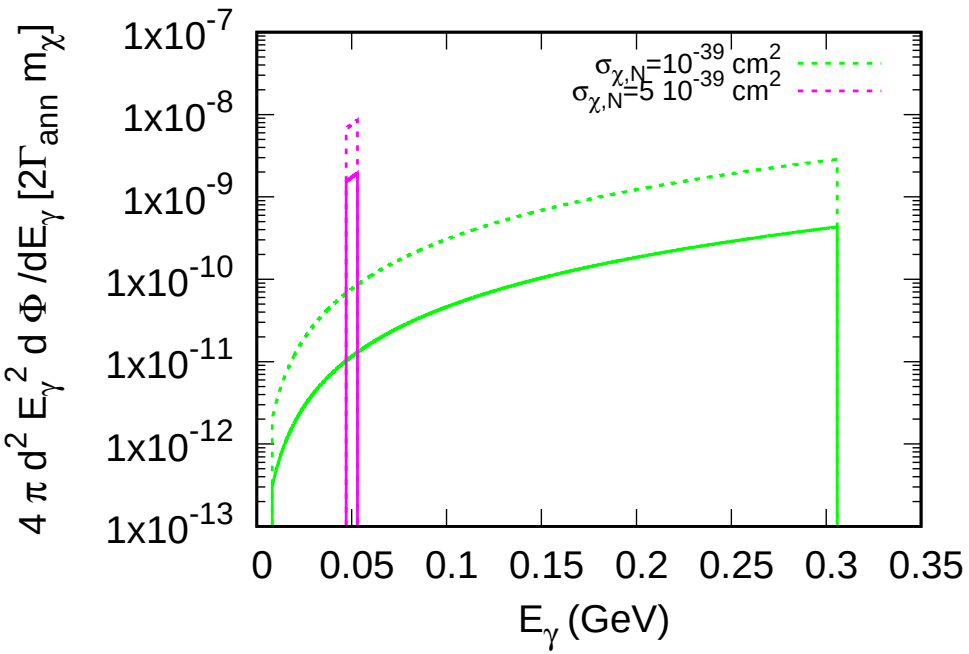

Neutron stars and white dwarfs

- NSs and WDs are formed at the end of the life of a luminous star
- $0.4M_{\odot} \lesssim M_{prog} \lesssim 8M_{\odot} \Rightarrow$ WD
- $M_{prog} \gtrsim 8\ \mathrm{M}_{\odot} \Rightarrow$ NS o BH

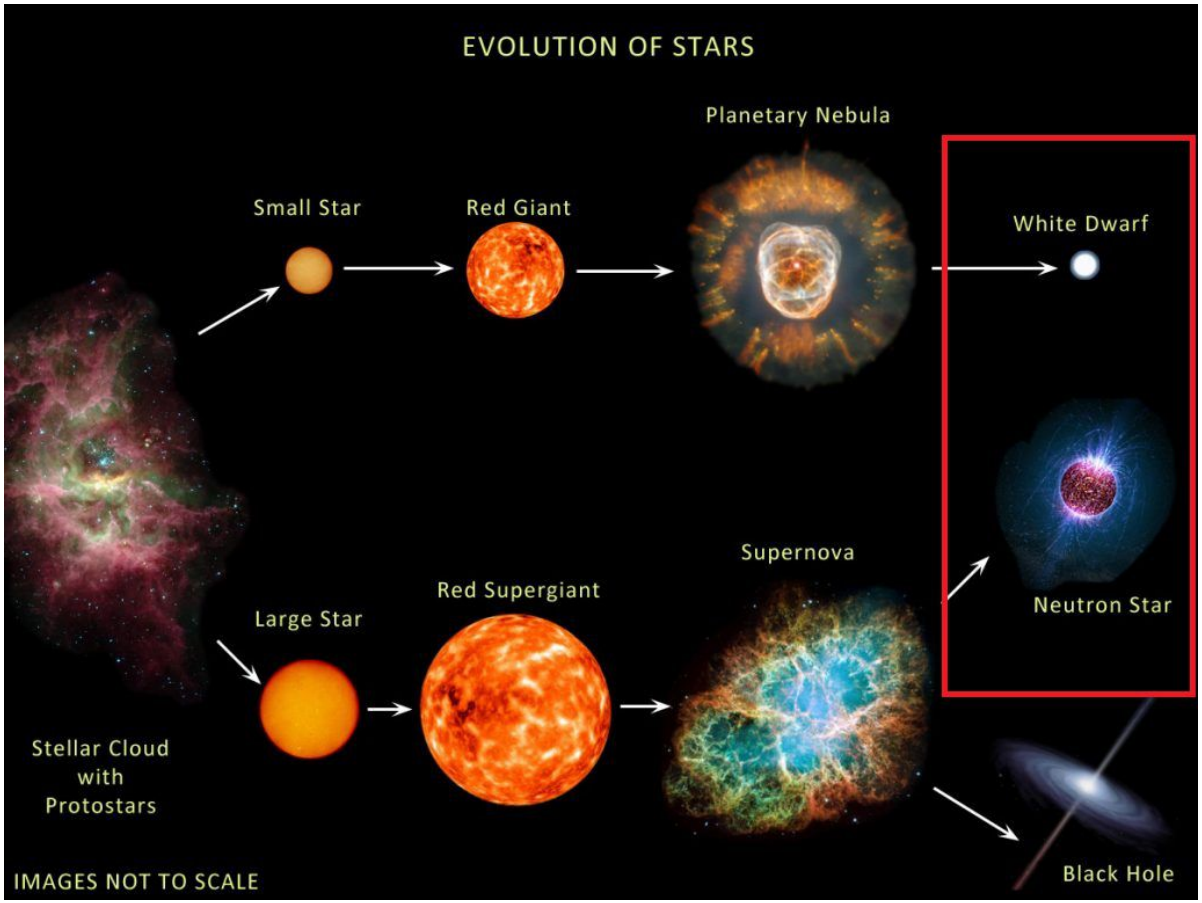

Neutron stars and white dwarfs

- $R_{NS} \sim 10$ km, $M_{NS} \sim 1.45\ \mathrm{M}_\odot$, $C = M_{NS}/R_{NS} \sim 0.1$, $\rho_{NS} \sim 10^{14}$ g/cm^3
- $R_{WD} \sim 0.12 R_\odot$, $M_{WD} \sim 0.6\ \mathrm{M}_\odot$, $C = M_{WD}/R_{WD} \sim 10^{-5}$, $\rho_{WD} \sim 10^5 - 10^7$ g/cm^3
- $R_\odot = 6.95\ 10^5$ km, $M_\odot = 1.989\ 10^{30}$ kg, $C = \frac{M_\odot}{R_\odot} \sim 10^{-6}$, $\rho_\odot \sim 1.6\ 10^2$ g/cm^3

White Dwarf

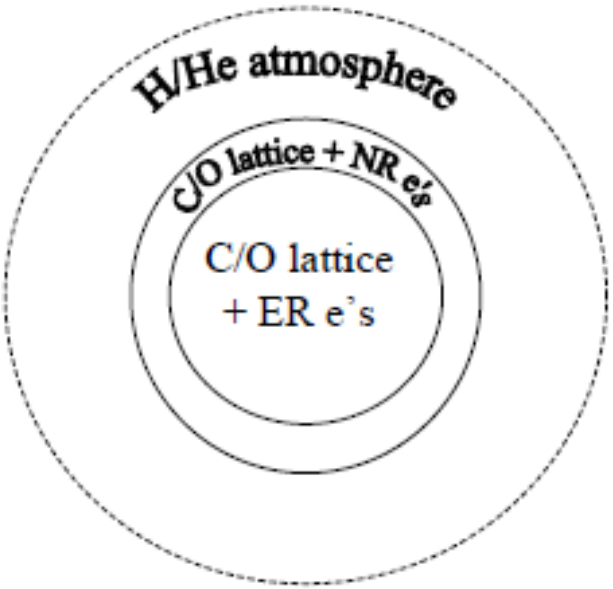

Neutron Star

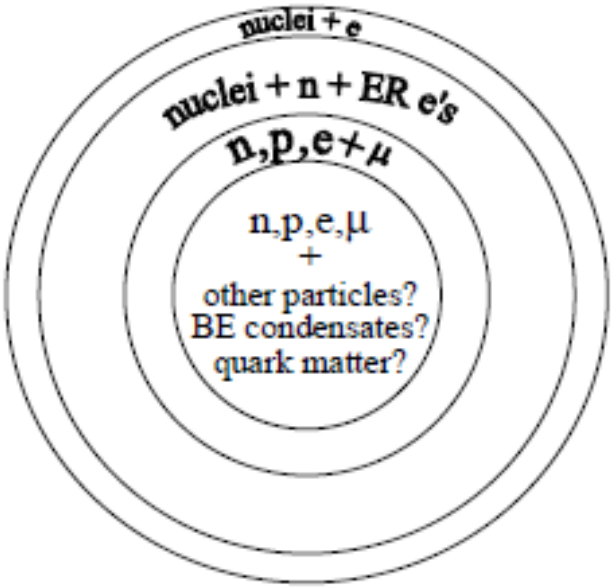

Neutron stars and white dwarfs

- WD internal temperatures $T \sim 0.1 - 1$ keV and surface temperatures $T_s \sim 10^{-5} - 10^{-4}$ keV
- NSs are born in supernova explosions with $T \sim 10$ MeV, after $t \sim 10$ s become transparent for ν's generated in their interior and cool by emitting them achieving $T \sim 1$ keV in $t \sim 10^6$ yrs

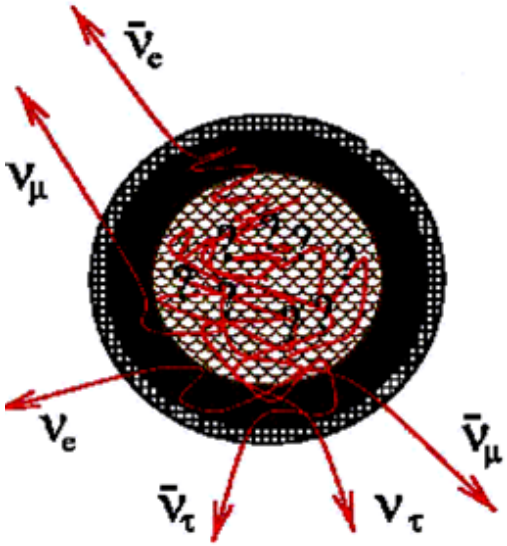

- WD interior, supported by degenerate e^- pressure, can be described by a polytropic equation of state (EoS) $P = K\rho^{1+\frac{1}{n}}$

  $n = \frac{3}{2}$ for $\rho_c \ll 10^6$ g/cm^3 (non relativistic e^-)

  $n = 3$ for $\rho_c \gg 10^6$ g/cm^3 (relativistic e^-)

- Vast number of EoS for NSs depending on different compositions of inner cores

DM accretion in dense stars

- The distribution of NSs in the MW peaks at $\langle r \rangle \lesssim 4$ kpc, where $\rho_\chi \sim 30\, \rho_{\chi,0}^{ambient}$, some globular clusters (GCs) with a core DM density $\rho_\chi \sim 100\ \mathrm{GeV/cm^3}$
  Lorimer et al., MNRAS 372 (2006) 777, G. Bertone, M. Fairbairn, PRD 77 (2008) 043515, M. McCullough, M. Fairbairn, PRD 81 (2010) 083520
- Capture rate, *Gould, ApJ 321 (1987) 571, Güver et al., JCAP 05 (2014) 03*

$$\Gamma_{\mathrm{capt}} = \frac{8}{3}\pi^2 \frac{\rho_\chi}{m_\chi} \frac{GMR}{1 - \frac{2GM}{R}} \bar{v}^2 \left(\frac{3}{2\pi \bar{v}^2} \right)^{\frac{3}{2}} f$$

- $\bar{v}$ is the average χ velocity in the existing DM distribution at the star location
- $f \sim 1$ for $\sigma_{\chi,i} \gtrsim \sigma_0$, with $\sigma_{\chi,i}$ the DM-i-th type SM particle cross section and $\sigma_0 = \frac{\pi m_i R^2}{M}$ the geometrical cross section
- In WDs DM particles are captured due to their interaction with C and O nuclei, $\sigma_{\chi,A} \gtrsim \sigma_0 \Rightarrow \sigma_{\chi,N} \gtrsim 10^{-39}\ \mathrm{cm^2} \Rightarrow$ efficient capture. If $\sigma_{\chi,A} < \sigma_0, f \sim \frac{\sigma_{\chi,A}}{\sigma_0}$
  Bramante, PRL 115 (2015) 141301
- For the NS case, capture due to DM-nucleon interaction ($90\,\%$ neutrons, $10\,\%$ protons), $\sigma_{\chi,N} \gtrsim \sigma_0 \sim 10^{-45}\mathrm{cm^2} \Rightarrow$ efficient capture. If $\sigma_{\chi,N} < \sigma_0, f \sim 0.45 \frac{\sigma_{\chi,N}}{\sigma_0}$
  Güver et al., JCAP 05 (2014) 03

DM accretion in dense stars

- The number of DM particles inside the star *Gaisser et al., PRD 34 (1986) 2206*

$$\frac{dN_\chi}{dt} = \Gamma_{\rm capt} - 2\Gamma_{\rm ann}$$

- $\Gamma_{\rm ann} = \frac{1}{2}\int d^3\vec{r}\, n_\chi^2(\vec{r})\langle\sigma_a v\rangle = \frac{1}{2}C_a N_\chi^2$
- $\langle\sigma_a v\rangle$ the averaged annihilation cross section over the initial DM states
- $n_\chi(\vec{r})$ the DM number density at the position $\vec{r}$ inside the star
- For $t > \tau_{\rm eq} = \frac{1}{\sqrt{\Gamma_{\rm capt} C_a}}$ DM is thermalized inside the star, and taking $\rho(r) \simeq \rho_c$,

$$n_\chi(\vec{r}) = n_{0,\chi} e^{-\left(\frac{r}{r_{\rm th}}\right)^2},$$

  with $n_{0,\chi}$ central DM density, $\int_0^R n_\chi(\vec{r}) d^3\vec{r} = N_\chi$
- Thermal radius $r_{th} = \sqrt{\frac{9T}{8\pi G\rho_c mx}}$
- For $t \gg \tau_{\rm eq}$, $N_\chi \sim \sqrt{\frac{\Gamma_{\rm capt}}{C_a}} \Rightarrow \Gamma_{\rm ann} = \frac{1}{2}\Gamma_{\rm capt}$

DM thermalisation in NSs

Garani, Genolili, Hambye, JCAP 05 (2019) 035

$$t_{th} \approx 10700 \text{ yrs } \frac{m_\chi/m_n}{(1+m_\chi/m_n)^2} \left(\frac{10^5 \text{ K}}{T}\right)^2 \left(\frac{10^{-45} \text{ cm}^2}{\sigma_\chi}\right)$$

More about thermalization in *Garani, Gupta, Raj, PRD 103 (2021) 043019*

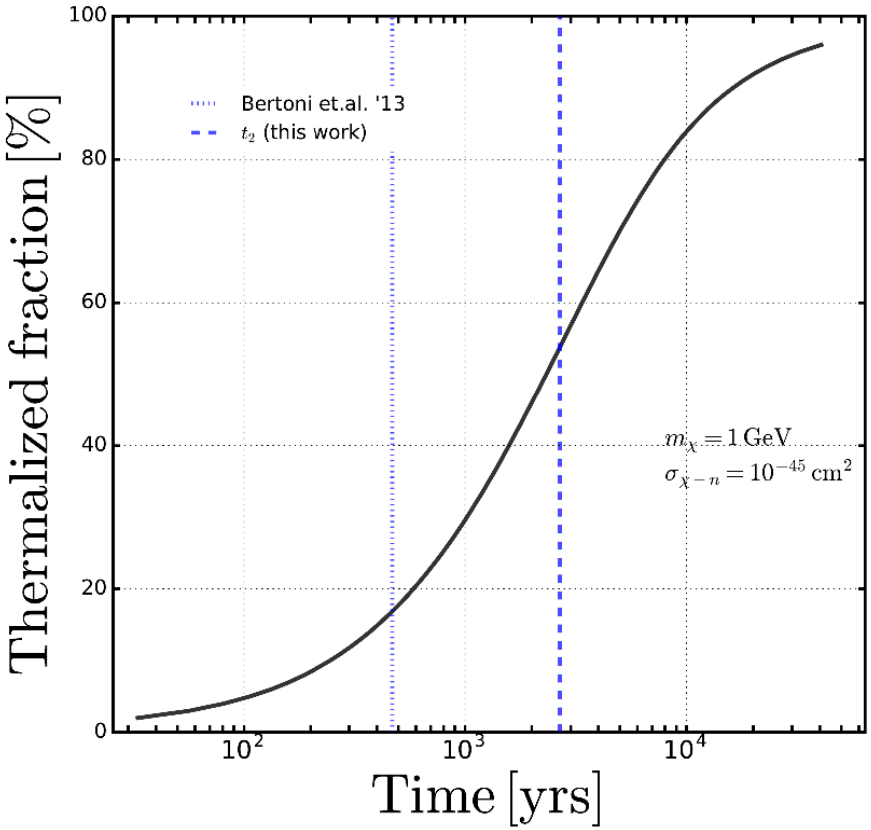

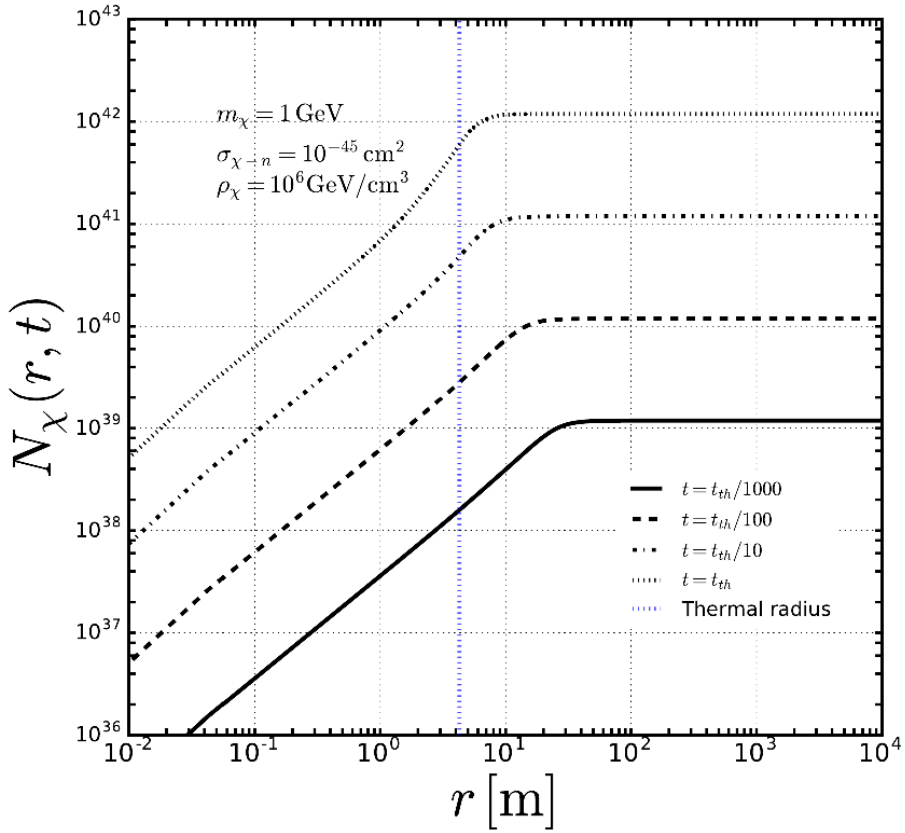

Figure 9: *Left:* Thermalized fraction $f = N_\chi^{th}/N_\chi^{tot}$ as a function of time for 1 GeV DM mass and $\sigma_{\chi-n} = 10^{-45}\,\text{cm}^2$. The vertical lines correspond to the times t_2 defined Eq. (42) (dashed line), and the discrete estimate from Ref. 30 (dotted line). *Right:* Evolution of number of DM particles within a sphere of radius r. The several times 't' considered are fractions of the thermalization time t_{th}.

DM inside NSs

- DM reaches the star at $v = \sqrt{\frac{2M_{NS}}{R_{NS}}} \sim 0.6$
- If capture is efficient $\sigma_{\chi,N} \gtrsim \sigma_0 \sim 10^{-45}\ \mathrm{cm}^2$, after $t \sim \tau_{eq}$ DM thermalizes, $v \sim \sqrt{\frac{T}{m_\chi}}$

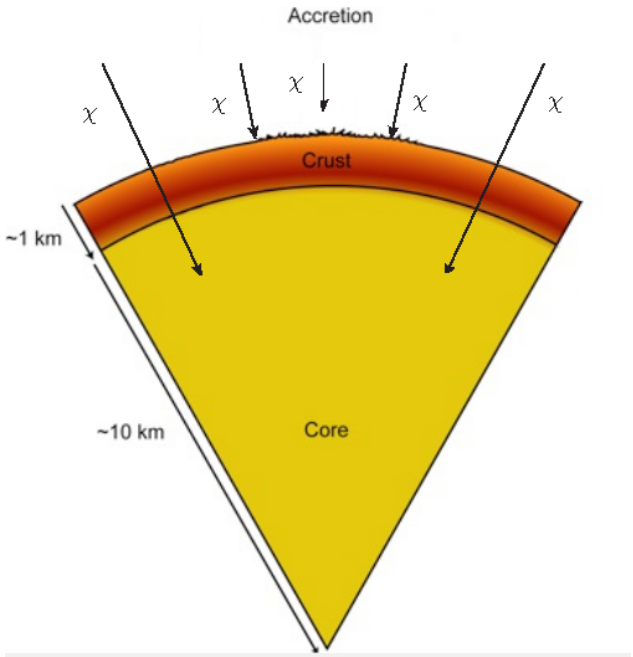

- Medium effects: density and temperature
  - Pauli blocking, Fermi Dirac distribution functions, $f_N(E) = \frac{1}{1+e^{(E-\mu_N^*)/T}}$, restrict the outgoing N phase space
  - Effective values for the chemical potential, μ_N^*, and for the nucleon mass m_N^* due to the presence of mesonic fields

    Serot and Walecka, Adv. Nucl. Phys. (1986)

Diffusion of DM in the NS core

- Fermionic LDM, $m_\chi \lesssim 1$ GeV, at $v \lesssim 0.6$ scatters off N's of the NS core
- Scalar and vector effective interactions

$$\mathcal{L}_\mathcal{I} = g_{Ns}\chi\overline{\chi}N\overline{N} + g_{Nv}\chi\gamma^\mu\overline{\chi}N\gamma_\mu\overline{N}$$

g_{Ns} and g_{Nv} scalar and vector χ−N couplings

$p = (E, \vec{p})$, $p' = (E', \vec{p'})$, $k = (\omega, \vec{k})$, $k' = (\omega', \vec{k'})$

$q = p' - p = k - k'$, $q_0 = E' - E = \omega - \omega'$

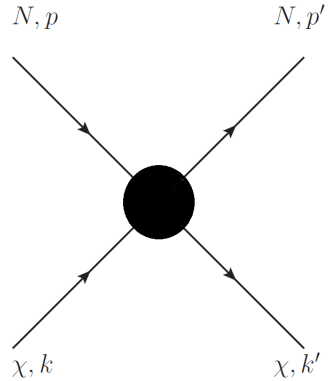

- The DM mean free path in the Sun or in the Earth can be estimated as $\lambda_\chi \simeq \frac{1}{\sigma_{\chi N} n}$, with n the baryonic number density
- Inside NSs medium effects have to be taken into account, $\lambda_\chi = \left(\frac{\sigma_{\chi N}}{V}\right)^{-1}$

  ***Cermeño**, Pérez-García and Silk PRD 94 (2016) 023509*

$$\lambda_\chi^{-1} = \frac{m_N^*}{4(2\pi)^3}\int_{q_{0,min}}^{\omega - m_\chi} dq_0 \int_{|\vec{k}|-|\vec{k'}|}^{|\vec{k}|+|\vec{k'}|} d|\vec{q}| \int_{|\vec{p}_-|}^{\infty} d|\vec{p}| \frac{|\overline{\mathcal{M}}_\mathcal{N}|^2 |\vec{p}| f_N(E)(1 - f_N(E'))}{4E'|\vec{k}|\sqrt{E^2\omega^2 - m_N^{*2}m_\chi^2}}$$

- Limits: $|\vec{p}_-| = \frac{m_N^*}{|\vec{q}|}\left(q_0 - \frac{|\vec{q}|^2}{2m_N^*}\right)$, $q_{0,min} = 0$ for $T = 0$ and $q_{0,min} = -\infty$ for $T \neq 0$

Diffusion of DM in the NS core

- NS core density $n \lesssim 2n_{sat}$, $n_{sat} = 0.17\ \text{fm}^{-3}$
- For evolved NSs $T \sim 1\ \text{keV} \ll E_F \Rightarrow T \sim 0$
- We take $g_{Ns} \sim 10^{-15}\ \text{MeV}^{-2}$, $g_{Nv} \sim 10^{-12}\ \text{MeV}^{-2}$

***Cermeño**, Pérez-García and Silk PRD 94 (2016) 023509*

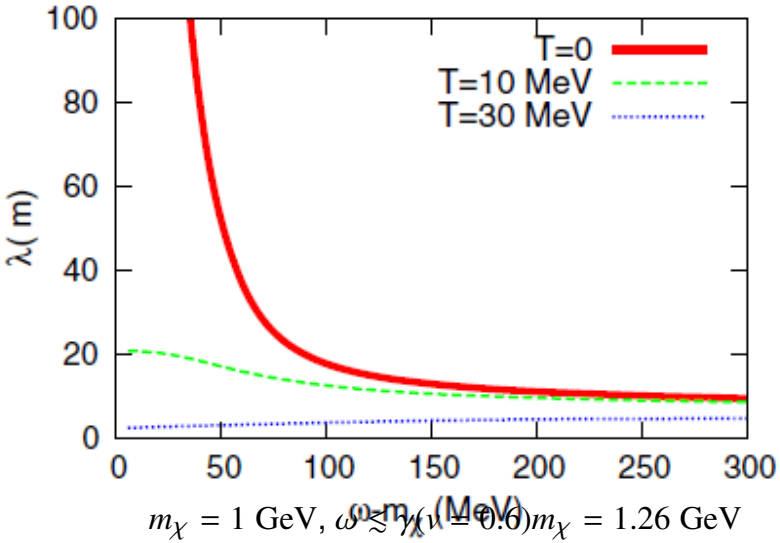

$m_\chi = 1$ GeV, $\omega \lesssim m_\chi (v = 0.6) m_\chi = 1.26$ GeV

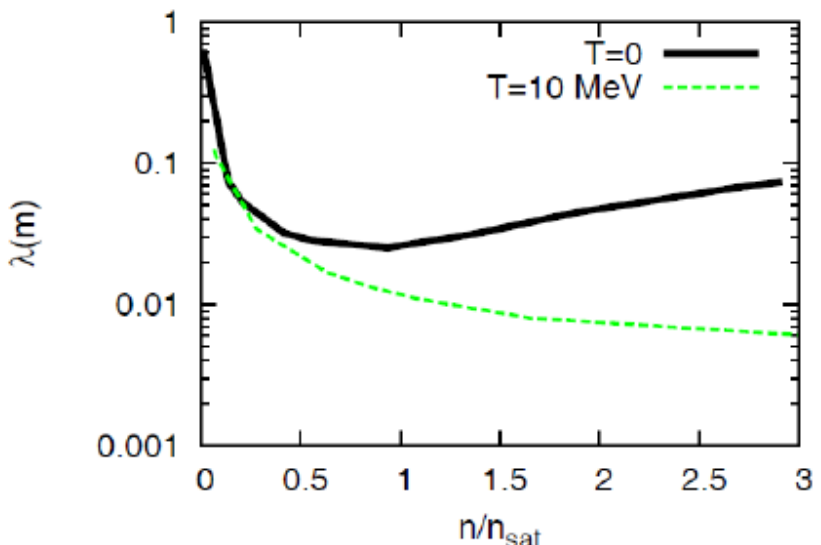

$m_\chi = 1$ GeV, $\omega = 1.26$ GeV ($v = 0.6$)

$\mu_N^* = E_F = \frac{(3\pi^2 n)^{\frac{2}{3}}}{2m_N^*}$, $m_N^* = 0.7 m_N$, $n(T = 0) = n_{sat}$, $n\,(T = 10\ \text{MeV}) = 0.174\ \text{fm}^{-3}$

$n\,(T = 30\ \text{MeV}) = 0.209\ \text{MeV}$

effective (nude) nucleon mass for $T = 0$ ($T \neq 0$)

$\lambda \ll R_{NS} \Rightarrow$ Diffusive scattering

DM interaction in the NS outer crust

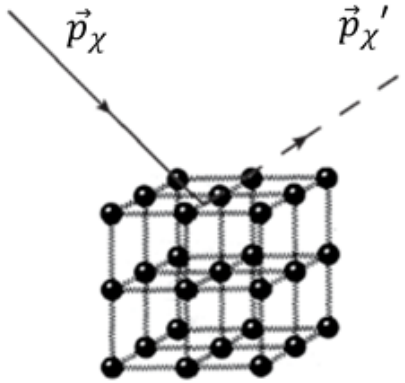

- Fermionic LDM, $m_\chi \lesssim 500$ MeV, scatters off (scalar and vector interaction) nuclei A of the NS outer crust, $\rho \simeq 2\,10^6 - 4\,10^{11}\,\mathrm{g/cm^3}$
- Scattering $\chi - A$ in the lattice $\Rightarrow$ phonon excitation
- Acoustic phonons ($\omega_k \lesssim 3$ MeV *Di Gallo et al., PRC 84 (2011) 045801*), linear dispersion relation $\omega_k = c_l|\vec{k}|$, with $\vec{k}$ the phonon momentum and c_l the sound speed
- BCC lattice, $c_l = \frac{T_p/3}{(6\pi^2 n_A)}$ with $T_p = \sqrt{\frac{4\pi n_A Z^2 e^2}{m_A}}$ the plasma temperature associated to a medium of ions with number density n_A, baryonic number A and electric charge Ze

  W. J. Carr, Phys. Rev. 122, 1437 (1961)
- $T_U < T < T_D$, $T_U \simeq 0.07 T_D$ minimum temperature for which the approximation of free electrons holds and $T_D \simeq 0.45 T_p$ the Debye temperature

  Ziman, Electrons and Phonons (1960)

Phonon excitation rate

- Acoustic phonon excitation rate $R^{(0)}_{\vec{k}} = 2\pi\delta(E_f - E_i)|\langle f|\mathcal{V}|i\rangle|^2$
- $\mathcal{V}(\vec{r}) = \sum_j \delta^3(\vec{r} - \vec{r_j})\ \frac{2\pi a}{m_\chi}$ interaction potential, a scattering length
- $\sigma_{\chi A} \simeq 4\pi a^2$ in the CM frame using the Born approximation, $|(\vec{p_\chi} - \vec{p'_\chi}).\vec{r'}| \ll 1$, with $|\vec{r'}|$ typical target size
- $\frac{d\sigma_{\chi,A}}{d\Omega} = \frac{|\overline{\mathcal{M}}_{\chi A}|^2}{64\pi^2(p_A+p_\chi)^2} \Rightarrow \sigma_{\chi,A} \simeq \frac{m_A^2\left(\frac{Z}{m_p}\sqrt{|\tilde{\mathcal{M}}_p|^2}+\frac{(A-Z)}{m_n}\sqrt{|\tilde{\mathcal{M}}_n|^2}\right)^2}{64\pi^2(m_A+m_\chi)^2}$,
  with $|\tilde{\mathcal{M}}_N|^2 \equiv \int_{-1}^{1} 2\pi d(cos\ \theta_\chi)|\overline{\mathcal{M}}_{\chi\mathcal{N}}|^2$
- The acoustic phonon excitation rate per unit volume

  ***Cermeño**, Pérez-García and Silk PRD 94 (2016) 063001*

$$R^{(0)}_k = \frac{8\pi^4 n_A^2}{(2\pi)^6 m_\chi^2 m_A c_l}\int_0^\infty |\vec{p_\chi}|d|\vec{p_\chi}|f_\chi(\vec{p_\chi})a^2|E_\chi - |\vec{k}|c_l|, \text{con}\ \ E_\chi \gg |\vec{k}|c_l$$

- $f_\chi(\vec{p_\chi}) = \frac{n_\chi}{4\pi T m_\chi^2 K_2(\frac{m_\chi}{T})} e^{-\frac{m_\chi}{T}\sqrt{1+\frac{|\vec{p_\chi}|^2}{m_\chi^2}}}$ Maxwell-Jüttner distribution function for relativistic incoming DM, $n_\chi = \rho_\chi/m_\chi$ the local DM density and $K_2(\frac{m_\chi}{T})$ the modified Bessel function of second kind

Phonon excitation rate

***Cermeño**, Pérez-García and Silk PRD 94 (2016) 063001*

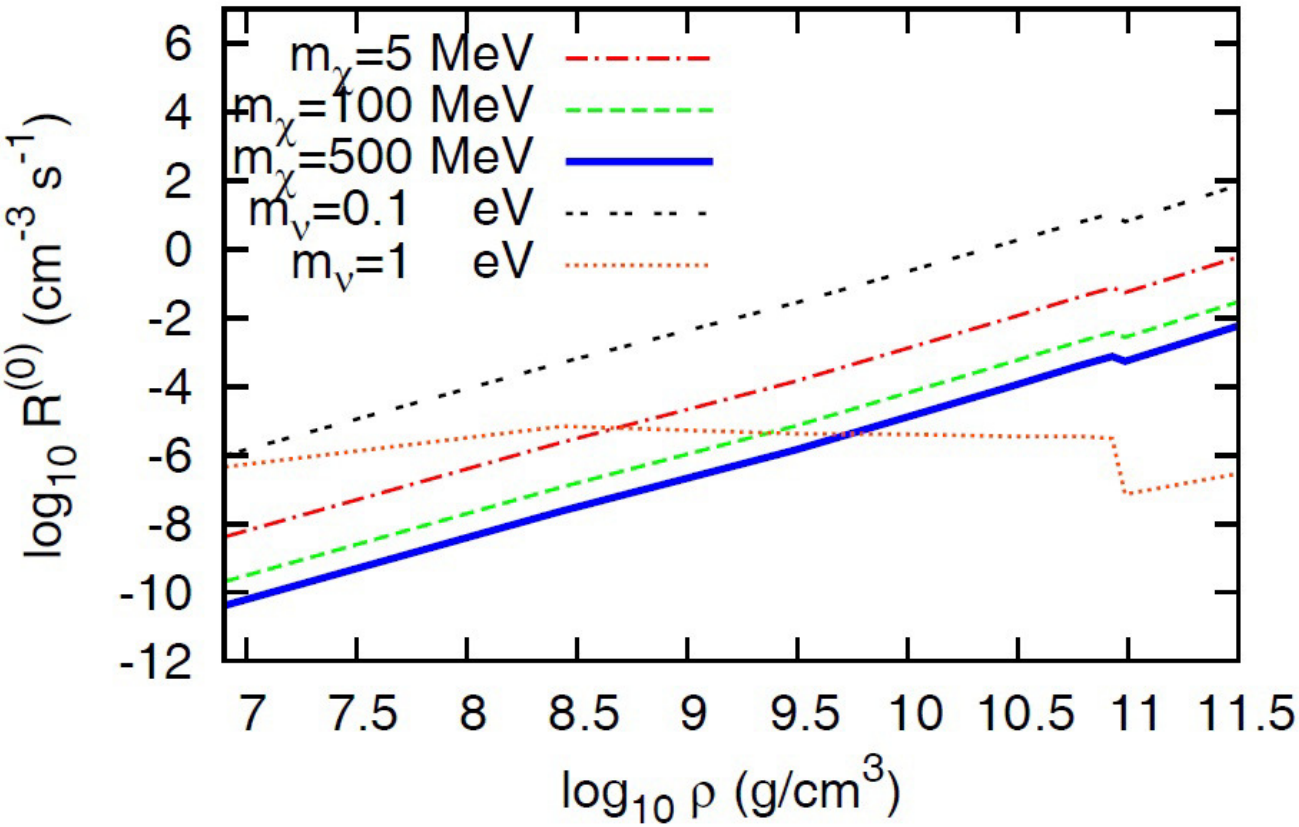

$m_\chi = 500, 100$ and 5 MeV, $\rho_\chi / \rho_{\chi,0}^{ambient} = 10$.

Neutrino contribution at $|\vec{k}| \to 0$, $R_{\nu 0}$, is also shown for $m_\nu = 0.1, 1$ eV, with $R_\nu^{(0)}(\vec{k}) = R_{\nu 0} e^{\frac{-b|\vec{k}|}{1\text{eV}}}$ and b a constant value which depends on the neutrino mass

Impact on thermal conductivity

- Total thermal conductivity $\kappa = \kappa_e + \kappa_i$, $\kappa_i^{-1} = \kappa_{ii}^{-1} + \kappa_{ie}^{-1}$
- $\kappa_{ii} \equiv \kappa_{ph} = \frac{1}{3} C_A n_A c_l L_{ph}$ and κ_{ie} are the phonon-phonon and phonon-electron partial conductivities *Ziman, Electrons and Phonons (1960)*
- C_A the heat capacity *per ion* (dimensionless) due to phonons
- At temperature T the phonon mean free path $L_{ph} \propto 1/N_{0,k}$, $N_{0,k} = (e^{\omega_k/T} - 1)^{-1}$, with a proportional factor which depends on the lattice properties
- The net number of phonons N_k that results from the competition of thermal and scattering excitation and stimulated emission

  ***Cermeño**, Pérez-García and Silk PRD 94 (2016) 063001*

$$N_k \simeq N_{0,k} + R_k^{(0)} \delta V \delta t - \int \frac{d^3\vec{p}}{n_\chi} f_\chi(\vec{p}) \tilde{R}_k^{(0)} N_{0,k} e^{\frac{\omega_k + \vec{k}.\vec{v}}{(\gamma(\vec{p_\chi})-1)m_\chi}} \delta V \delta t$$

where $\tilde{R}_k^{(0)}$ is the single phonon excitation rate for each particular momentum value, $\gamma(\vec{p_\chi}) = \frac{1}{\sqrt{1-\left(\frac{|\vec{p_\chi}|}{E_\chi}\right)^2}}$ Lorentz factor and $v \sim 10^{-2}$ the NS galactic drift velocity

Ion-ion thermal conductivity

***Cermeño**, Pérez-García and Silk PRD 94 (2016) 063001*

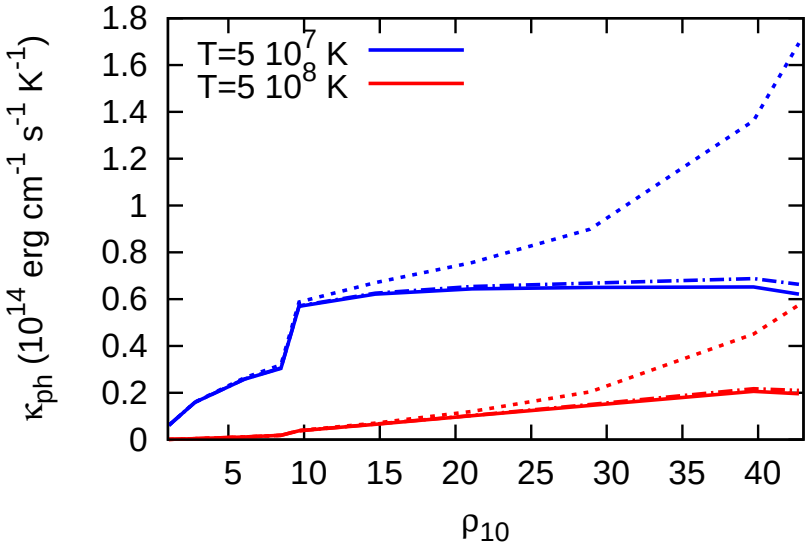

$m_\chi = 100$ MeV. Solid, dash-dotted and dashed lines depict the cases with no DM and with LDM for $\rho_\chi/\rho_{\chi,0}^{ambient} = 10, 100$.

We fix $|\vec{k}| = \frac{0.01}{a_i}$, $a_i = (4\pi n_A/3)^{\frac{1}{3}}$.

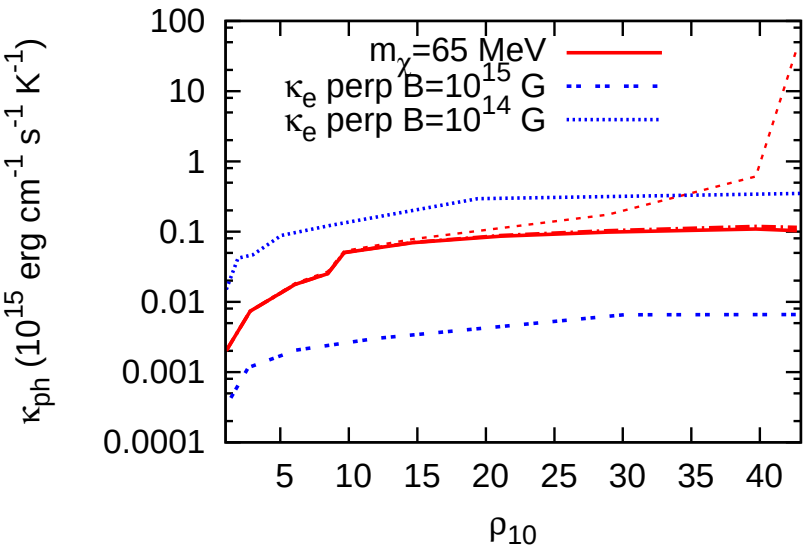

$T = 10^8$ K and $m_\chi = 65$ MeV.Solid, dash-dotted and dashed lines depict the cases with no DM and with LDM for $\rho_\chi/\rho_{\chi,0}^{ambient} = 10,\ 100$. We fix $|\vec{k}| = \frac{0.01}{a_i}$.

Secluded DM annihilation inside NSs

- Fermionic DM interacts with the SM sector through a pseudoscalar mediator a

  C. Boehm et al., JCAP 1405 (2014) 009; M. J. Dolan et al., JHEP 1503 (2015) 171; C. Arina et al., PRL 114 (2015) 011301

$$\mathcal{L}_I = -i\frac{g_\chi}{\sqrt{2}} a\bar{\chi}\gamma_5\chi - ig_0\frac{g_f}{\sqrt{2}} a\bar{f}\gamma_5 f$$

g_χ DM-mediator coupling

g_f SM fermions and mediator coupling

$g_f = 1$ flavor-universal model, g_0 scaling factor

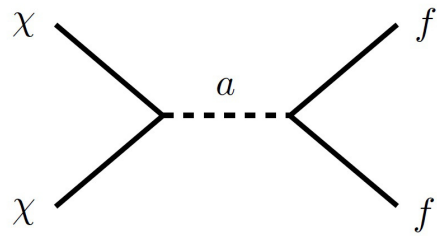

- For $m_\chi < m_{\text{Higgs}}$, $m_a < m_\chi$, the main annihilation channels

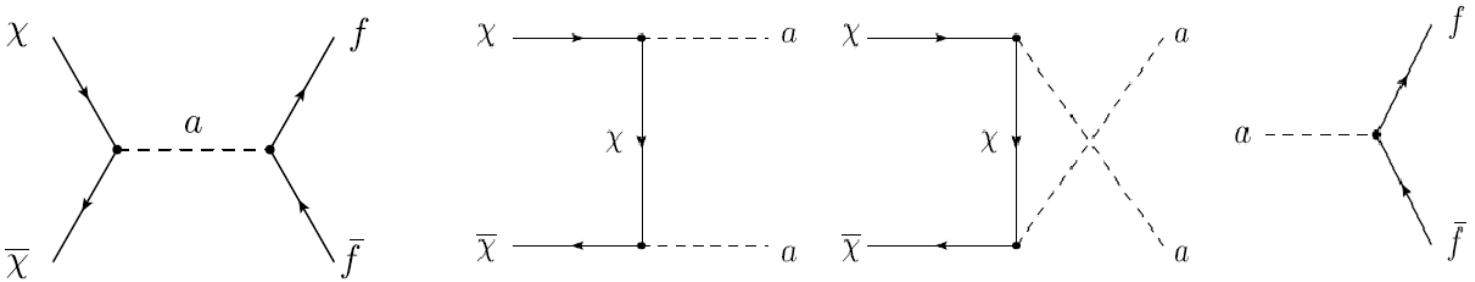

Neutrino local energy emissivity

- Energy emissivity $Q_E = \frac{dE}{dVdt} = 4 \int d\Phi (E_1 + E_2) \, |\overline{\mathcal{M}}|^2 \, f(f_1, f_2, f_3, f_4)$
- $d\Phi = \frac{d^3p_1}{2(2\pi)^3 E_1} \frac{d^3p_2}{2(2\pi)^3 E_2} \frac{d^3p_3}{2(2\pi)^3 E_3} \frac{d^3p_4}{2(2\pi)^3 E_4} (2\pi)^4 \delta^4(p_1 + p_2 - p_3 - p_4)$
- For $\chi\chi \to f\bar{f}$, $\quad f(f_1, f_2, f_3, f_4) = f_\chi(E_1) f_{\bar{\chi}}(E_2)(1 - f_f(E_3))(1 - f_{\bar{f}}(E_4))$
- For $\chi\chi \to aa$, $\quad f(f_1, f_2, f_3, f_4) = f_\chi(E_1) f_{\bar{\chi}}(E_2) f_a(E_3) f_a(E_4)$
- f_χ, f_f and f_a are the local stellar distribution functions for DM, fermionic and pseudoscalar particles

- $f_\chi = \left(\frac{1}{2\pi m_\chi T} \right)^{\frac{3}{2}} n_\chi(r) e^{\frac{-|\vec{p_i}|^2}{2m_\chi T}}$ for DM thermalized inside the NS
- We restrict our final states to $\nu's$
- As standard ν's do not get trapped $f_\nu \sim 0$
- We take $f_a \sim 1$ for simplicity

Neutrino local energy emissivity

Model	m_χ [GeV]	m_a [GeV]	g_χ	g_0
A	0.1	0.05	7.5×10^{-3}	7.5×10^{-3}
B	1	0.05	1.2×10^{-1}	2×10^{-3}
C	30	1	6×10^{-1}	5×10^{-5}

***Cermeño**, Pérez-García and Lineros, ApJ 863 (2018) 157*

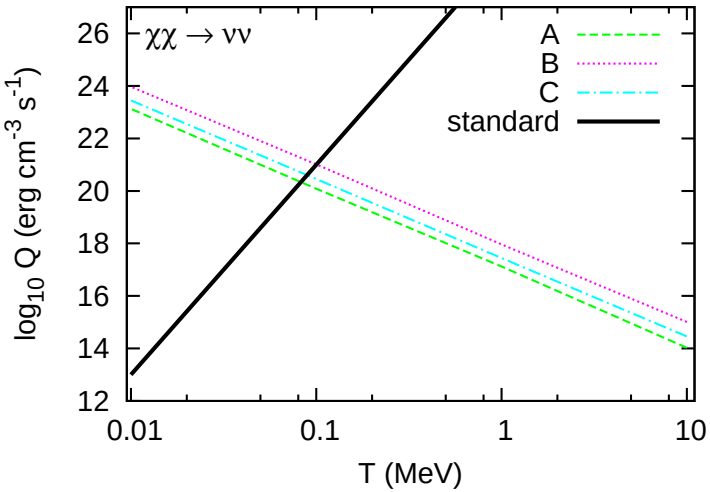

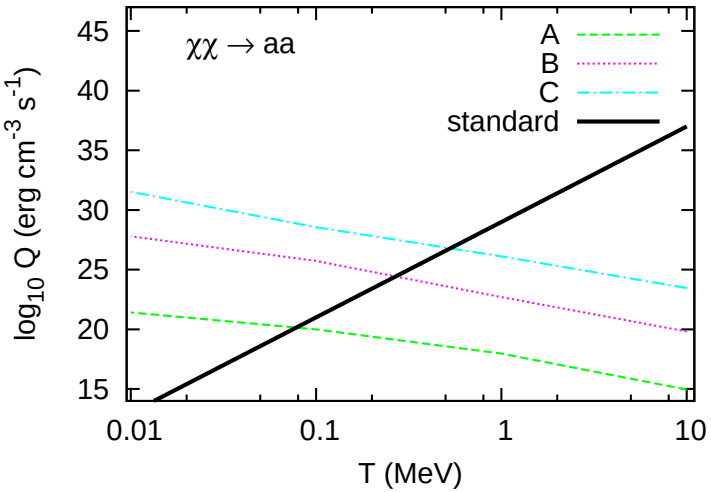

$$Q_E(T, N_\chi) = Q_0 \left(\frac{N_\chi}{N_{0,\chi}}\right)^2 \left(\frac{T}{1\ \mathrm{MeV}}\right)^{-3}$$

$$N_{\chi,0} = 1.5 \times 10^{39} \left(\frac{\rho_\chi}{\rho_{\chi,0}^{ambient}}\right)\left(\frac{1\ \mathrm{GeV}}{m_\chi}\right)\left(\frac{\sigma_{\chi,N}}{10^{-43}\ \mathrm{cm}^2}\right)$$

Kouvaris and Tinyakov, PRD (2010) 82

Localized emission in $\lesssim 7\,\%$ of the total stellar volume for $T \lesssim 10^{10}$ K

$Q_E(T, N_\chi) > Q_{MURCA}$ for $T \in [0.01, 0.1]$ MeV during the NS entire lifetime for model C

Secluded DM annihilation inside WDs

- Less dense objects and more experimental data, stellar magnitudes and distances of the WDs in the M4 GC

  L. R. Bedin et al., ApJ 697 (2009) 965, M. McCullough, M. Fairbairn, Phys. Rev. D 81, 083520

- Mostly model independent framework, no asumption about the type of coupling
- LDM, $m_\chi \lesssim 500$ MeV, interaction with the SM through a metastable mediator Y
- $m_Y \lesssim m_\chi$
- SIMPs $10^{-40}\ \mathrm{cm}^2 \lesssim \sigma_{\chi,N} \lesssim 10^{-34}\ \mathrm{cm}^2$, $\sigma_{\chi,A} = A^2\sigma_{\chi,N}$
- Main annihilation channel $\chi\bar{\chi} \to YY$, $Y \to \gamma\gamma$
- Indirect signals will depend on the Y lifetime, $\tau = \gamma_Y \tau_{rest}$, $\gamma_Y = \frac{1}{\sqrt{1-v_Y^2}}$ Lorentz factor and $\tau_{rest} \lesssim 1$ s lifetime at rest
- $t_{\mathrm{age}} \sim 10^9$ years $\gg \tau_{\mathrm{eq}} \Rightarrow \Gamma_{\mathrm{ann}} = \frac{\Gamma_{\mathrm{capt}}}{2}$
- DM thermalized inside the WD annihilates into Y's which may interact with nuclei, $\sigma_{Y,A} = A^2\sigma_{Y,N}$, with a mean free path $\lambda_{int} \sim \frac{1}{\sigma_{Y,A} n_A}$

Mediator attenuation inside the WD

- If $\tau > \lambda_{int}$, Y energy losses. Initially, $p_{Y,0} = \sqrt{m_\chi^2 - m_Y^2}$, after one interaction $p_Y = q p_{Y,0}$, $0 < q < 1$
- Continuous energy losses $\Rightarrow p_Y(r) = \sqrt{m_\chi^2 - m_Y^2}\, e^{\frac{-(1-q)A\sigma_{Y,N}\rho_c}{m_N} \int_0^r \omega(r')^{\frac{3}{2}} dr'}$
- $\omega(r)$ the approximated analytic solution of the Lane-Emden equation for a polytrope with $n = \frac{3}{2}$, accurate to $1\,\%$ to the numerical one *Liu, MNRAS 281 (1996) 1197*

***Cermeño** and Pérez-García, PRD 98 (2018) 063002*

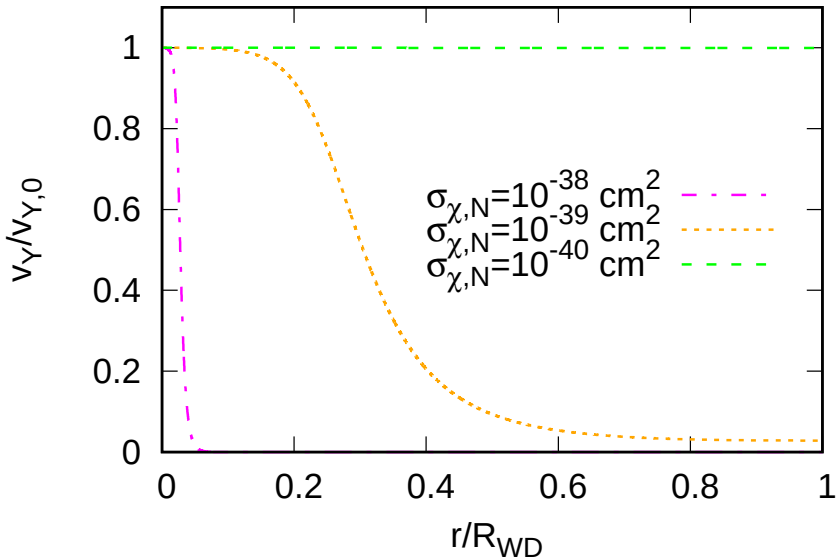

$m_\chi = 0.5$ GeV, $m_Y = 0.01$ GeV, $\sigma_{\chi,N} = \sigma_{Y,N}$,
$\rho_c = 3.78\ 10^6$ g/cm^3, $M = 0.95 M_\odot$

Internal luminosity

- Internal luminosity, ***Cermeño*** *and Pérez-García, PRD 98 (2018) 063002*

$$L_\chi = \Gamma_{\rm ann} \int_0^R N\, e^{-\int_0^r \frac{m_Y dr'}{\tau_{\rm rest} E_Y(r')}} \int_{E_-(r)}^{E_+(r)} E_\gamma \frac{dN_\gamma(r)}{dE_\gamma} dE_\gamma dr$$

- Decay probability density

$$\frac{dP_{\rm dec}}{dr} = N\, e^{-\int_0^r \frac{m_Y dr'}{\tau_{\rm rest} E_Y(r')}}, \quad N\left(\int_0^R e^{-\int_0^r \frac{m_Y dr'}{\tau_{\rm rest} E_Y(r')}} dr + \int_R^\infty e^{-\int_0^r \frac{m_Y dr'}{\tau_{\rm rest} E_Y(R)}} dr\right) = 1$$

- $\frac{dN_\gamma}{dE_\gamma} = \frac{4}{\Delta E}\Theta(E_\gamma - E_-)\Theta(E_+ - E_\gamma)$, $\Delta E = E_+ - E_-$ and $E_\pm = \frac{1}{\gamma_Y(r)}\frac{m_Y}{2}(1 \mp v_Y(r))^{-1}$
- $v_Y(r) \to 0 \Rightarrow \gamma_Y(r) \to 1$, $E_- \to E_+$ and $\Delta E \to 0$

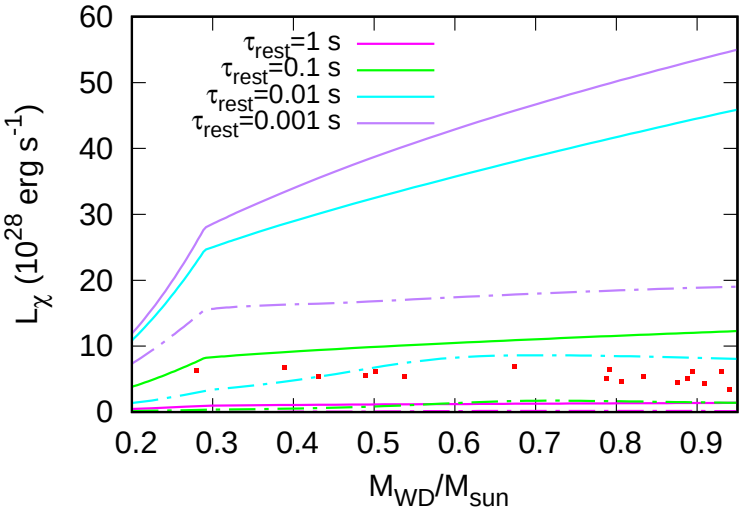

Cermeño *and Pérez-García, PRD 98 (2018) 063002*

$m_\chi = 0.5$ GeV, $\sigma_{\chi,N} = \sigma_{Y,N} = 10^{-39}$ cm^2, $q = 0.5$

solid lines $m_Y = 0.375$ GeV,

dashed lines $m_Y = 0.01$ GeV

red points L_{exp} in the M4 GC from
M. McCullough and M. Fairbairn, PRD 81 (2010) 083520

Internal luminosity and constraints

- If $L_\chi > 1.5 L_{exp}$ for all the experimental data ($50\,\%$ of tolerance)$\Rightarrow$ we exclude those points of the parameter of space
- The lower limit of τ_{rest}, $\tau_{\rm limit}$, depends on $\frac{m_Y}{m_\chi}$ in a different way depending on $\sigma_{\chi,N}$ and $\sigma_{Y,N}$, left plot
- For the most restrictive case $m_Y \sim m_\chi \Rightarrow$ excluded values of τ_{rest} as a function of $\sigma_{\chi,N}$, pink region of the rigth plot

Cermeño *and Pérez-García, PRD 98 (2018) 063002*

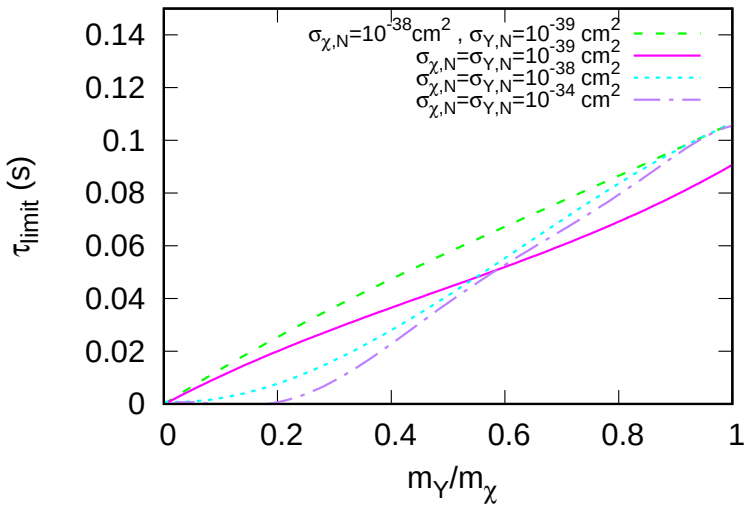

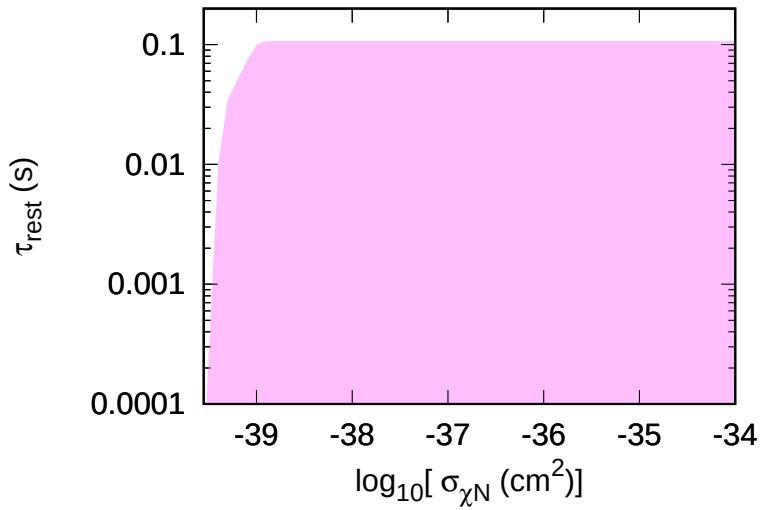

DM density in some active galactic nuclei

Adiabatic growth of a super-massive black hole in a region with an initial DM distribution $\rho^0_{\rm DM}(r) \propto \rho_0 \, (r/r_0)^{-\gamma} \Rightarrow$ **DM spike formation** *Gondolo, Silk, PRL 83 (1999) 1719*

$$\rho_{DM}(r) = \begin{cases} 0 & r < 4R_{\rm S} \\ \frac{\rho_{\rm sp}(r)\rho_{\rm sat}}{\rho_{\rm sp}(r)+\rho_{\rm sat}} & 4R_{\rm S} \leq r < R_{\rm sp} \\ \rho_0 \left(\frac{r}{r_0}\right)^{-\gamma} \left(1+\frac{r}{r_0}\right)^{-2} & r \geq R_{\rm sp} \end{cases},$$

- $R_S = 5 \times 10^{-6}$ pc the Schwarzschild radius
- $R_{sp} = \alpha_\gamma r_0 \left(\frac{M_{BH}}{\rho_0 r_0^3}\right)^{1/(3-\gamma)}$ the spike radius, with α_γ a normalization constant that depends on γ and can be obtained numerically
- The spike distribution

$$\rho_{\rm sp}(r) = \rho_R g_\gamma(r) \left(\frac{R_{\rm sp}}{r}\right)^{\gamma_{\rm sp}}, \quad \rho_R = \rho_0 \left(\frac{R_{\rm sp}}{r_0}\right)^{-\gamma}, \quad g_\gamma(r) \simeq \left(1 - \frac{4R_S}{r}\right)^3, \quad \gamma_{sp} = \frac{9-2\gamma}{4-\gamma}$$

- The maximum density allowed by DM annihilations, $\rho_{\rm sat} \simeq \frac{m_\chi}{\langle\sigma v\rangle t_{BH}}$, during $t_{\rm BH} \sim 10^{10}$ yr
- We take $\gamma = 1$, NFW profile for $r \geq R_{\rm sp}$ and $\gamma_{\rm sp} = 7/3$

DM density in Cen A

$$\rho_{DM}(r) = \begin{cases} 0 & r < 4R_S \\ \frac{\rho_{sp}(r)\rho_{sat}}{\rho_{sp}(r)+\rho_{sat}} & 4R_S \leq r < R_{sp} \\ \rho_0 \left(\frac{r}{r_0}\right)^{-1} \left(1+\frac{r}{r_0}\right)^{-2} & r \geq R_{sp} \end{cases},$$

$$\rho_{sp}(r) = \rho_0 \left(\frac{R_{sp}}{r_0}\right)^{-1} \left(1-\frac{4R_S}{r}\right)^3 \left(\frac{R_{sp}}{r}\right)^{7/3},$$

$$\rho_{sat} \simeq \frac{m_\chi}{\langle\sigma v\rangle t_{BH}}$$

with $R_S = 5\times10^{-6}$ pc, $r_0 = 20$ kpc, $\rho_0 \sim 1$ GeV/cm^3, $R_{sp} = 10^8 R_S$

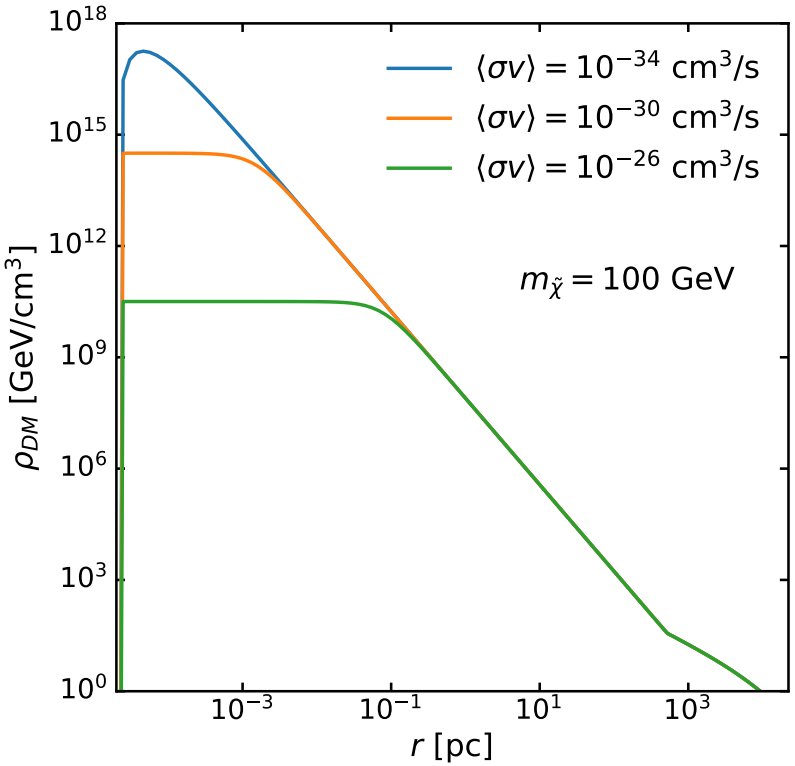

M. Cermeño, *C. Degrande, L. Mantani, PRD 105 (2022) 8, 083019, arXiv: 2201.07247*

The model

$$\mathcal{L}_{DM} = i\bar{\psi}_{\tilde{\chi}}(\not{D} - m_{\tilde{\chi}})\psi_{\tilde{\chi}} + D_\mu\varphi^\dagger D^\mu\varphi - m_\varphi\varphi^\dagger\varphi + (a_R\,\bar{e}_R\,\psi_{\tilde{\chi}}\,\varphi + h.c.)\,.$$

Bringmann et al., JCAP 07 (2012) 054, Garny et al., JCAP 12 (2013) 640, Kopp, Michaels, Smirnov, JCAP 04 (2014) 022, Okada, Toma, PLB 750 (2015) 266, Garny, Ibarra, Vogl, Int.J.Mod.Phys.D 24 (2015) 07, 1530019

$\tilde{\chi}$ Majorana fermion, φ charged scalar mediator, e_R right-handed electrons

- $m_\varphi \gtrsim m_{\tilde{\chi}}$ and $\Delta M = m_\varphi - m_{\tilde{\chi}} \ll m_\varphi, m_{\tilde{\chi}}$
- $\tilde{\chi}\tilde{\chi} \to e^+e^-$ velocity suppressed
- Relevant annihilation channels $\tilde{\chi}\tilde{\chi} \to \gamma\gamma, \tilde{\chi}\tilde{\chi} \to e^-e^+\gamma \Rightarrow$ line-like signatures
- Resonantly enhanced DM scattering off electrons in the AGN jet

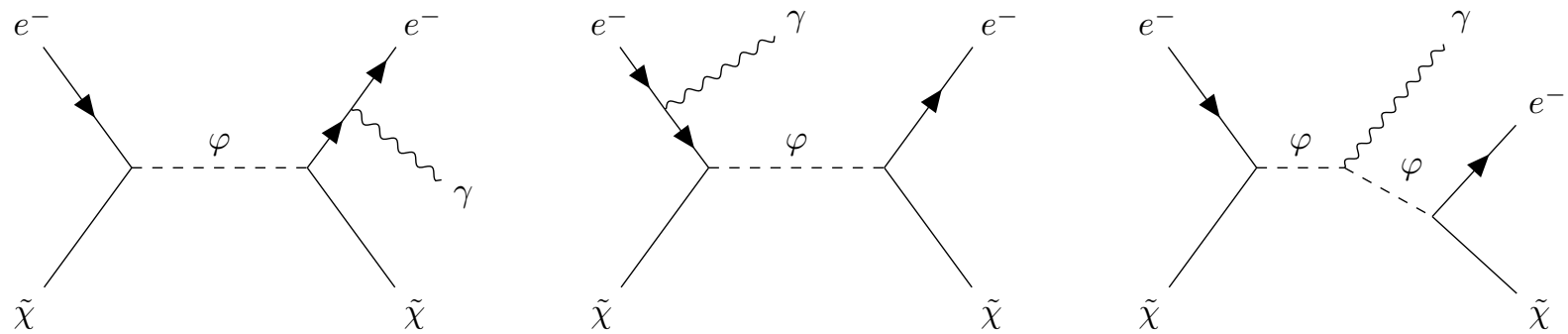

Circular polarised photons

- A net circular polarisation signal is generated when there is an excess of one photon polarisation state over the other
- Parity must be violated in at least one of the dominant photon emission processes

$$\mathcal{A}_- \neq \mathcal{A}_+$$

$$\mathcal{A}_\pm = \sum_{spins} |\epsilon^\mu_\pm \mathcal{M}_\mu|^2$$

$$\epsilon^\mu_\pm(k) = \frac{1}{2}(\mp\epsilon^\mu_1(k) - i\epsilon^\mu_2(k))$$

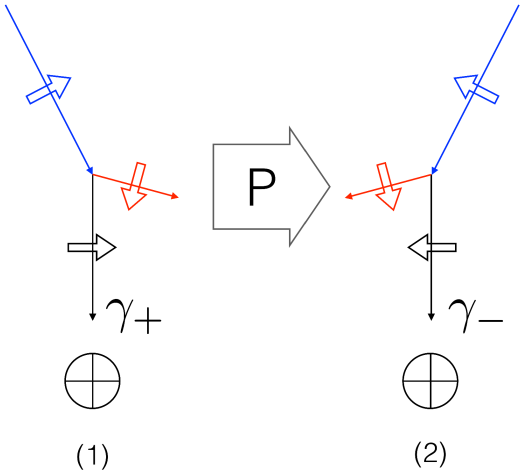

Boehm et al., JCAP 05 (2017) 043

- There must be an asymmetry in the number density of one of the particles in the initial state or CP must be violated
- A P violating interaction like $e^-\tilde{\chi} \to e^-\tilde{\chi}\gamma$ in a region with an abundance of electrons over positrons → circularly polarised photons *Boehm et al. JCAP 05 (2017) 043*
  The circular polarisation asymmetry can reach $90\,\%$ for interactions in the GC
  M. Cermeño, *C. Degrande, L. Mantani, Phys.Dark Univ. 34 (2021) 100909*
- No net polarisation from $\tilde{\chi}\tilde{\chi} \to e^-e^+\gamma$, initial state is a CP-eigenstate

Circular polarised photon flux from Cen A

The flux of circularly polarised photons from $e^-\tilde{\chi} \to e^-\tilde{\chi}\,\gamma_\pm$ at $d_{\rm AGN} \sim 3.8$ Mpc

M. Cermeño, *C. Degrande, L. Mantani, PRD 105 (2022) 8, 083019, arXiv: 2201.07247*

$$\frac{d\Phi_{\gamma,pol}}{dE_\gamma} = \frac{1}{d^2_{AGN}} \frac{\delta_{DM}}{m_\chi} \int dE_e \frac{d\Phi_e^{AGN}}{dE_e} \left| \frac{d^2\sigma_+}{dE_\gamma d\Omega_\gamma}(E_e, E_\gamma, \theta_0) - \frac{d^2\sigma_-}{dE_\gamma d\Omega_\gamma}(E_e, E_\gamma, \theta_0) \right|$$

- $\delta_{DM} \equiv \int_{r_{min}}^{r_0} \rho_{DM}(r) dr$ the integral of the DM density along the direction of the jet

  r_{min} minimum distance from the AGN center at which the scattering takes place

  r_0 the distance at which the AGN jet fades

- $\frac{d^2\sigma_\pm}{dE_\gamma d\Omega_\gamma}(E_e, E_\gamma, \theta_0)$ the differential cross section for $e^-\tilde{\chi} \to e^-\tilde{\chi}\,\gamma_\pm$, with Ω_γ the solid angle between the emitted photon and the incoming electron.

  The polar coordinate θ_γ is fixed at θ_0, angle between the position of the AGN jet of electrons with respect the line of sight

- $\frac{d\Phi_e^{AGN}}{dE_e}$ the electron energy spectrum in units of erg^{-1} s^{-1}

The electron energy spectrum in the jet

Assuming that the gamma-ray photons coming from the Cen A core are due to synchrotron self-Compton radiation from two emitting zones (both located at $\theta_0 = 30°$ with respect to the line of sight), the electron energy spectrum can be derived *Abdalla et al., A & A 619 (2018) A71*

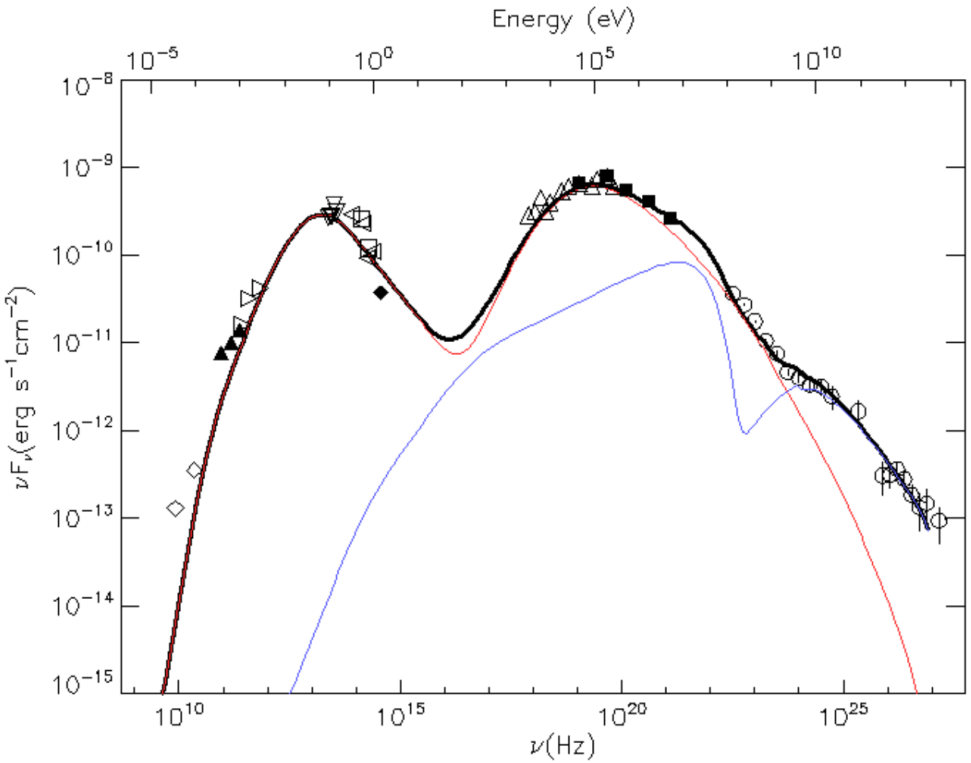

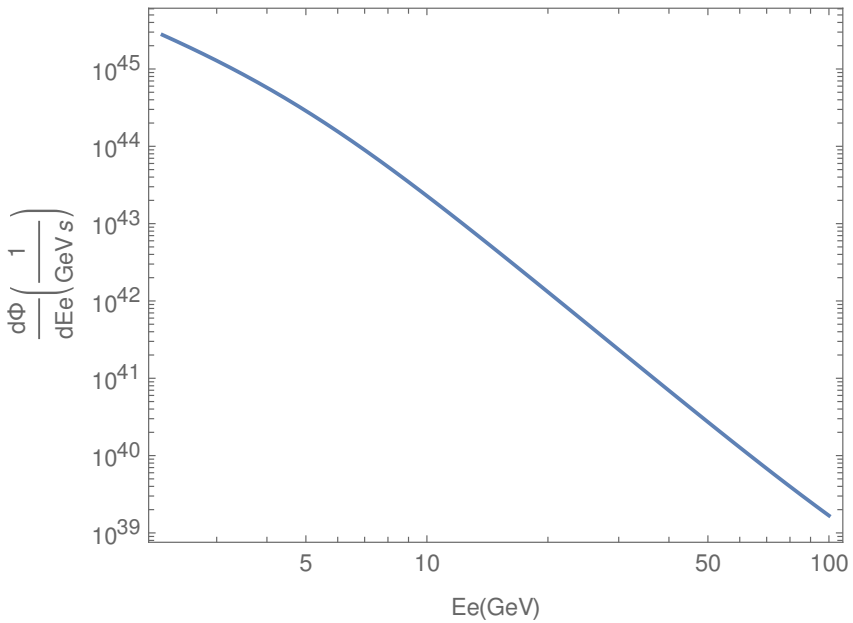

We use this photon flux as our background to measure the signals and to put constraints

Exclusion from annihilation and circular polarised flux

- Allowed DM candidates $m_{\tilde{\chi}} \sim 40 - 200$ GeV and $a_R \lesssim 10^{-2}$
- ΔM for the survived parameter space points fixed by the relic density and span from $\Delta M = 3\,(1)$ GeV for $m_{\tilde{\chi}} = 50\,(200)$ GeV *M. Cermeño, C. Degrande, L. Mantani, PRD 105 (2022) 083019*

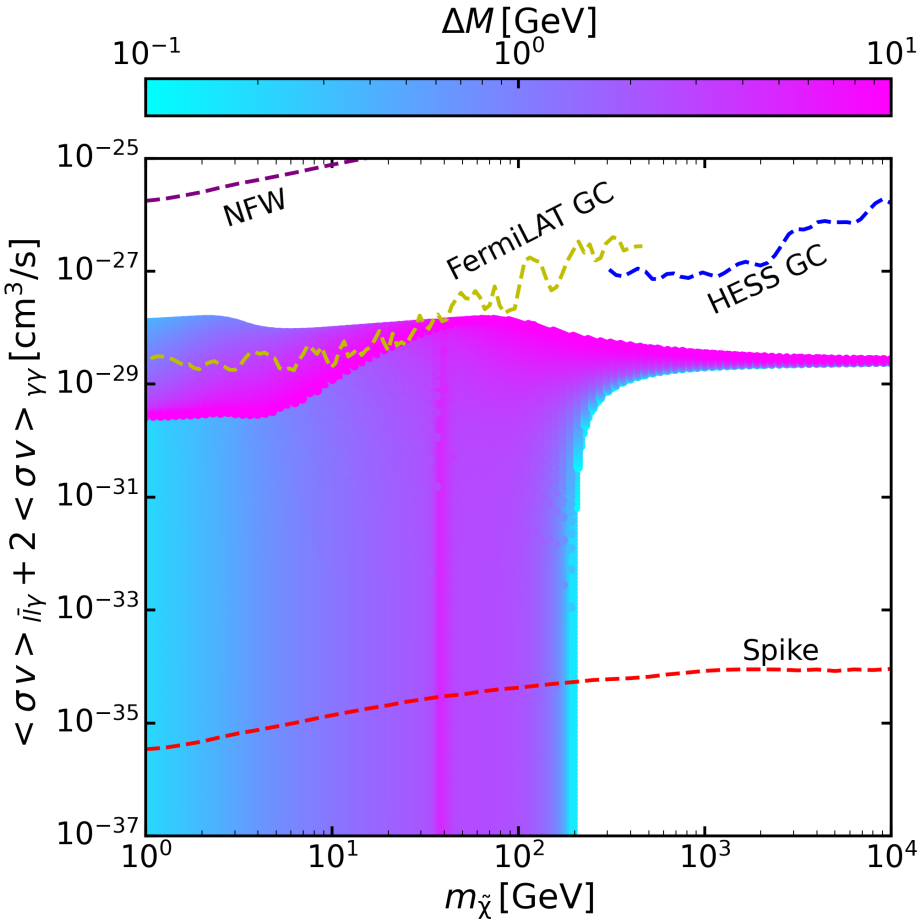

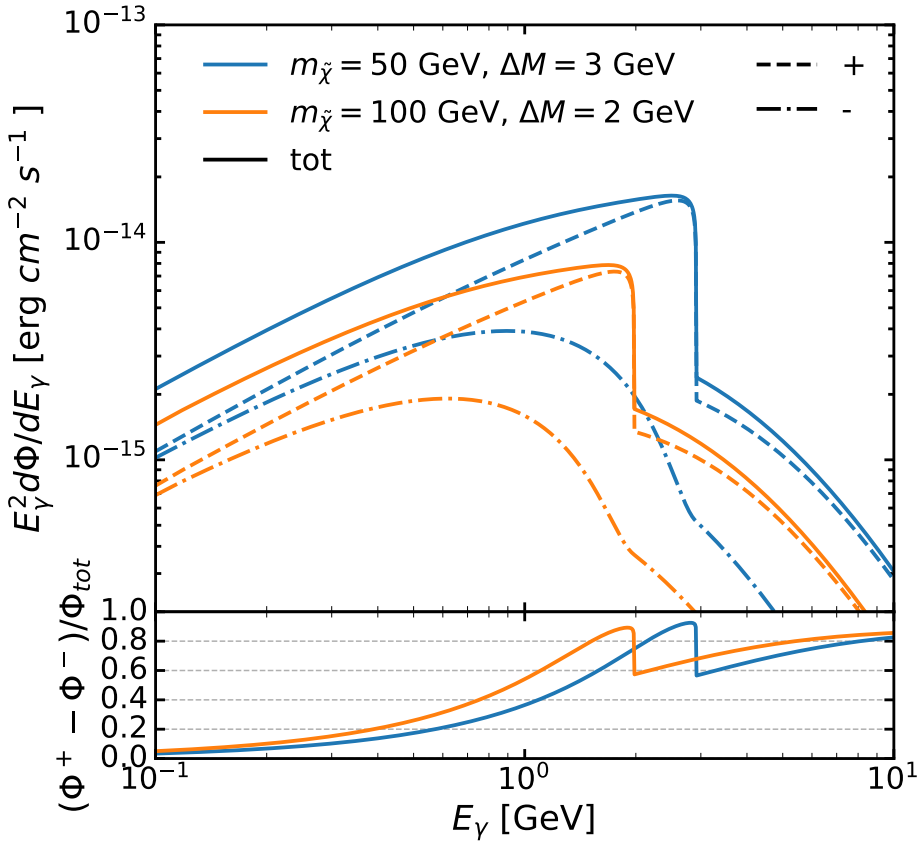

Asymmetries close to 100 %

Sensitivity of Fermi-LAT to measure this flux around $5\ 10^{13}$ erg cm^{-2} s^{-1}

DM distribution in the Galaxy

- Well-motivated DM density profiles in our galaxy by the study of rotation curves and N-body simulations *Einasto, Trudy Inst. Astrofiz. Alma-Ata 5 (1965) 87, Navarro, Frenk, White, ApJ 462 (1996) 563, Navarro et al., MNRAS 402 (2010) 21, Ludlow, Angulo MNRAS 465 (2017) L84*

$$\rho_{\rm NFW}(r) = \rho_s \frac{r_s}{r}\left(1+\frac{r}{r_s}\right)^2$$

$$\rho_{\rm Ein}(r) = \rho_s \exp\left\{-\frac{2}{\alpha}\left[\left(\frac{r}{r_s}\right)^{\alpha}-1\right]\right\}$$

Profiles	Einasto	NFW
$\rho_{\rm s}$ $({\rm GeVcm}^{-3})$	0.079	0.307
$r_{\rm s}$ (kpc)	20.0	21.0
$\alpha_{\rm s}$	0.17	/

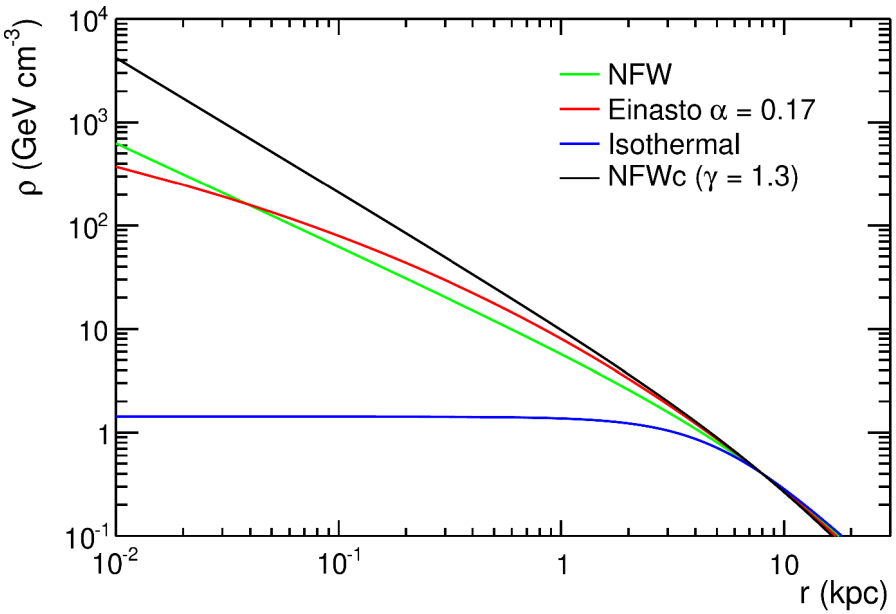

The Fermi-LAT Collaboration PRD 91 (2015) 122002

- The local DM density $\rho_{\chi,0} = 0.385 \pm 0.027\ {\rm GeV/cm}^3$ at $r_\odot = 8.5$ kpc from the Galactic Center (GC) *Catena and Ullio JCAP08 (2010) 004*

Relic density

- Thermal DM production, $(m_{\tilde{\chi}}, \Delta M) \Rightarrow a_R$ that yields $\Omega_\chi h^2 = 0.120 \pm 0.001$

$$\Omega_\chi h^2 \sim \frac{1}{\sigma v_{eff}}, \quad \sigma v_{eff} = \sigma v_{\tilde{\chi}\tilde{\chi}} + \sigma v_{\tilde{\chi}\varphi} e^{-\frac{\Delta M}{T}} + \sigma v_{\varphi\varphi} e^{-\frac{2\Delta M}{T}},$$

$\sigma v_{\tilde{\chi}\tilde{\chi}} \sim \frac{a_R^4}{m_\chi^2}$, $\sigma v_{\tilde{\chi}\varphi} \sim \frac{a_R^2 g^2}{m_\chi^2}$, $\sigma v_{\varphi\varphi} \sim \frac{g^4}{m_\chi^2}$, where g is a gauge coupling

M. Cermeño, *C. Degrande, L. Mantani, Phys.Dark Univ. 34 (2021) 100909*

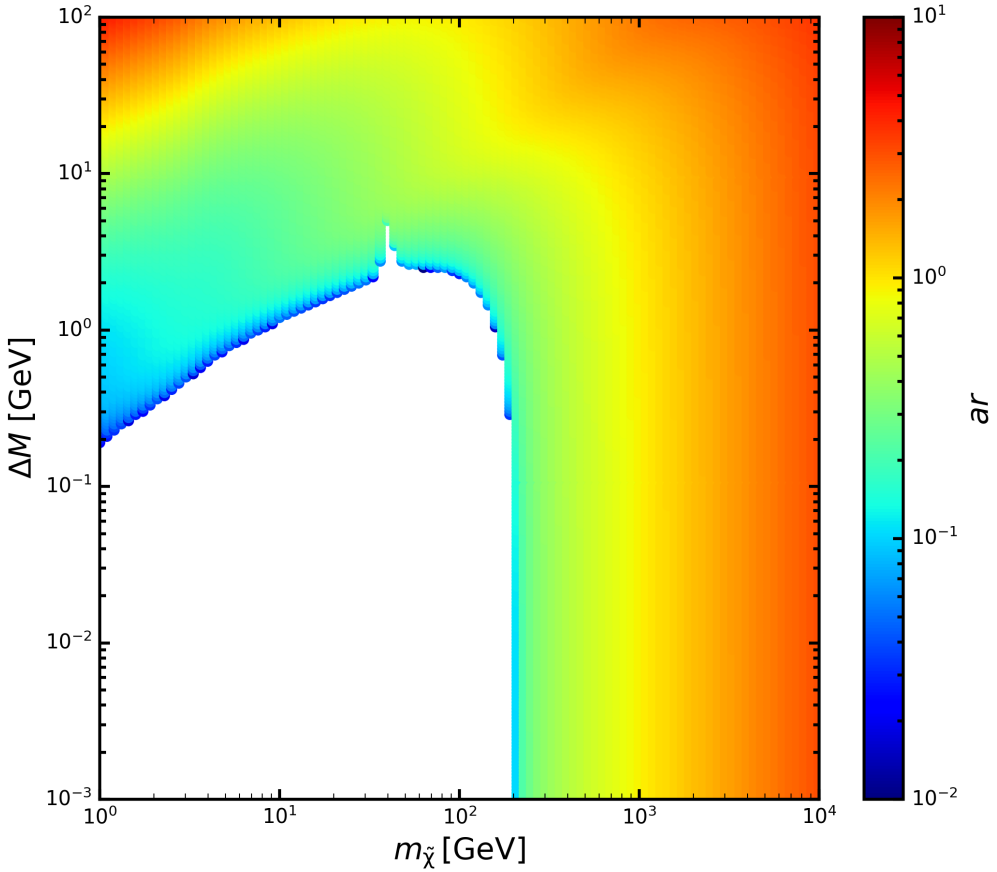

Indirect detection constraints

- $\tilde{\chi}\tilde{\chi} \to e^+e^-$ velocity suppressed
- $\tilde{\chi}\tilde{\chi} \to e^-e^+\gamma$ and $\tilde{\chi}\tilde{\chi} \to \gamma\gamma$ relevant channels
- yellow and blue lines are the upper limits from Fermi-LAT and HESS

  Ackermann et al., PRD 727 D 91 (2015) 122002, Abdallah et al., PRL 731120 (2018) 201101
- For $m_\chi \gtrsim 200$ GeV cases with $\Delta M < 10^{-1}$ GeV overlap with the rest of the solutions

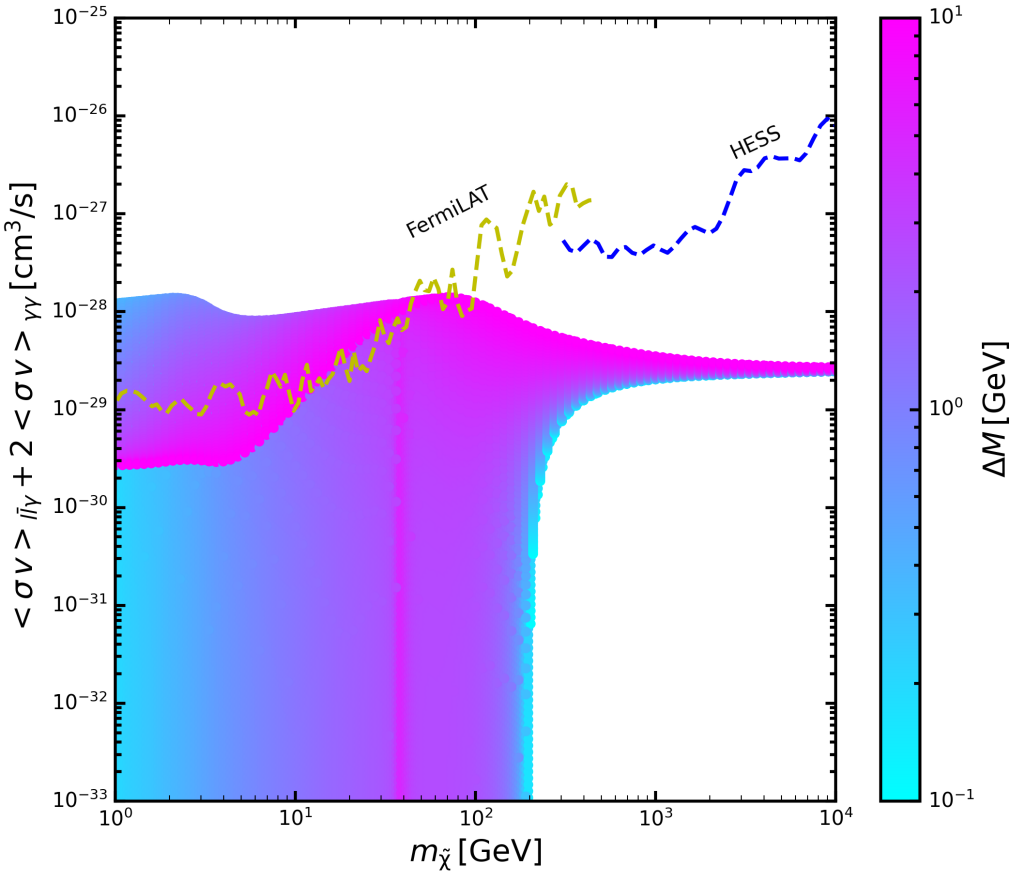

M. Cermeño, *C. Degrande, L. Mantani, Phys.Dark Univ. 34 (2021) 100909*

Collider constraints

- φ pair produced through electro-weak interactions
- Contraints from $\varphi \to \tilde{\chi} e^-$, unless ΔM is too small
- LHC excludes only $m_\varphi \lesssim 100$ GeV for $\Delta M \sim$ few GeV
- LEP constraints evaded $\frac{m_\varphi}{m_\chi} \leq 1.03$
- Constraints from mono-photon events at LEP less stringent than the ones from Fermi LAT and HESS

  Kopp, Michaels, Smirnov, JCAP 04 (2014) 022
- Strongest constraint $\Rightarrow$ Z width, $m_\varphi > M_Z/2 = 45$ GeV

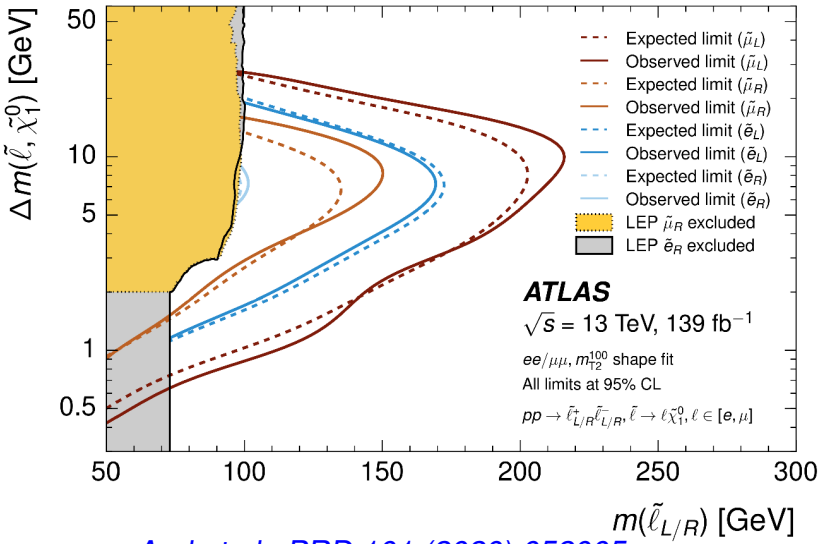

Aad et al., PRD 101 (2020) 052005

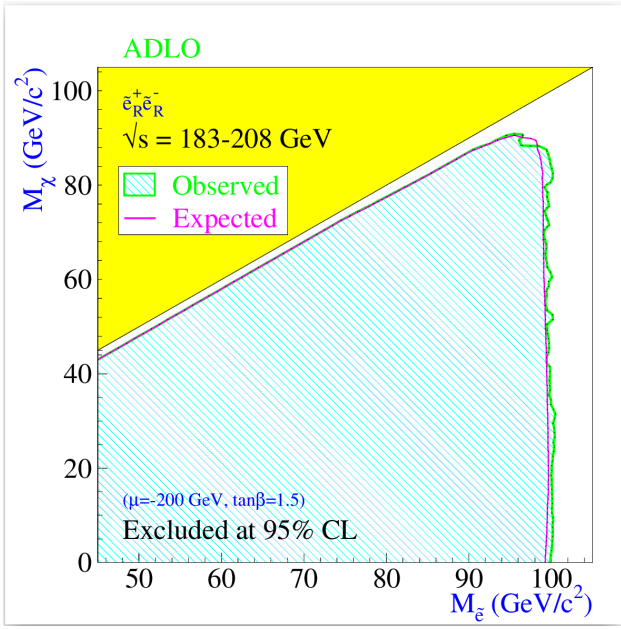

LEP2 SUSY Working Group (2004)

Direct detection constraints

$$\mathcal{L}_{eff} = \mathcal{A}\bar{\psi}_{\tilde{\chi}}\gamma^{\mu}\gamma^{5}\psi_{\tilde{\chi}}\partial^{\nu}F_{\mu\nu}$$

$\mathcal{A}$ the anapole form factor

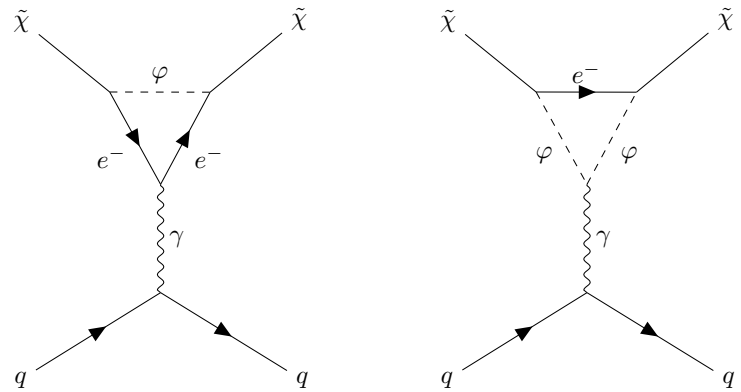

M. Cermeño, *C. Degrande, L. Mantani, Phys.Dark Univ. 34 (2021) 100909*

- Upper bounds by XENON1T (solid) and the projected LZ (dashed)

  Aprile et al., PRL 121 (2018) 111302,

  Mount et al., arXiv:1703.09144

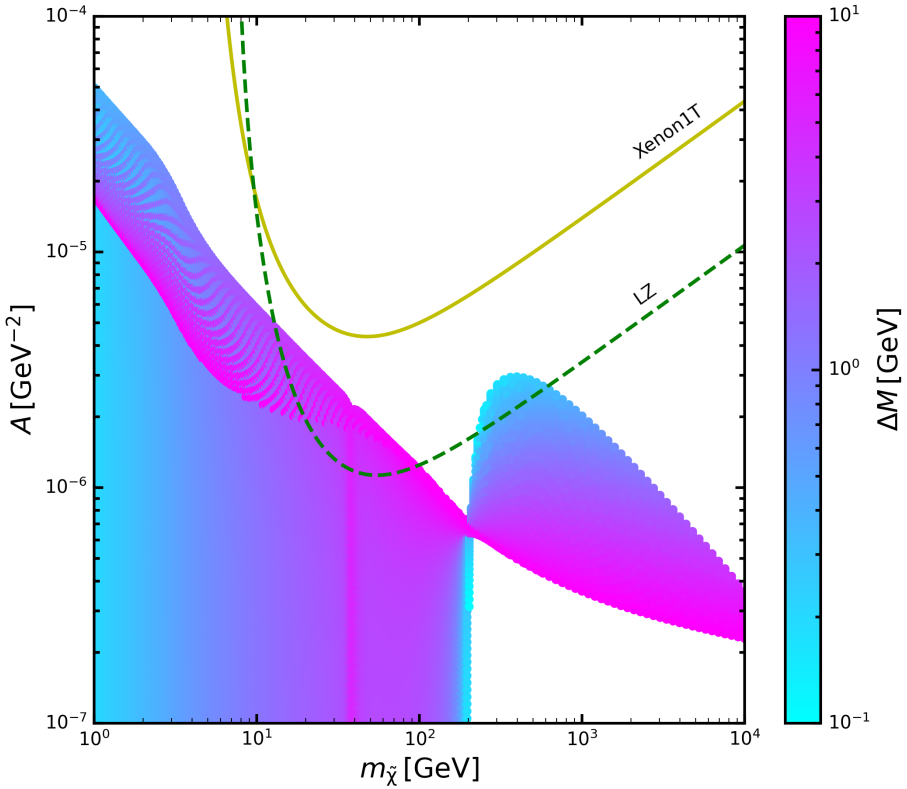

Anapole form factor

Our Majorana DM particle can interact via one loop anapole moment

$$\mathcal{L}_{eff} = \mathcal{A}\bar{\psi}_{\tilde{\chi}}\gamma^{\mu}\gamma^{5}\psi_{\tilde{\chi}}\partial^{\nu}F_{\mu\nu}.$$

The anapole form factor for $|q^2| \ll m_e^2$

$$\mathcal{A} = -\frac{ea_R^2}{32\pi^2 m_{\tilde{\chi}}^2}\left[\frac{-10 + 12\log\left(\frac{\sqrt{|q^2|}}{m_{\tilde{\chi}}}\right) - (3+9r^2)\log(r^2-1) - (3-9r^2)\log r^2}{9(r^2-1)}\right]$$

Kopp, Michaels, Smirnov, JCAP 04 (2014) 022, Baker, Thamm, JHEP 10 (2018) 187

- $\sqrt{|q^2|} = \sqrt{2E_r m_T}$ the transferred momentum, where $E_r \sim \frac{1}{2}m_{\tilde{\chi}}v_{\tilde{\chi}}^2$ is the recoil energy and m_T the mass of the target of the experiment
- $r = \frac{m_\varphi}{m_{\tilde{\chi}}}$, for $r^2 \lesssim 1.001$ the perturbation theory is not valid anymore, need of the next term in the expansion

Mono-photon searches

Mono-photon events coming from $e^- e^+ \to \tilde{\chi}\tilde{\chi}\gamma$ at LEP and the future ILC

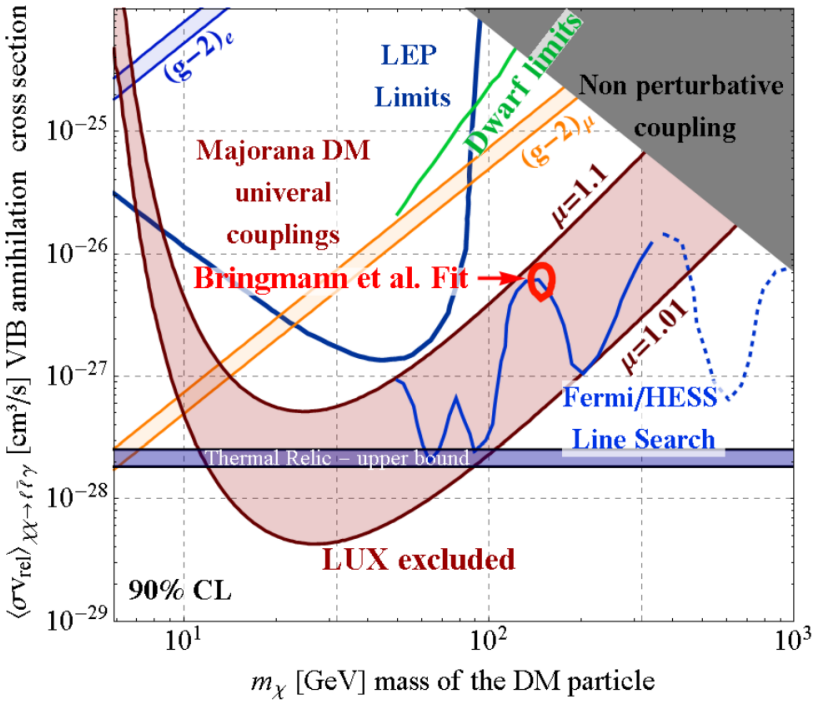

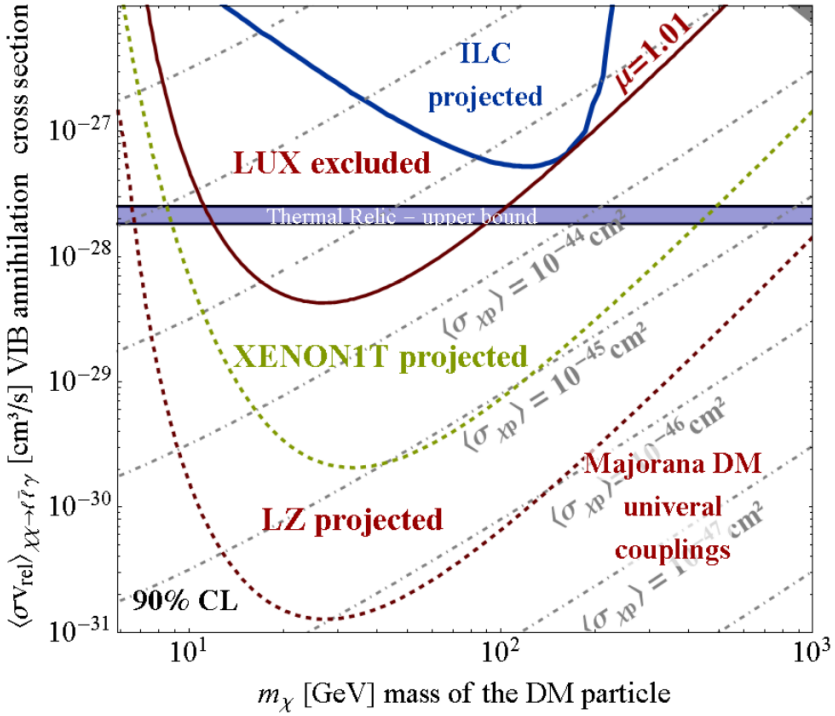

Mono-photon searches

Mono-photon events coming from $e^- e^+ \to \tilde{\chi}\tilde{\chi}\gamma$ at CLIC ($\sqrt{s} = 3$ TeV)

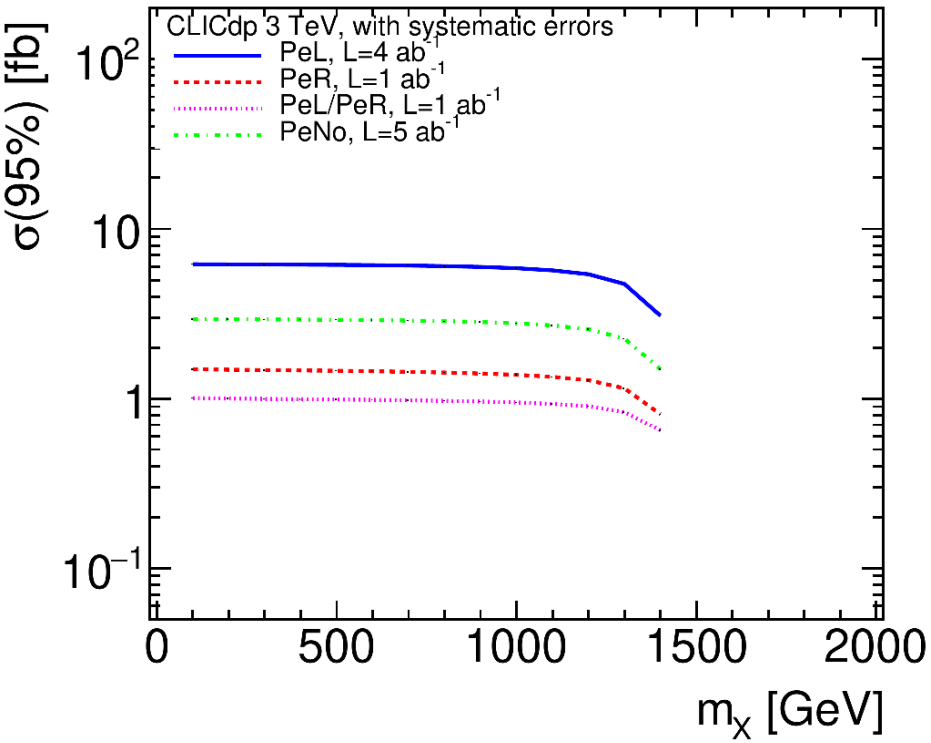

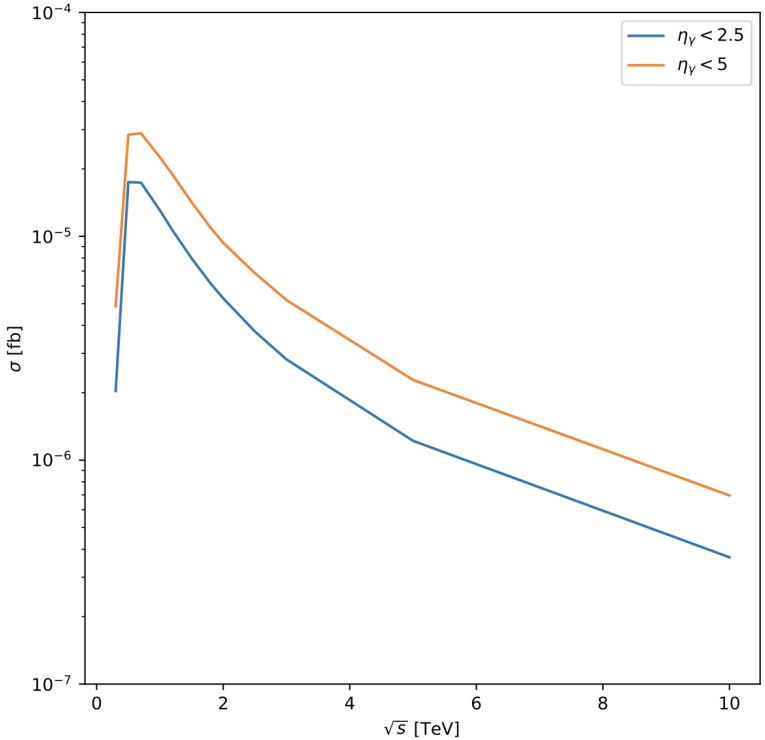

95 % confidence level upper limit cross section expected from CLIC

VS

cross section for monophoton events for our best fit point $m_{\tilde{\chi}} = 123$ GeV $a_R = 0.018$

Resonances of the process

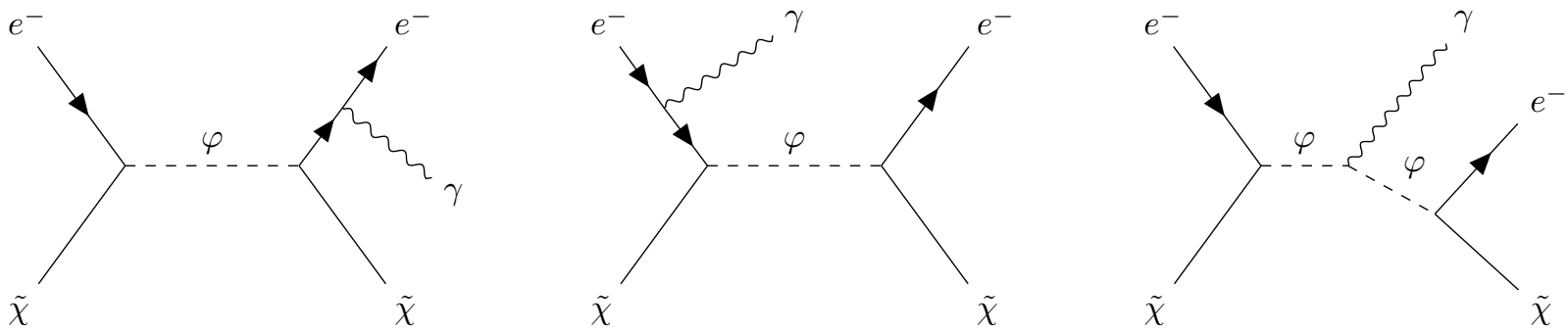

$p_{\tilde{\chi}} = (m_{\tilde{\chi}}, \vec{0})$, $p_e = (E_e, \vec{p}_e)$ the incoming DM and electron four-momenta,
$p'_{\tilde{\chi}} = (E'_{\tilde{\chi}}, \vec{p}'_{\tilde{\chi}})$, $p'_e = (E'_e, \vec{p}'_e)$ the outgoing ones

- Two resonances

$$s = (p_e + p_{\tilde{\chi}})^2 = m_\varphi^2 \Rightarrow E_{R1} = \frac{m_\varphi^2 - m_{\tilde{\chi}}^2}{2m_{\tilde{\chi}}} \approx \Delta M$$

$$s' = (p'_e + p'_{\tilde{\chi}})^2 = m_\varphi^2 \Rightarrow E_{R2} = \frac{m_\varphi^2 - m_{\tilde{\chi}}^2 + 2m_{\tilde{\chi}} E_\gamma}{2(m_{\tilde{\chi}} - E_\gamma(1 - \cos\theta_\gamma))}$$

θ_γ the angle between the emitted photon and the incoming CR electron

Resonances of the process

When the minimum electron energy

$$E_{\rm min} = \frac{E_\gamma}{1 - \frac{E_\gamma}{m_{\tilde{\chi}}} \cos\,\theta_\gamma}$$

is higher than E_{R1},

$$E_\gamma > \frac{m_{\tilde{\chi}}(m_\varphi^2 - m_{\tilde{\chi}}^2)}{2m_{\tilde{\chi}}^2 + (m_\varphi^2 - m_{\tilde{\chi}}^2)(1 - \cos\,\theta_\gamma)}$$

the first resonance cannot happen anymore.

The drop-off between $E_{\gamma,1} = \frac{m_{\tilde{\chi}}(m_\varphi^2 - m_{\tilde{\chi}}^2)}{2m_\varphi^2}$ and $E_{\gamma,2} = \frac{(m_\varphi^2 - m_{\tilde{\chi}}^2)}{2m_{\tilde{\chi}}}$.

For $\Delta M \ll m_\varphi \sim m_{\tilde{\chi}} \Rightarrow E_{\gamma,1} \sim E_{\gamma,2} \sim \Delta M$.

Beyond this energy, only the second resonance contributes to the flux.

The Narrow Width Approximation

- We are interested in cases with $\Delta M \ll m_\varphi$
- the total width of the mediator is

$$\Gamma_{\rm tot} \sim \Gamma_{\varphi \to e^- \tilde{\chi}} = \frac{1}{8\pi} a_R^2 \frac{(m_\varphi^2 - m_{\tilde{\chi}}^2)^2}{2m_\varphi^3} \approx \frac{1}{4\pi} a_R^2 \frac{(\Delta M)^2}{m_\varphi}$$

- $\frac{\Gamma_{\rm tot}}{m_\varphi} \propto \left(\frac{\Delta M}{m_\varphi}\right)^2 \ll 1 \Rightarrow$ NWA

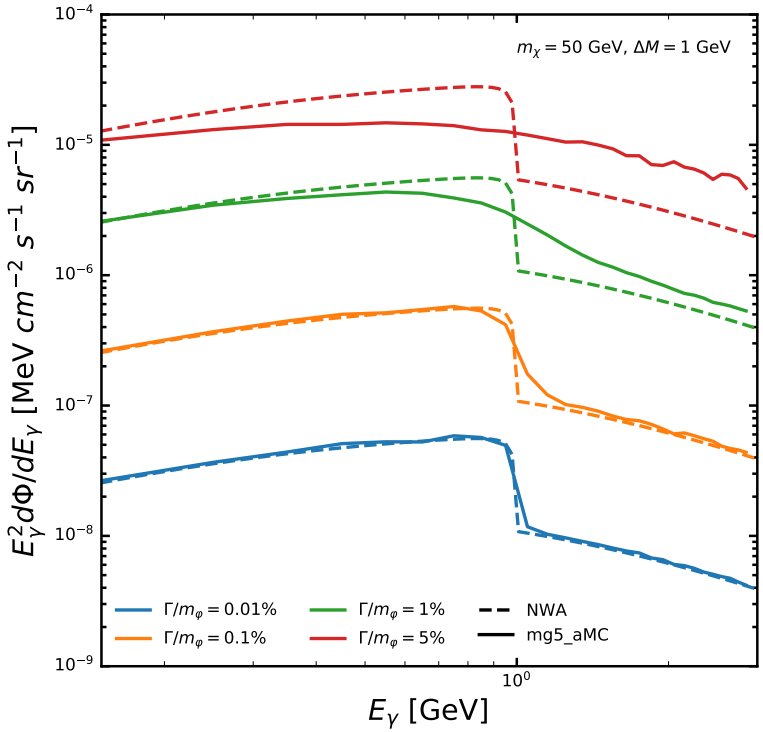

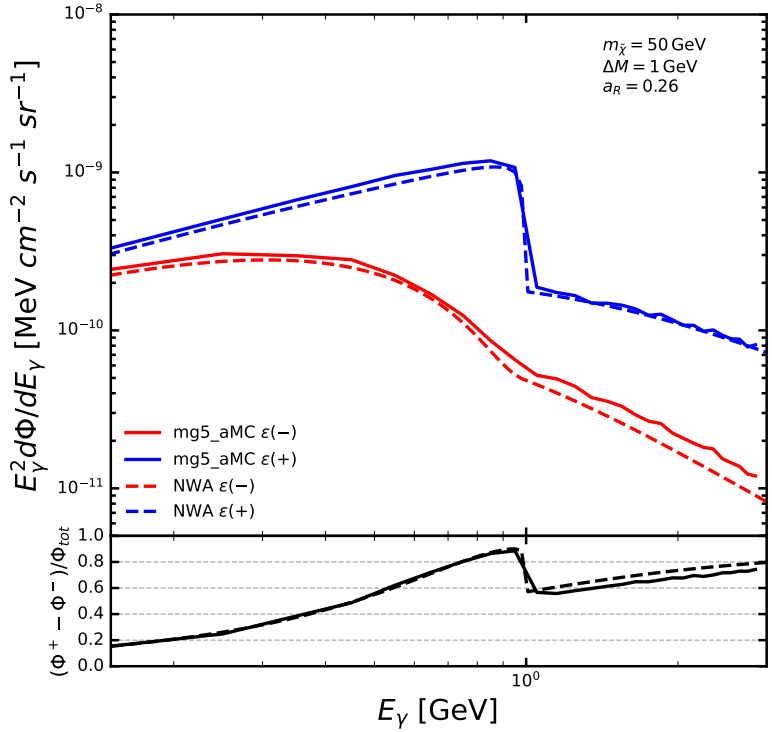

The Narrow Width Approximation

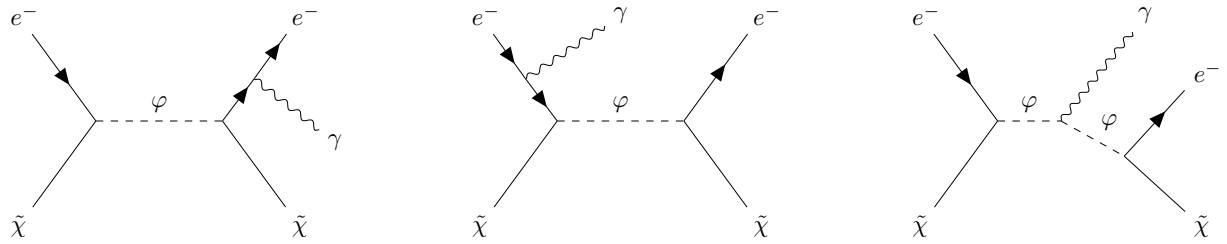

$$\frac{d\tilde{\Phi}_{e\tilde{\chi},\pm}}{dE_\gamma} \equiv \frac{m_{\tilde{\chi}}}{\bar{J}} \frac{d\Phi_{e\tilde{\chi},\pm}}{dE_\gamma} = \int dE_e \frac{d\phi}{dE_e} \frac{d\sigma_\pm}{dE_\gamma}(E_e, E_\gamma),$$

$$\frac{d\tilde{\Phi}_{e\tilde{\chi},\pm}}{dE_\gamma} = \int \frac{d\phi}{dE_e} \frac{d\tilde{\sigma}_{1\pm}}{dE_\gamma} \mathrm{d}E_e + \int \frac{d\phi}{dE_e} \frac{d\tilde{\sigma}_{2\pm}}{dE_\gamma} \mathrm{d}E_e,$$

the differential cross section for the first diagram

$$\frac{d\tilde{\sigma}_{1\pm}}{dE_\gamma} = \sigma_{e^-\tilde{\chi}\to\varphi}(E_e) \frac{d\Gamma_{\varphi\to e^-\tilde{\chi}\gamma^\pm}}{dE_\gamma}(E_\gamma) \frac{1}{\Gamma_{\mathrm{tot}}}$$

the differential cross section for the other two

$$\frac{d\tilde{\sigma}_{2\pm}}{dE_\gamma} = \frac{d\sigma_{e^-\tilde{\chi}\to\varphi\gamma^\pm}}{dE_\gamma}(E_e, E_\gamma) \frac{\Gamma_{\varphi\to e^-\tilde{\chi}}}{\Gamma_{\mathrm{tot}}}$$

with $\Gamma_{\mathrm{tot}} = \Gamma_{\varphi\to e^-\tilde{\chi}} + \Gamma_{\varphi\to e^-\tilde{\chi}\gamma^\pm}$

DM density spike formation

Assumptions taken

- Adiabatic growth
- Collisionless DM
- Cuspy initial profile
- Growth in the center of the DM halo
- The DM halo did not undergo a merger

The spike is expected to smooth down because of dynamical relaxation due to the scattering of DM with stars if the relaxation time is smaller than the age of the Universe, i.e.,

$$t_r \sim 2\ 10^9\ \mathrm{yr} \left(\frac{M_{\mathrm{BH}}}{4.3\ 10^6\ M_\odot} \right) < H_0^{-1} \sim 10^{10}\ \mathrm{yr}$$

- For the MW $t_r \sim 2$ Gyr
- For Cen A $t_r \sim 10^2$ Gyr

DM density in Cen A

$$\rho_{DM}(r) = \begin{cases} 0 & r < 4R_S \\ \frac{\rho_{sp}(r)\rho_{sat}}{\rho_{sp}(r)+\rho_{sat}} & 4R_S \leq r < R_{sp} \\ \rho_0 \left(\frac{r}{r_0}\right)^{-1} \left(1+\frac{r}{r_0}\right)^{-2} & r \geq R_{sp} \end{cases}, \qquad \delta_{DM} \equiv \int_{4R_S}^{r_0} \rho_{DM}(r) dr$$

$$\rho_{sp}(r) = \rho_0 \left(\frac{R_{sp}}{r_0}\right)^{-1} \left(1 - \frac{4R_S}{r}\right)^3 \left(\frac{R_{sp}}{r}\right)^{7/3}, \quad \rho_{sat} \simeq \frac{m_\chi}{\langle\sigma v\rangle t_{BH}}$$

with $R_S = 5 \times 10^{-6}$ pc, $r_0 = 20$ kpc, $\rho_0 \sim 1$ GeV/cm^3, $R_{sp} = 10^8 R_S$

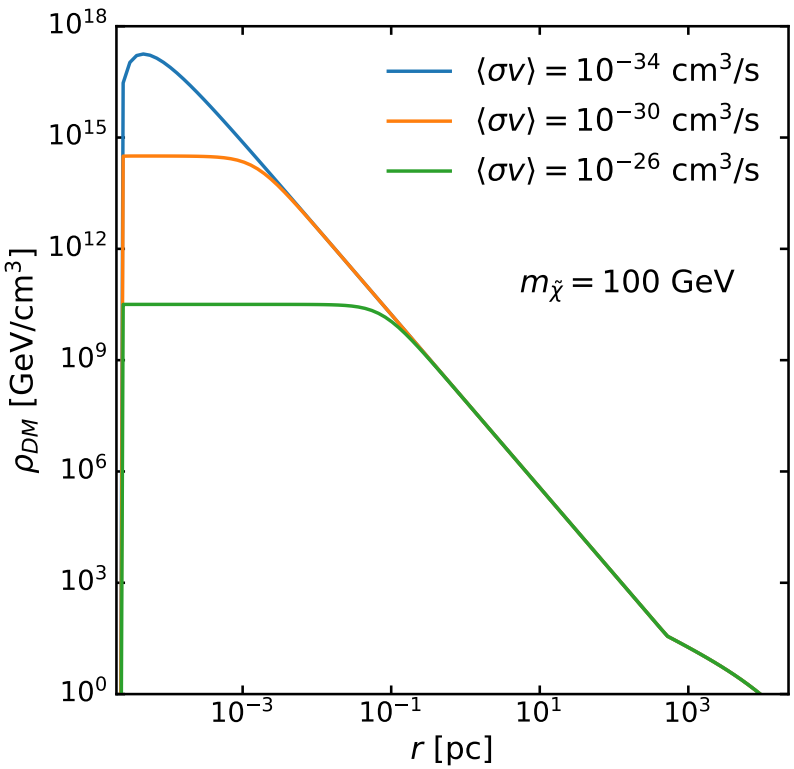

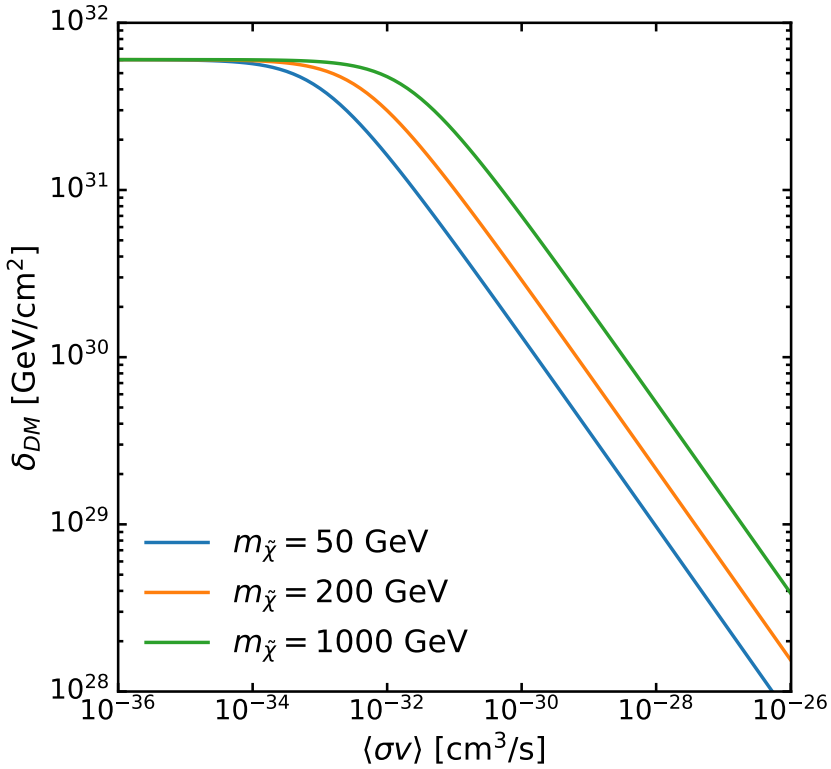

M. Cermeño, C. Degrande, L. Mantani, PRD 105 (2022) 8, 083019, arXiv: 2201.07247

The electron energy spectrum in the jet

Assuming that the gamma-ray photons coming from the Cen A core are due to synchrotron self-Compton radiation from two emitting zones (both located at $\theta_0 = 30°$ with respect to the line of sight), the electron energy spectrum can be derived *Abdalla et al., A & A 619 (2018) A71*

At least part of the photon emission at $E_\gamma > 300$ GeV arises on large scales *Abdalla et al., Nature 582 (2020) 356*

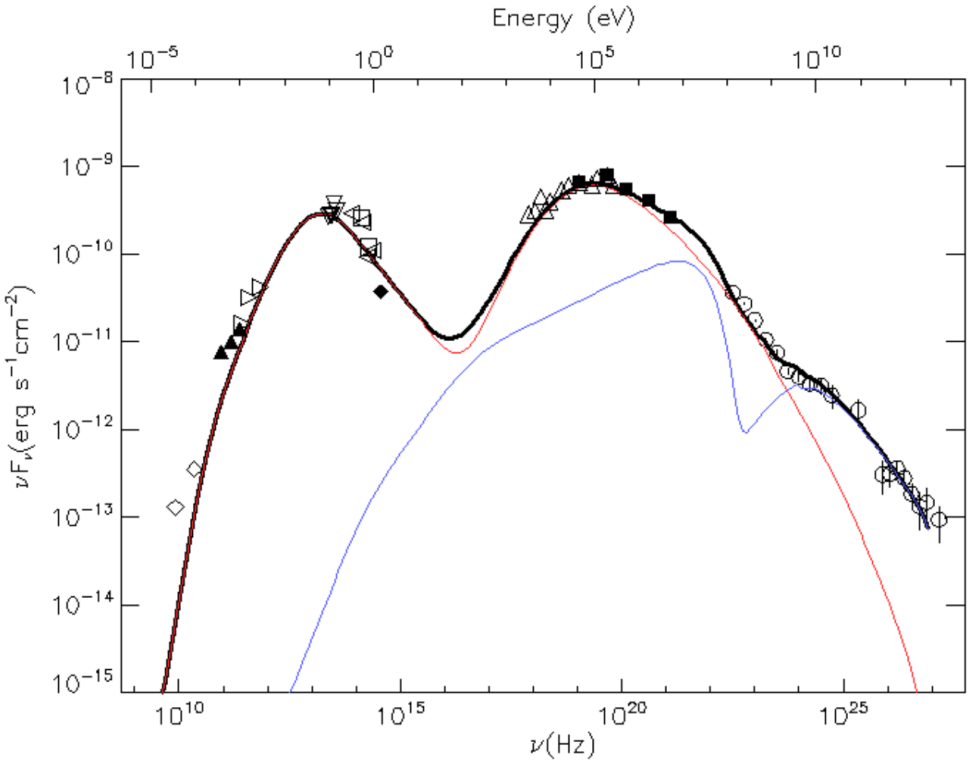

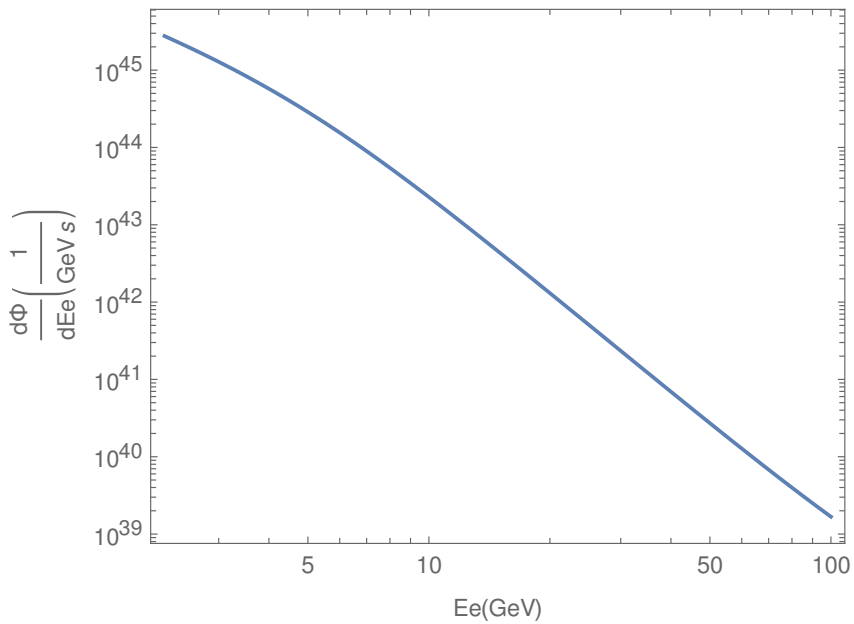

We use this photon flux as our background to measure the signals and to put constraints

The electron energy spectrum in the jet

Assuming that the gamma-ray photons coming from the Cen A core are due to synchrotron self-Compton (SSC) the electron energy spectrum can be derived *Abdalla et al., A & A 619 (2018) A71*

$$\frac{1}{d_{\rm AGN}^2}\frac{d\Phi_e^{\rm AGN}}{dE_e} = \frac{1}{d_{\rm AGN}^2\, m_e}\int_{0.9}^{1}\frac{d\mu}{\Gamma_B\,(1-\beta_B\mu)}\frac{d\Phi_e^{\rm AGN}}{d\gamma}$$

,

$$\frac{d\Phi_e}{d\gamma}^{\rm AGN} = \frac{1}{2}k_e\left[\gamma\Gamma_B\,(1-\beta_B\mu)\right]^{-s_1}\left[1+\left(\gamma\,(\Gamma_B\,(1-\beta_B\mu))\,/\gamma'_{br}\right)^{s_2-s_1}\right]^{-1}$$

$$\Gamma_B = (1-\beta_B^2)^{-\frac{1}{2}} \sim 7, \quad \delta = \left[\Gamma_B(1-\beta_B\,\cos\theta_0)\right]^{-1}, \quad \gamma_{\rm min} = \frac{\gamma'_{\rm min}}{\Gamma_B\,(1-\beta_B\mu)}, \quad \gamma_{\rm max} = \frac{\gamma'_{\rm max}}{\Gamma_B\,(1-\beta_B\mu)}$$

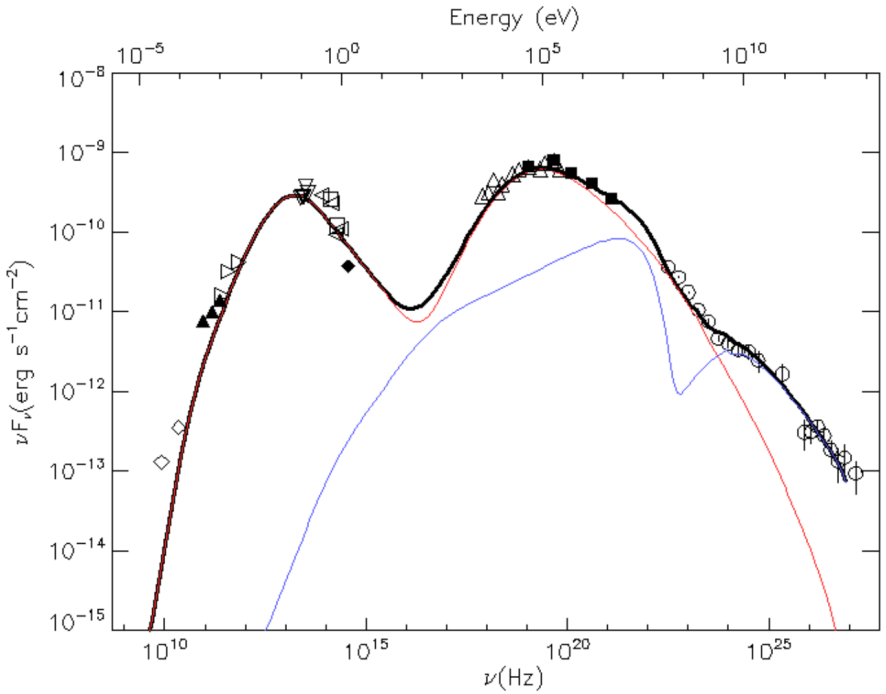

Parameter	the 1st SSC zone	the 2nd SSC zone
δ	1.0	1.0
θ_0	30°	30°
B (G)	6.2	17.0
$R_{\rm b}$ (cm)	3.0×10^{15}	8.8×10^{13}
s_1	1.8	1.5
s_2	4.3	2.5
$\gamma'_{\rm min}$	3×10^{2}	1.5×10^{3}
$\gamma'_{\rm max}$	1×10^{7}	1×10^{7}
$\gamma'_{\rm brk}$	8.0×10^{2}	3.2×10^{4}
L_e (erg s^{-1})	3.1×10^{43}	3×10^{40}

$$L_e = \int_{-1}^{1}\frac{d\mu}{\Gamma_B\,(1-\beta_B\mu)}\int_{\gamma_{\rm min}}^{\gamma_{\rm max}} d\gamma m_e\gamma\frac{d\Phi_e^{AGN}}{d\gamma}\left[\gamma\,(\Gamma_B\,(1-\beta_B\mu))\right]$$

The electron energy spectrum in the jet: other works

Other works as *Gorchtein, Profumo, Ubaldi, PRD 82 (2010) 083514, Huang, Rajaraman, and Tait, JCAP 05 (2012) 027, Gómez, Jackson, Shaughnessy, PRD 88 (2013) 015024* used the fit from *Abdo et al., ApJ 719 (2010) 1433 (2010)* taking $L_e = 10^{45}$ erg/s (Eddington limit)

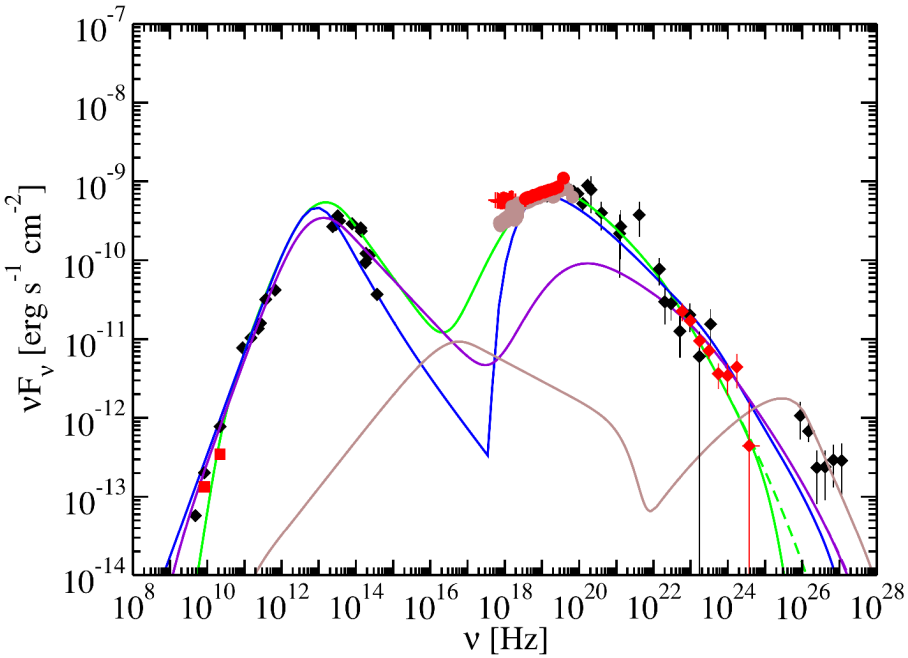

Parameter	Symbol	Green[1]	Blue[2]	Violet[3]	Brown[4]
Bulk Lorentz factor	Γ_j	7.0	$5 \rightarrow 2$	3.7	2.0
Doppler factor	δ_D	1.0	$1.79 \rightarrow 1.08$	3.9	3.1
Jet angle	θ	30°	25°	15°	15°
Magnetic field (G)	B	6.2	0.45	0.2	0.02
Variability timescale (s)	t_v	1.0×10^5		1×10^5	1×10^5
Comoving blob size scale (cm)	R_b	3.0×10^{15}	3×10^{15}	1.1×10^{16}	9.2×10^{15}
Low-energy electron spectral index	p_1	1.8	3.2	1.8	1.8
High-energy electron spectral index	p_2	4.3		4.0	3.5
Minimum electron Lorentz factor	$\gamma_{\rm min}$	3×10^2	1.3×10^3	8×10^2	8×10^2
Maximum electron Lorentz factor	$\gamma_{\rm max}$	1×10^8	1×10^7	1×10^8	1×10^8
Break electron Lorentz factor	$\gamma_{\rm brk}$	8×10^2		2×10^3	4×10^5
Jet power in magnetic field (erg s^{-1})	$P_{j,B}$	6.5×10^{43}	1.7×10^{41}	2.7×10^{41}	4.3×10^{38}
Jet power in electrons (erg s^{-1})	$P_{j,e}$	3.1×10^{43}	3.1×10^{42}	2.3×10^{42}	7.0×10^{40}

[1] SSC model.
[2] Decelerating Jet model (Georganopoulos & Kazanas 2003).
[3] SSC model excluding X-rays.
[4] SSC Fit to HESS data only.

The electron energy spectrum in the jet: other works

HESS demonstrated the alignment of a substantial part of the very high energy emission with the large-scale radio jet *H. Abdalla et al., Nature 582 (2020) 356*

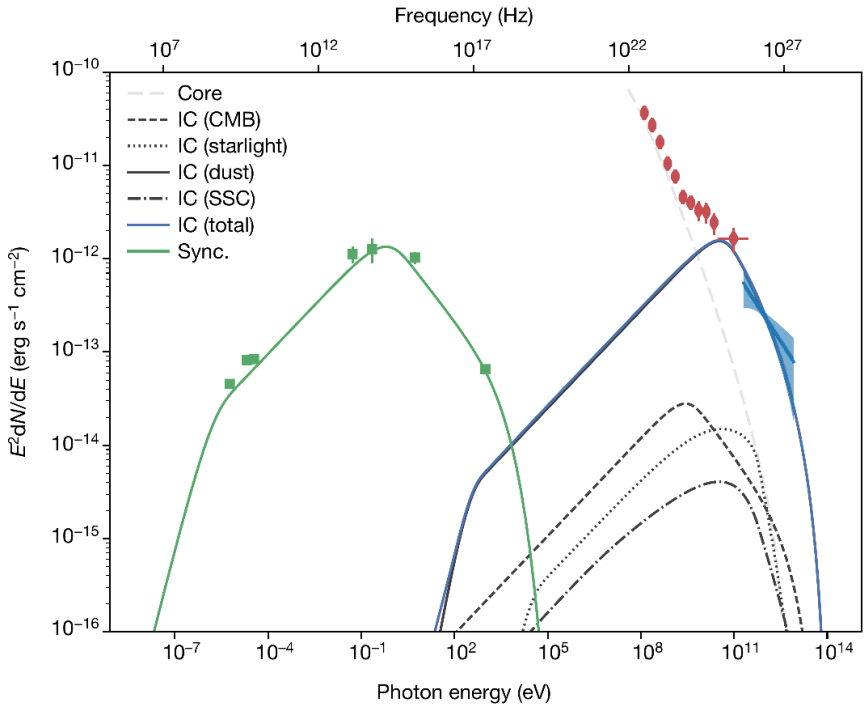

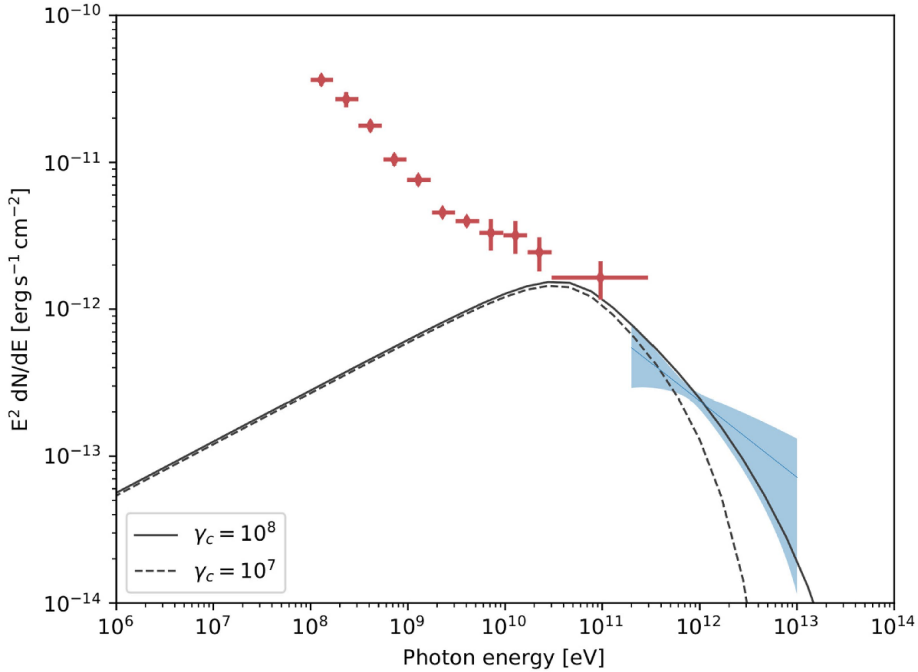

Total flux from scattering in the AGN

The total flux of photons coming from $\tilde{\chi} e^- \to \tilde{\chi} e^- \gamma$ in the AGN jet cannot reach values of the order of the sensitivity of Fermi LAT ($\sim 5\ 10^{13}$ erg/s) unless $m_\varphi < 45$ GeV

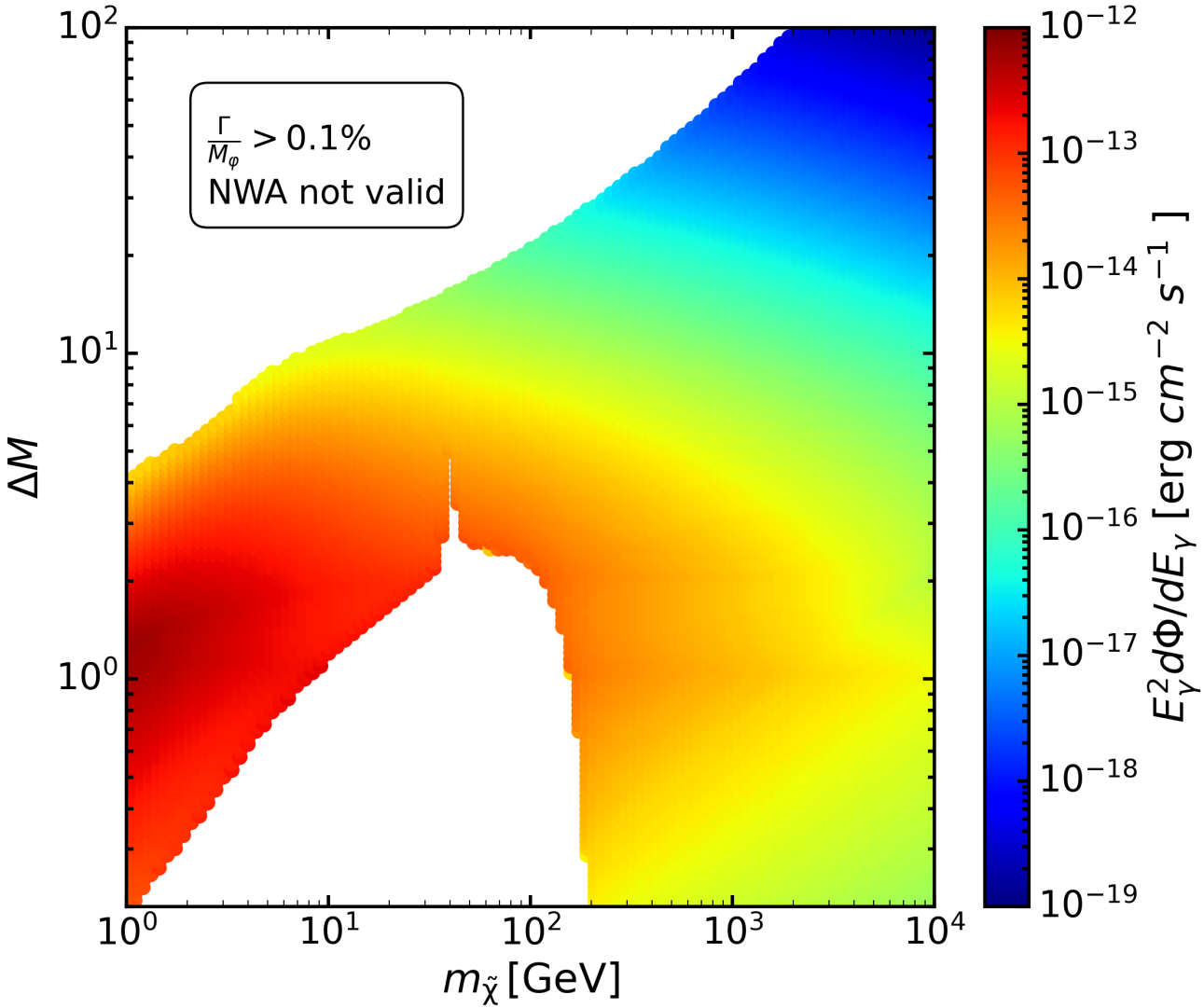

Sensitivity Fermi-LAT Cen A

$$\epsilon \sim 0.1\,,\; A_{\rm eff} \sim 10^4\ {\rm cm}^2$$

$$\frac{N_{\rm signal}}{\sqrt{N_{\rm back}}} \sim 3 \Rightarrow \frac{\frac{d\Phi_{e\chi}}{dE_\gamma}}{\sqrt{\frac{d\Phi_{\rm back}}{dE_\gamma}}} \sqrt{2\epsilon E_{\gamma,{\rm peak}} A_{\rm eff} \Delta t} = 3$$

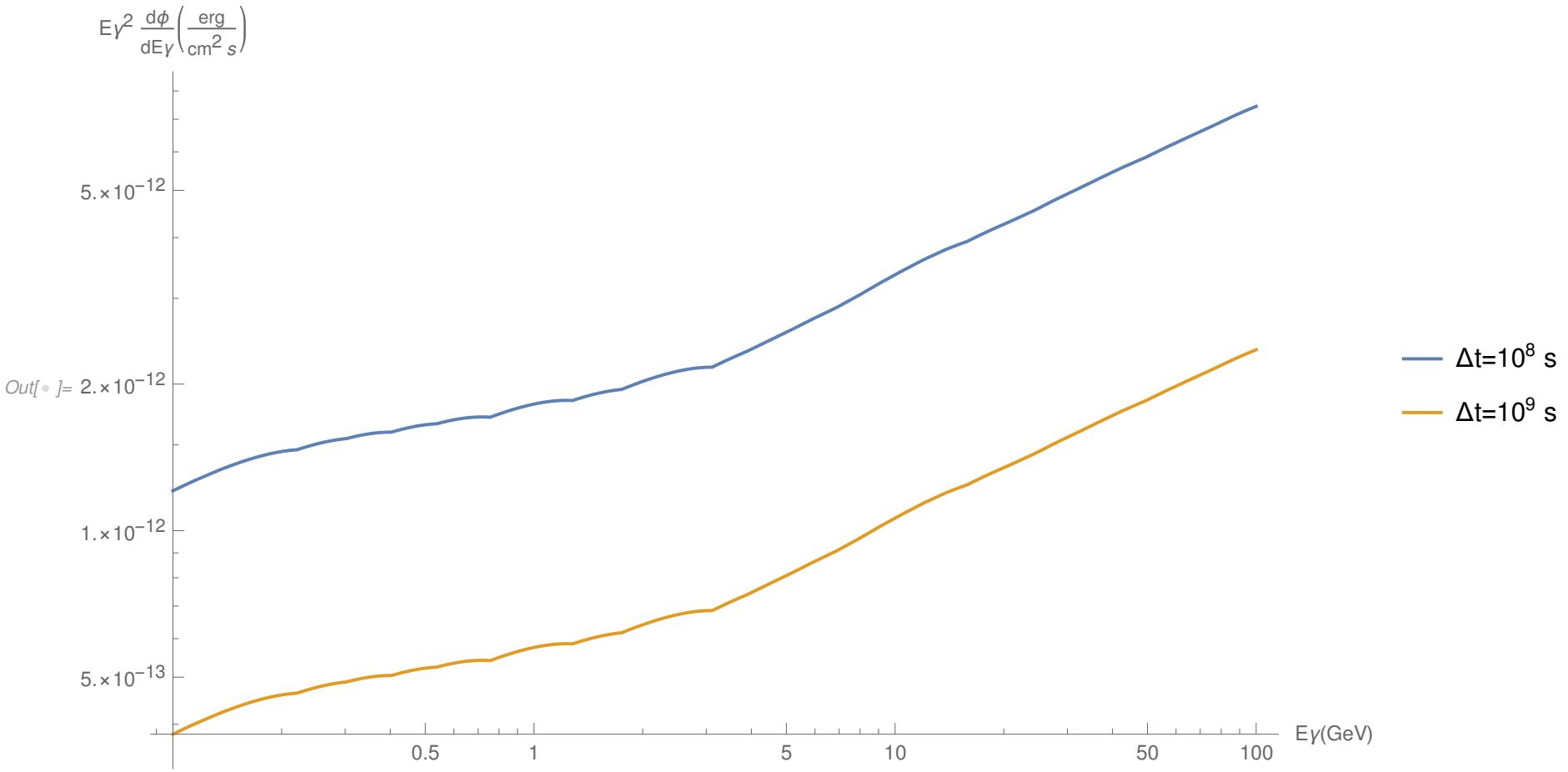

Fit of the Cen A excess

Assuming that the data measured by Fermi-LAT and HESS can be explained only partially with known astrophysical sources, we fit energies below 2.4 GeV and above 300 GeV with a broken power law

$$\frac{d\Phi^{back}}{dE_\gamma} = \begin{cases} kE_\gamma^{-\gamma_1} & E_\gamma \leq E_{br} \\ kE_{br}^{\gamma_2+\gamma_1} E_\gamma^{-\gamma_2} & E_\gamma > E_{br} \end{cases}$$

where $E_{br} = 2.4$ GeV and fit the remaining data with DM annihilation.
The total flux expression that we fit is therefore given by $\frac{d\Phi}{dE_\gamma} = \frac{d\Phi^{back}}{dE_\gamma} + \frac{d\Phi^{ann}}{dE_\gamma}$.

The annihilation flux $\frac{d\Phi^{ann}}{dE_\gamma} = \int_0^\infty dE'_\gamma K(E_\gamma, E'_\gamma) \frac{d\Phi^{ann}}{dE'_\gamma}(E'_\gamma)$, where $K(E_\gamma, E'_\gamma) = \frac{1}{\sqrt{2\pi}\sigma} e^{-\frac{(E_\gamma - E'_\gamma)^2}{2\sigma^2}}$ with $10\,\%$ uncertainty at the experimental level $\sigma = 0.1E'_\gamma$.

$\{k, \gamma_1, \gamma_2, a_R, m_{\tilde{\chi}}\}$ free parameters

$N_{data} = 19$, $N_{dof} = 19 - 5 = 14$

$\chi^2 = \sum_{i=0}^{N_{data}} \frac{(O^i_{meas} - O^i_{th})^2}{\sigma_i^2}$

O^i_{meas} the measured values, O^i_{th} the theoretical prediction and σ_i the uncertainty of the data

Best fit $m_{\tilde{\chi}} = 123$ GeV, $\Delta M = 2$ GeV and $a_R = 0.018$ with $\chi^2_{min} = 1.59$ and $\chi^2_{min,back} = 13.65$

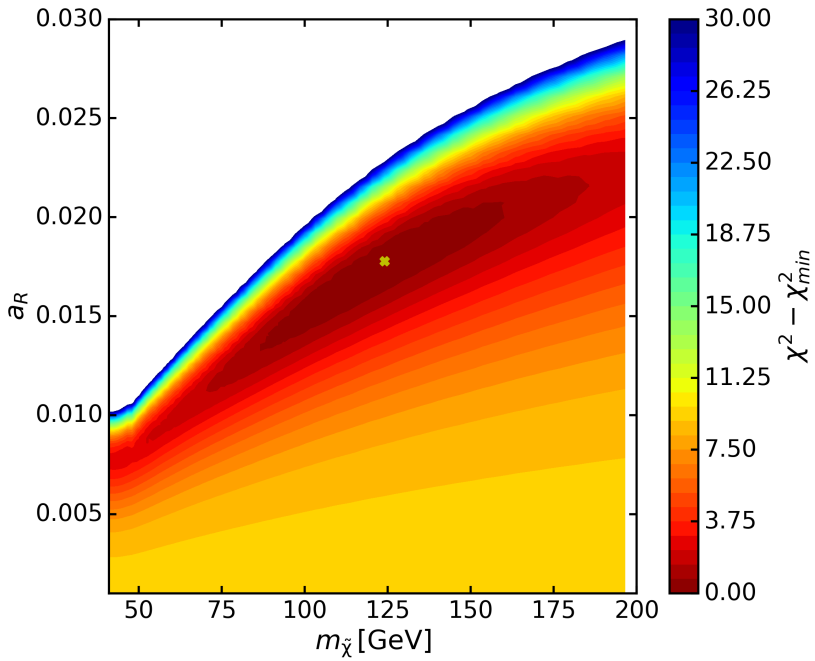

Fit of the Cen A photon excess with DM annihilation

- We fit energies below 2.4 GeV and above 300 GeV with a broken power law

$$\frac{d\Phi^{back}}{dE_\gamma} = \begin{cases} kE_\gamma^{-\gamma_1} & E_\gamma \leq E_{br} \\ kE_{br}^{\gamma_2+\gamma_1} E_\gamma^{-\gamma_2} & E_\gamma > E_{br} \end{cases}$$

  where $E_{br} = 2.4$ GeV, and the remaining data with DM annihilation

- Total flux $\frac{d\Phi}{dE_\gamma} = \frac{d\Phi^{back}}{dE_\gamma} + \frac{d\Phi^{ann}}{dE_\gamma}$
- Best fit value for $m_{\tilde{\chi}} = 123$ GeV, $\Delta M = 2$ GeV and $a_R = 0.018$ ($\chi^2_{min} = 1.59$)

M. Cermeño, *C. Degrande, L. Mantani, PRD 105 (2022) 8, 083019, arXiv: 2201.07247*

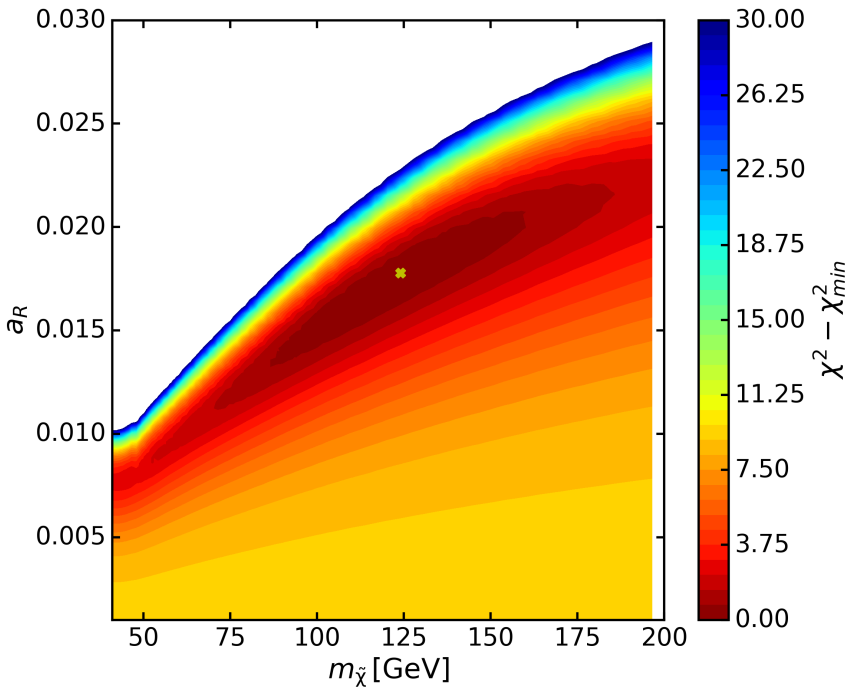

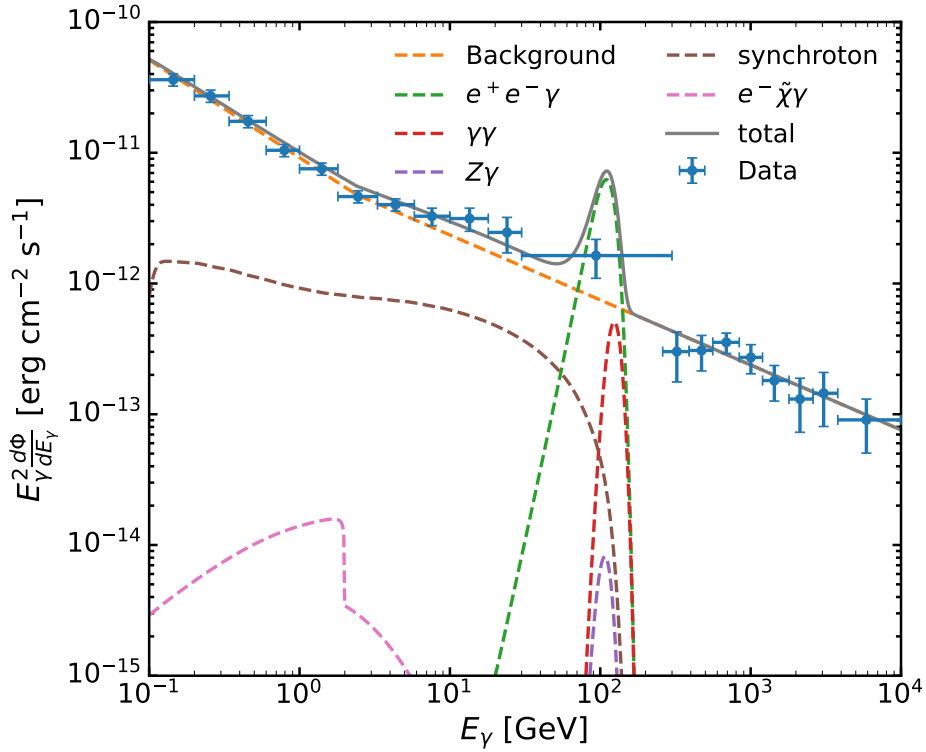

Fit of the Cen A excess binned

- The fit is performed by computing the differential binned flux, i.e. the integral of the differential flux in each bin divided by the bin width
- Best fit for $m_{\tilde{\chi}} = 123$ GeV, $\Delta M = 2$ GeV and $a_R = 0.018$

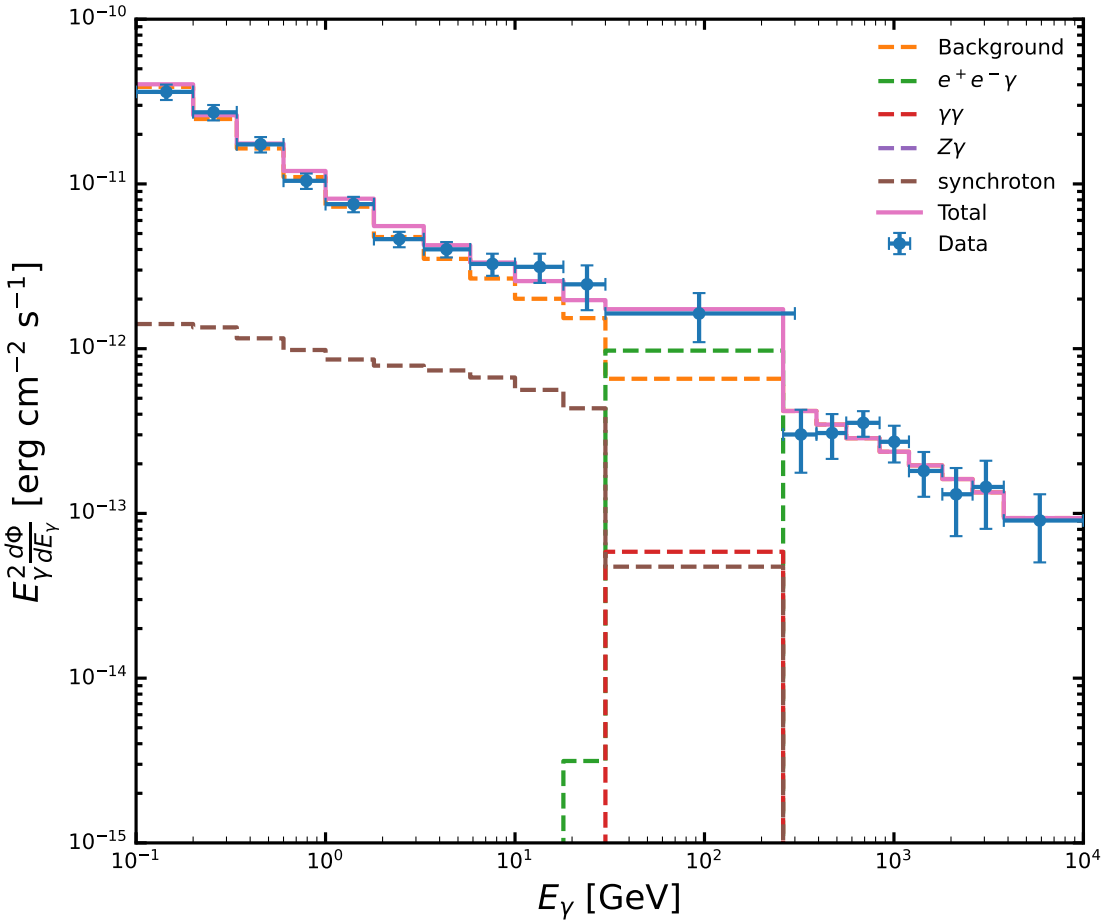

Synchrotron radiation

- Synchrotron radiation of the electrons from $\tilde{\chi}\tilde{\chi} \to e^- e^+ \gamma$ in the presence of a magnetic field
- Equipartition magnetic field model *Regis, Ullio, PRD 78 (2008) 043505, Lacroix, Boehm, Silk, PRD 92 (2015) 043510*

$$B(r) = \begin{cases} B_0 \left(\frac{r_c}{r_{acc}}\right)^2 \left(\frac{r}{r_{acc}}\right)^{-\frac{5}{4}} & r < r_{acc} \\ B_0 \left(\frac{r}{r_c}\right)^{-2} & r_{acc} \leq r < r_c \\ B_0 & r \geq r_c, \end{cases}$$

- $B_0 \sim 200\ \mu$G, obtained for a mean comoving magnetic field of $B \sim 10$ G
- $r_{acc} = 2GM_{BH}/v_{flow}^2$ accretion radius, $v_{flow} \sim 500 - 700$ km/s the velocity of the Galactic wind at the center of Cen A, and $r_c \sim 5$ kpc the size of the inner radio lobes
- The photon flux coming from the synchrotron radiation

$$E_\gamma^2 \frac{d\Phi_{syn}}{dE_\gamma} = \frac{8\pi E_\gamma}{d_{AGN}^2} \int_{4R_S}^{r_0} r^2 dr \int_{E_\gamma}^{m_\chi} dE P(r, E, E_\gamma) \psi_e(r, E)$$

- The electron and positron energy spectrum $\psi_e(r, E) = \frac{1}{2b(r,E)} \left(\frac{\rho_{DM}(r)}{m_{DM}}\right)^2 \int_E^{m_{DM}} dE_S \frac{d\sigma v_{e^-e^+\gamma}}{dE_S}$
- $b(r, E) = \frac{4}{3}\sigma_T \frac{B(r)^2}{2\mu_0} \gamma_L^2$ the total energy loss rate, $\gamma_L = \frac{E}{m_e}$
- The synchrotron emission spectrum $P(r, E, E_\gamma) = \frac{1}{4\pi\varepsilon_0} \frac{\sqrt{3}e^3 B(r)}{m_e} G_i\left(\frac{E_\gamma}{E_\gamma^c(r,E)}\right)$
- $G_i(x) = \frac{1}{2}\int_0^\pi G\left(\frac{x}{\sin\alpha}\right) \sin^2\alpha d\alpha$ the isotropic synchrotron spectrum, $E_\gamma^c(r, E) = \frac{3eE^2 B(r)}{4\pi m_e^3}$ critical photon energy, $G(t) = t\int_t^\infty K_{5/3}(u) du$, where $K_{5/3}$ is the modified Bessel function of order $5/3$

Circular polarised photon flux from the GC

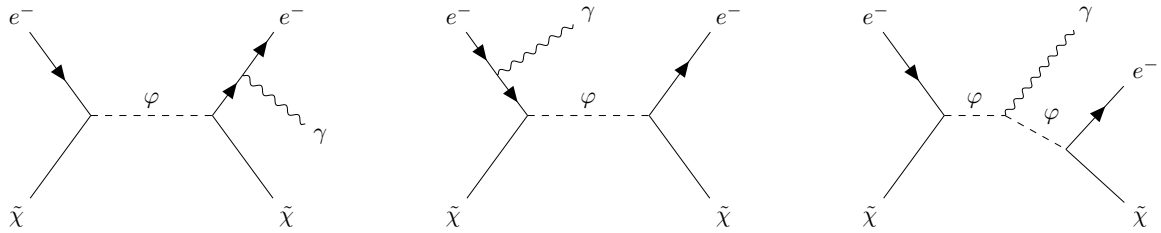

***M. Cermeño**, C. Degrande, L. Mantani, Phys.Dark Univ. 34 (2021) 100909*

$$\frac{d\Phi_{e\chi,pol}}{dE_\gamma} = \frac{\bar{J}(\Delta\Omega_{\rm obs})}{m_{\tilde{\chi}}} \int dE_e \frac{d\phi}{dE_e} \left| \frac{d\sigma_+}{dE_\gamma}(E_e, E_\gamma) - \frac{d\sigma_-}{dE_\gamma}(E_e, E_\gamma) \right|$$

- $\bar{J}(\Delta\Omega_{\rm obs}) = \frac{2\pi}{\Delta\Omega_{\rm obs}} \int_0^{\theta_{\rm obs}} d\theta \, \sin\theta \int_0^{2r_\odot} ds \, \rho(r(s,\theta)) \, f(r(s,\theta))$

  $f(r) = e^{-\frac{(r-r_\odot)}{r_0}}$ the spatial distribution of CR electrons, $r_0 = 4$ kpc

  Strong et al., A&A, 422 (2004) L47

  $\rho(r(s,\theta))$ the DM density profile

- $\frac{d\sigma_\pm}{dE_\gamma}(E_e, E_\gamma)$ the differential cross section for $e^-\tilde{\chi} \to e^-\tilde{\chi}\,\gamma_\pm$, with E_e the incoming electron energy, $m_{\tilde{\chi}}$ the DM mass and E_γ the photon energy
- $\frac{d\phi}{dE_e}$ the CR electron energy spectrum in units of $\mathrm{GeV}^{-1}\ \mathrm{cm}^{-2}\ \mathrm{s}^{-1}\ \mathrm{sr}^{-1}$

CR electron energy spectrum

The local interestellar spectrum (LIS)

$$E_e^{-1.2} \quad \text{for} \quad E_e < 0.05 \text{ GeV},$$
$$E_e^{-2} \quad \text{for} \quad 0.05 \text{ GeV} \lesssim E_e \lesssim 4 \text{ GeV},$$
$$E_e^{-3} \quad \text{for} \quad E_e > 4 \text{ GeV}.$$

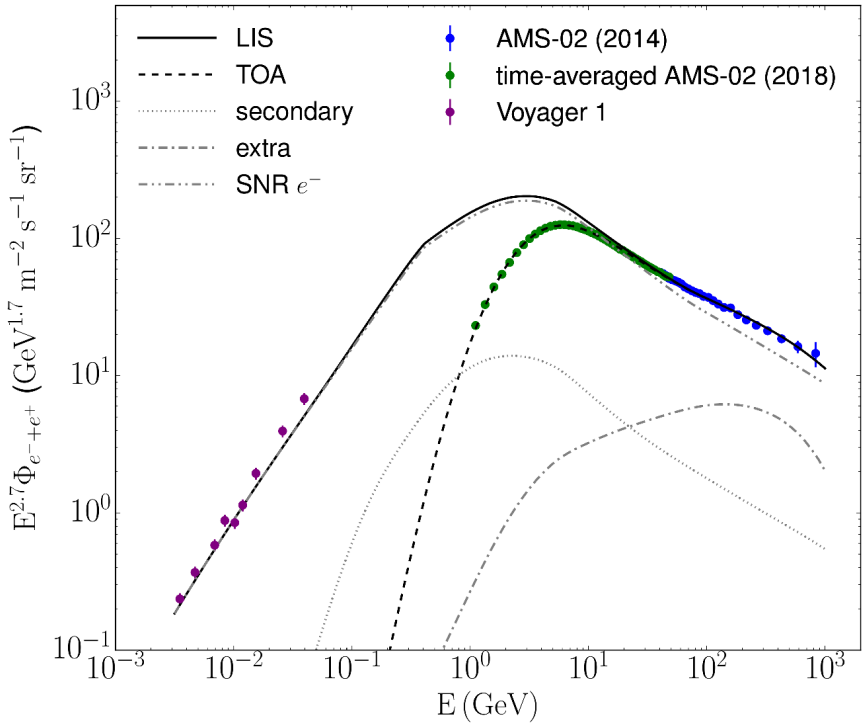

Injected spectrum

$$\frac{d\Phi_{\rm inj}}{dE_e} = \begin{cases} k_{e,\rm inj}\left(\frac{E_e}{\rm GeV}\right)^{-2.13} & \text{for } E_e \le 0.109 \text{ GeV} \\ \frac{k_{e,\rm inj}}{8.9\ 10^{-3}}\left(\frac{E_e}{0.109\ \rm GeV}\right)^{-2.57} & \text{for } E_e > 0.109 \text{ GeV} \end{cases}$$

with $k_{e,\rm inj} = 6.98\ 10^{-3}\ \text{GeV}^{-1}\ \text{cm}^{-2}\ \text{s}^{-1}\ \text{sr}^{-1}$.

Vittino et al., PRD 100 (2019) 043007

Photon flux and circular polarisation GC

LIS $E_e^{-1.2}$ for $E_e < 0.05$ GeV
E_e^{-2} for $0.05\ \text{GeV} \lesssim E_e \lesssim 4\ \text{GeV}$

Injected $E_e^{-2.13}$ for $E_e \leq 0.109$ GeV
$E_e^{-2.57}$ for $E_e > 0.109$ GeV

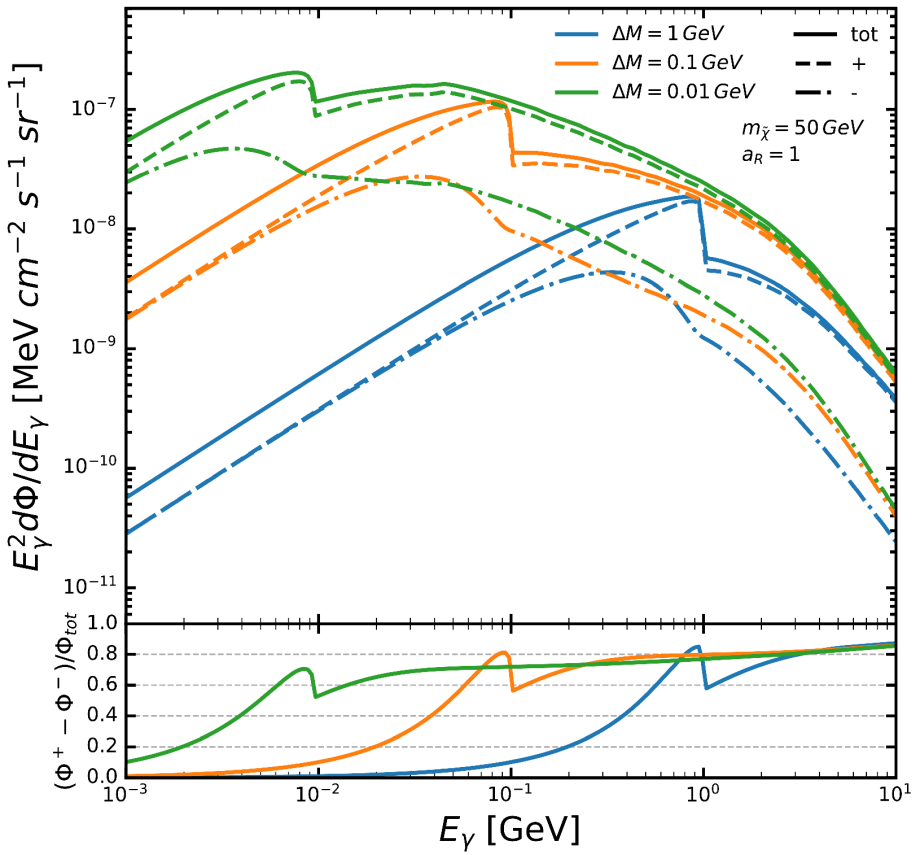

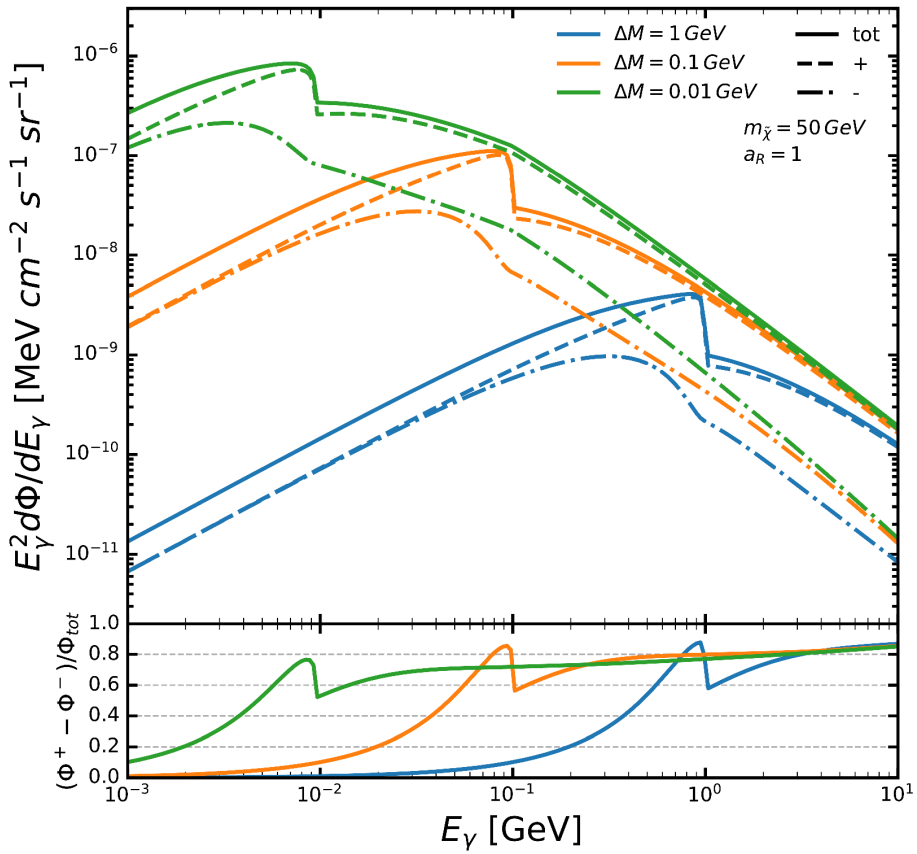

M. Cermeño, *C. Degrande, L. Mantani, Phys.Dark Univ. 34 (2021) 100909*

$$\frac{\Phi^+ - \Phi^-}{\Phi_{\text{tot}}} \equiv \frac{\frac{d\Phi_{e\tilde{\chi},pol}}{dE_\gamma}}{\frac{d\Phi_{e\tilde{\chi}}}{dE_\gamma}}, \qquad \frac{d\Phi_{e\tilde{\chi},pol}}{dE_\gamma} = \frac{d\Phi_{e\tilde{\chi},+}}{dE_\gamma} - \frac{d\Phi_{e\tilde{\chi},-}}{dE_\gamma}$$

Asymmetries up to $90\,\%$

Flux scales as a_R^2/m_χ^2

CR electron energy spectrum GC

The local interestellar spectrum (LIS)

$$E_e^{-1.2} \quad \text{for} \quad E_e < 0.05\ \text{GeV}\,,$$
$$E_e^{-2} \quad \text{for} \quad 0.05\ \text{GeV} \lesssim E_e \lesssim 4\ \text{GeV}\,,$$
$$E_e^{-3} \quad \text{for} \quad E_e > 4\ \text{GeV}\,.$$

Injected spectrum

$$\frac{d\Phi_{\rm inj}}{dE_e} = \begin{cases} k_{e,\rm inj}\left(\frac{E_e}{\rm GeV}\right)^{-2.13} & \text{for } E_e \le 0.109\ \text{GeV} \\ \frac{k_{e,\rm inj}}{8.9\ 10^{-3}}\left(\frac{E_e}{0.109\ \rm GeV}\right)^{-2.57} & \text{for } E_e > 0.109\ \text{GeV} \end{cases}$$

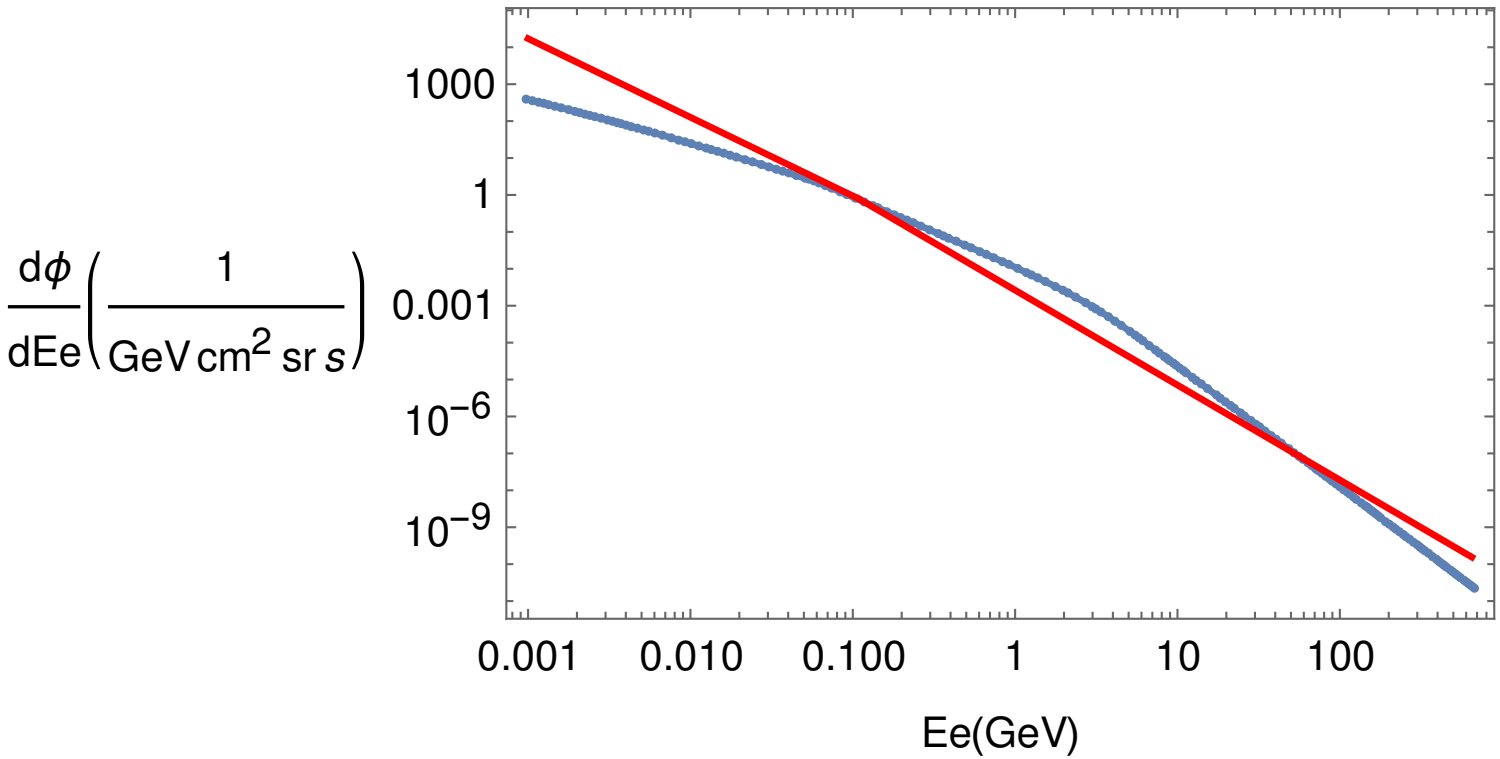

CR electron energy spectrum GC

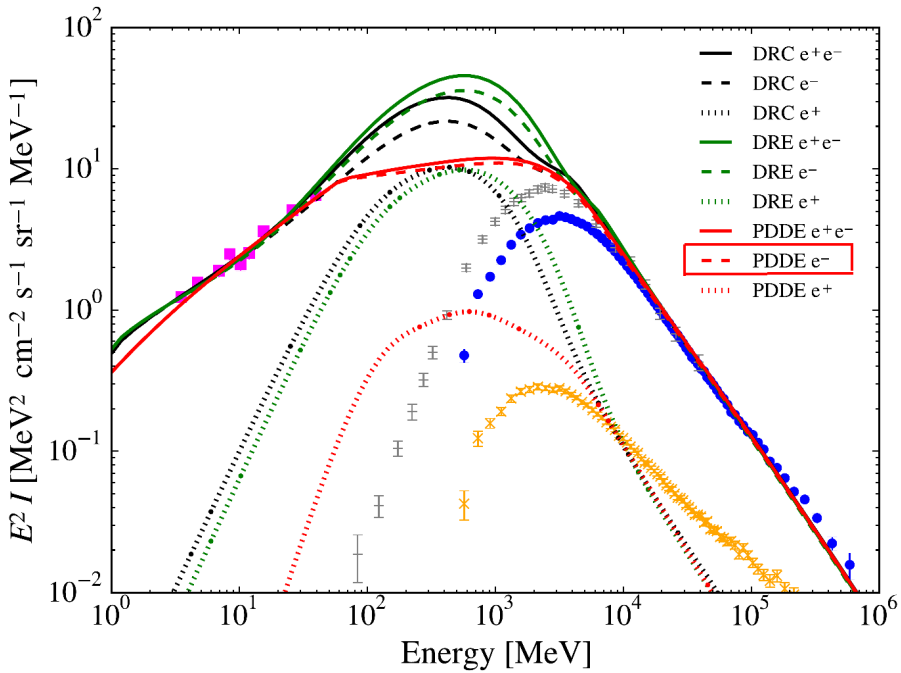

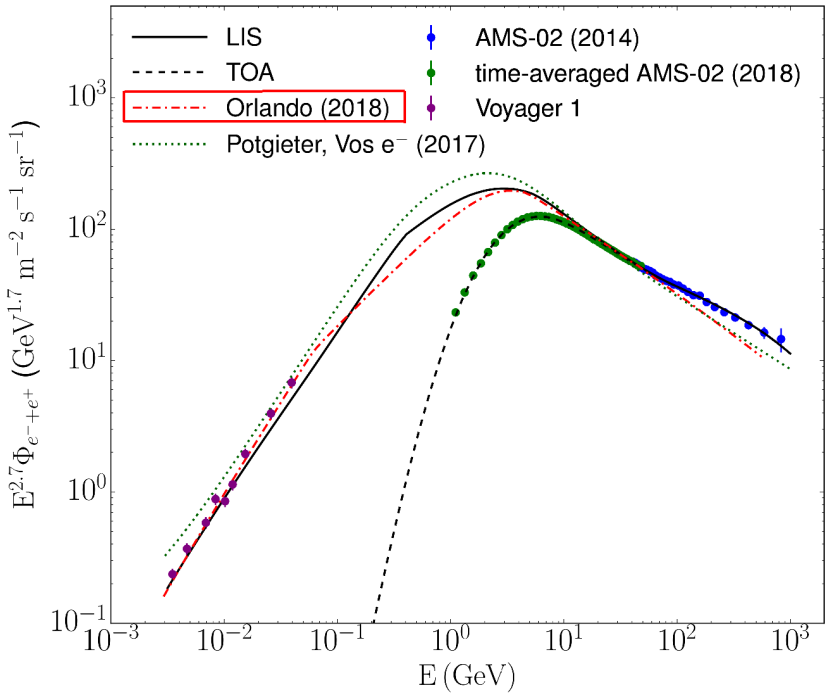

Orlando, MNRAS 475 (2018) 2724

Vittino et al., PRD 100 (2019) 043007

Scattering vs annihilation GC

The annihilation rate

$$q_{\tilde{\chi}\tilde{\chi}} \sim \langle \sigma v \rangle \frac{\rho_0}{m_{\tilde{\chi}}} \sim \frac{a_R^4 e^2}{(4\pi)^2 m_{\tilde{\chi}}^2} v_{\tilde{\chi}} \frac{\rho_0}{m_{\tilde{\chi}}}$$

The CR scattering rate

$$q_{e\tilde{\chi}} \sim \sigma_{e\tilde{\chi}} E_e \frac{d\phi}{dE_e} \sim \frac{a_R^2 e^2}{4\pi m_{\tilde{\chi}}^2} E_e \frac{d\phi}{dE_e}$$

The ratio

$$\frac{q_{e\tilde{\chi}}}{q_{\tilde{\chi}\tilde{\chi}}} \sim 10^{-6} a_R^{-2} \left(\frac{E_e \frac{d\phi}{dE_e}}{\mathrm{cm}^{-2}\ \mathrm{s}^{-1}} \right) \left(\frac{m_{\tilde{\chi}}}{\mathrm{GeV}} \right)$$

Sensitivity e-ASTROGAM GC

$$\epsilon = 0.013\,,\ A_{\rm eff} = 50 - 560\ {\rm cm}^2,\ E_\gamma = 0.3 - 10\,{\rm MeV}$$

$$\epsilon = 0.3\,, A_{\rm eff} = 215 - 1810\ {\rm cm}^2,\ E_\gamma = 10 - 3000\,{\rm MeV}$$

$$\frac{N_{\rm signal}}{\sqrt{N_{\rm back}}} \sim 3$$

$$\frac{\frac{d\Phi_{e\chi}}{dE_\gamma}}{\sqrt{\frac{d\Phi_{\rm back}}{dE_\gamma}}} \sqrt{2\epsilon E_{\gamma,{\rm peak}} \Delta\Omega A_{\rm eff} \Delta t} = 3$$

$$E_\gamma^2 \frac{d\phi_{\rm back}}{dE_\gamma} \sim 10^{-2}\ {\rm MeV\ cm^{-2}\ s^{-1}\ sr^{-1}}$$

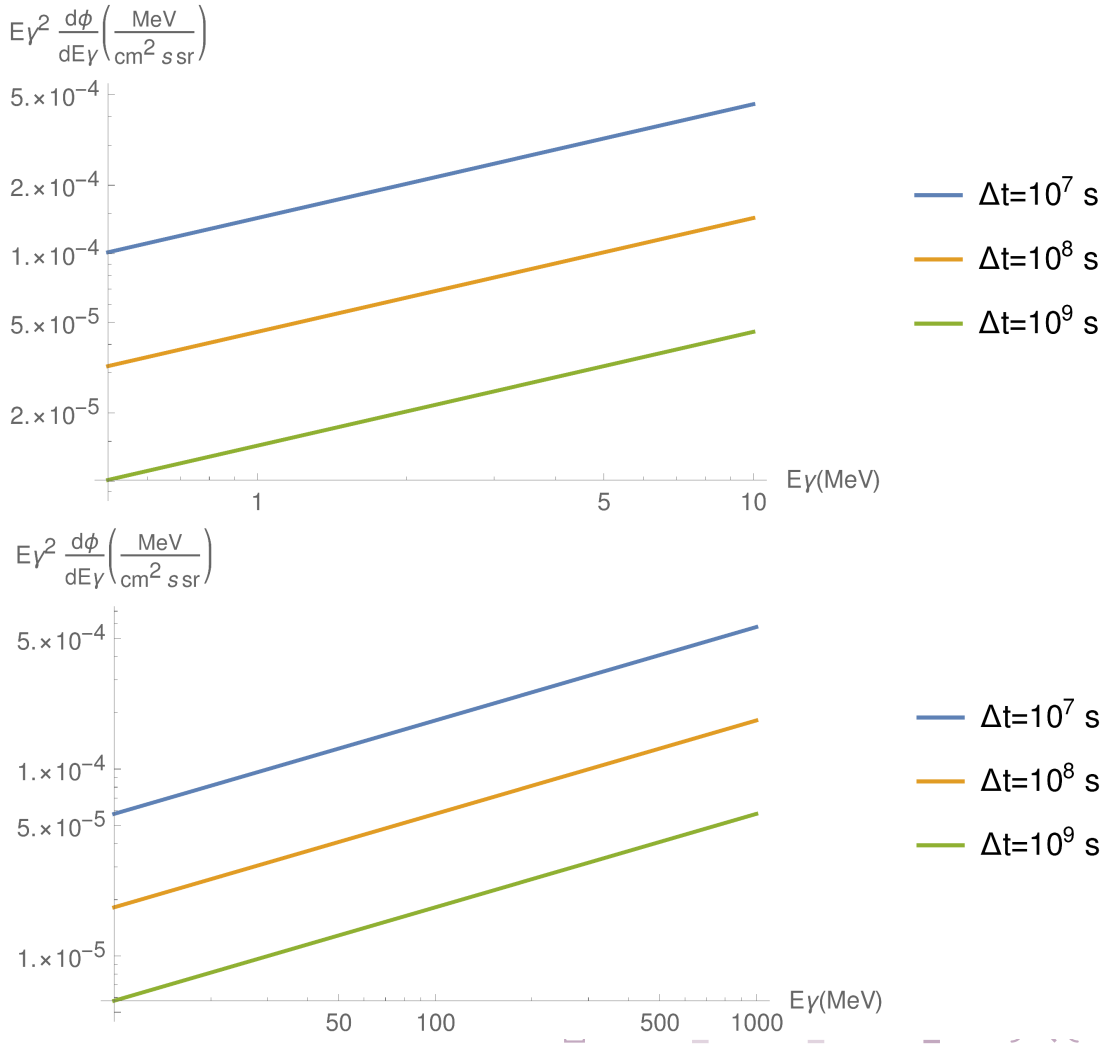

Results: Photon flux and circular polarisation from the GC

- Left: LIS
- Right: injected spectrum
- Einasto profile, $\frac{\bar{J}_{\rm NFW}}{\bar{J}_{\rm Ein}} \sim 0.7$

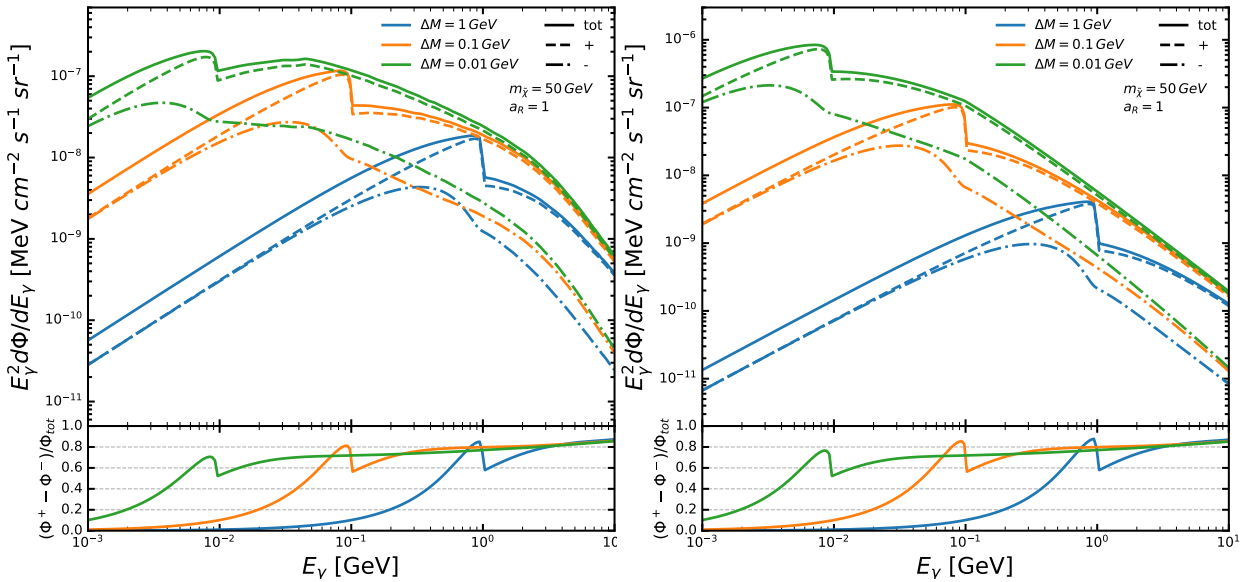

- Thermal relic DM, rescale flux by a_R^2
- $m_{\tilde{\chi}} = 50$ GeV underabundant
- Dirac DM, rescale flux by $\frac{\rho_{\bar{\chi}}}{\rho_\chi + \rho_{\bar{\chi}}}$
- $m_\varphi \geq 45$ GeV cannot be easily evaded

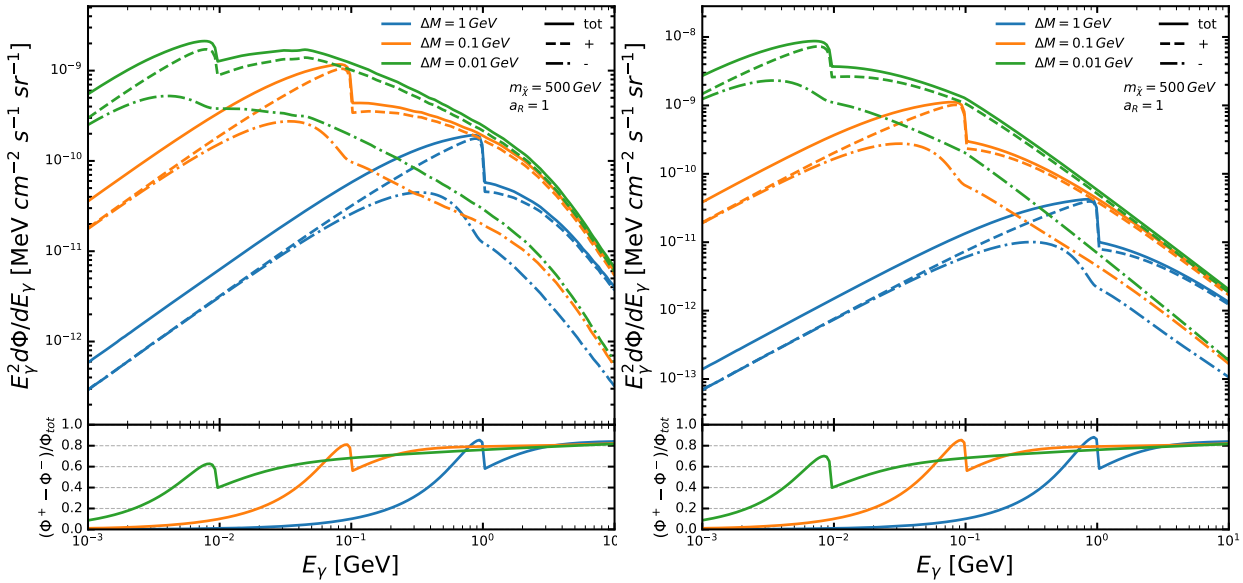

Results: Photon flux and circular polarisation from the GC

- Energy spectrum $\frac{d\Phi}{dE_e} = k_e \left(\frac{E_e}{\mathrm{GeV}}\right)^{-3}$, $k_e = 10^{-2}\ \mathrm{GeV}^{-1}\ \mathrm{cm}^{-2}\ \mathrm{s}^{-1}\ \mathrm{sr}^{-1}$

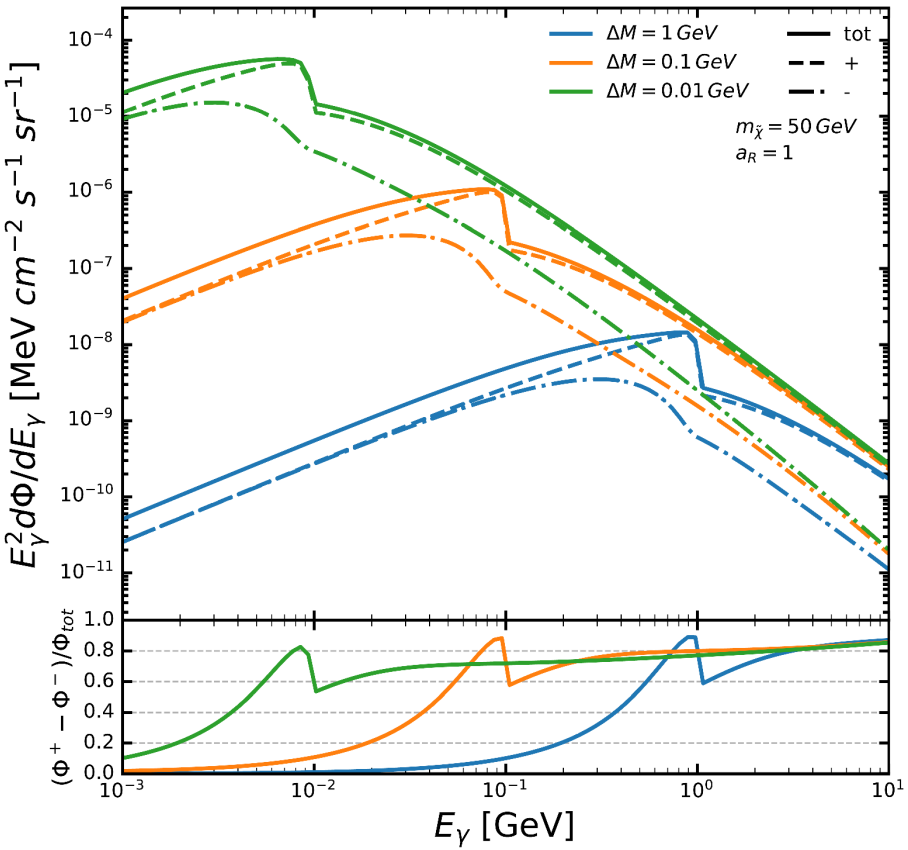

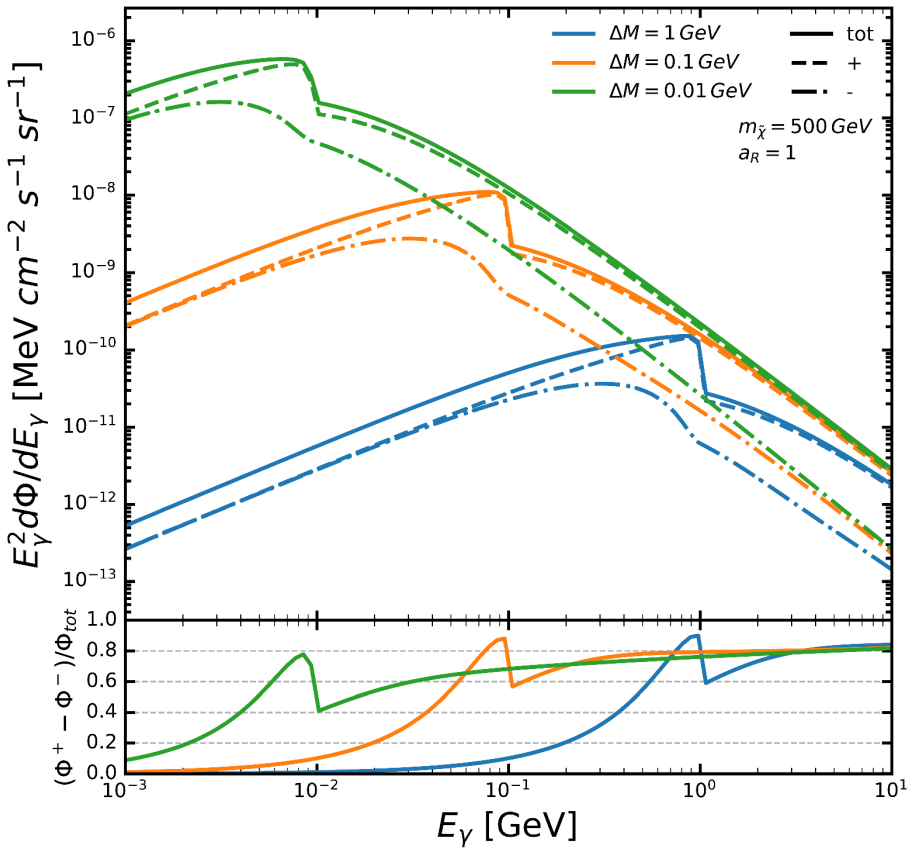

- The electron energy spectrum has a relevant impact on the final results
- Higher circular polarised fluxes could be obtain close to other astrophysical electron sources (AGNs, pulsars, SNRs...)

Impact of the first resonance on the asymmetry

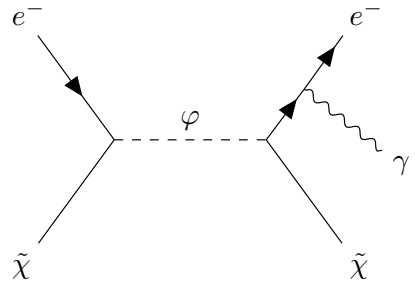

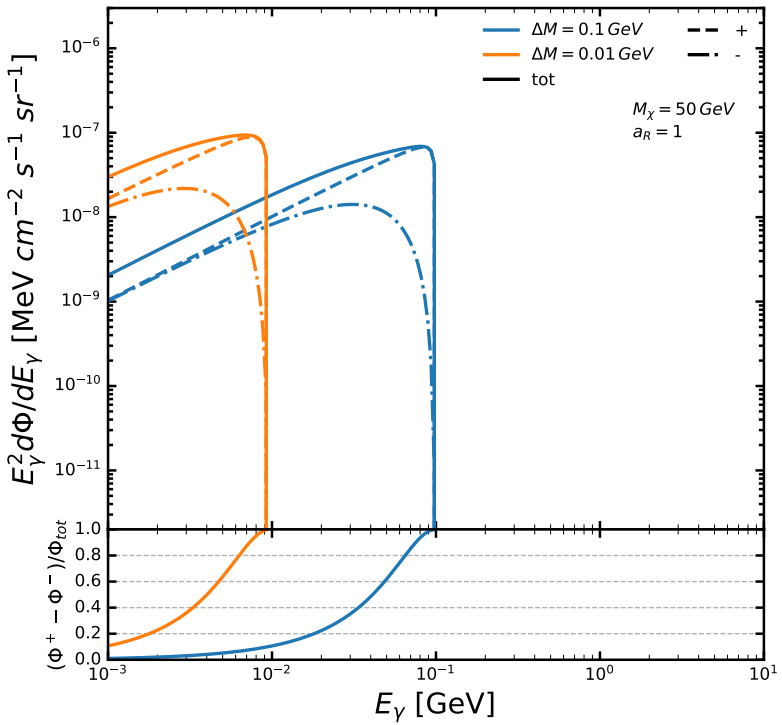

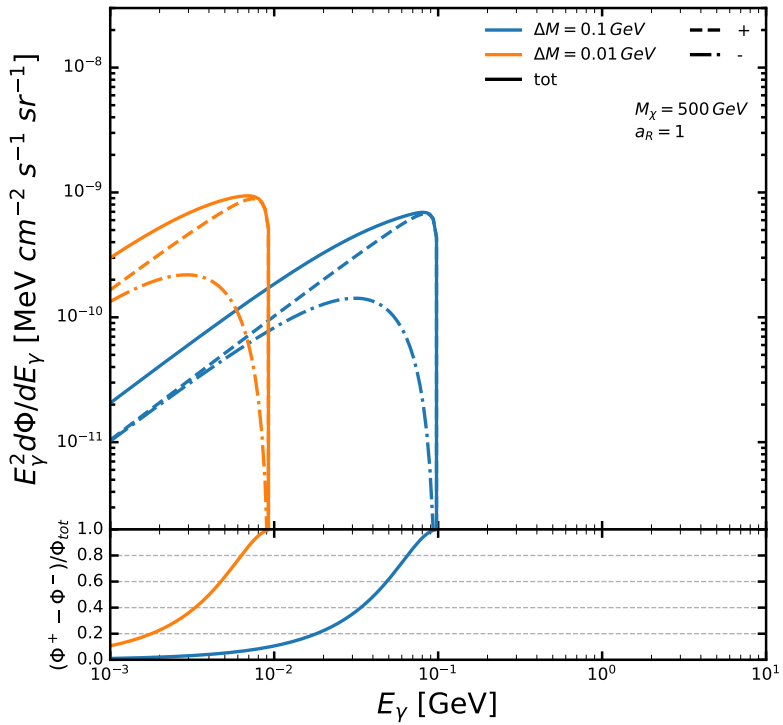

LIS spectrum

Impact of the second resonance on the asymmetry

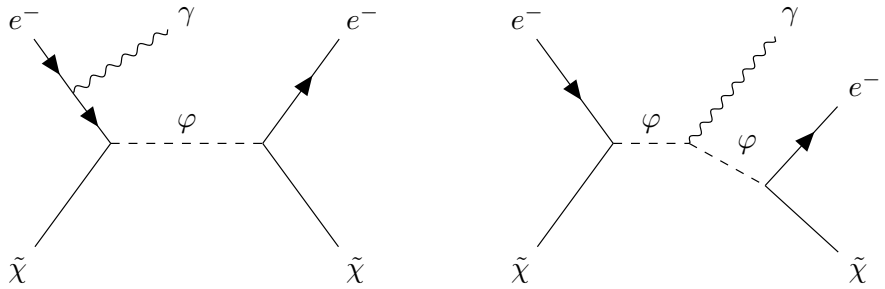

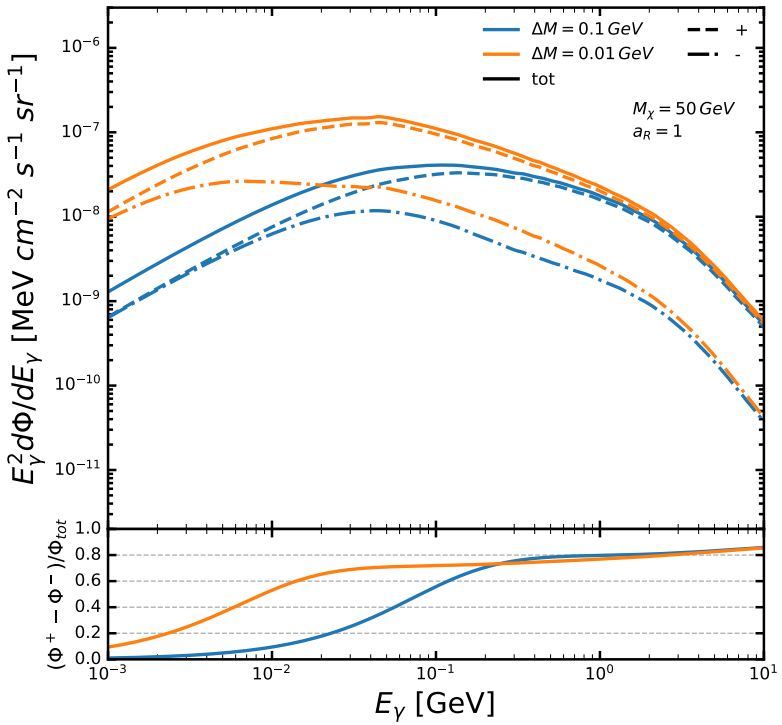

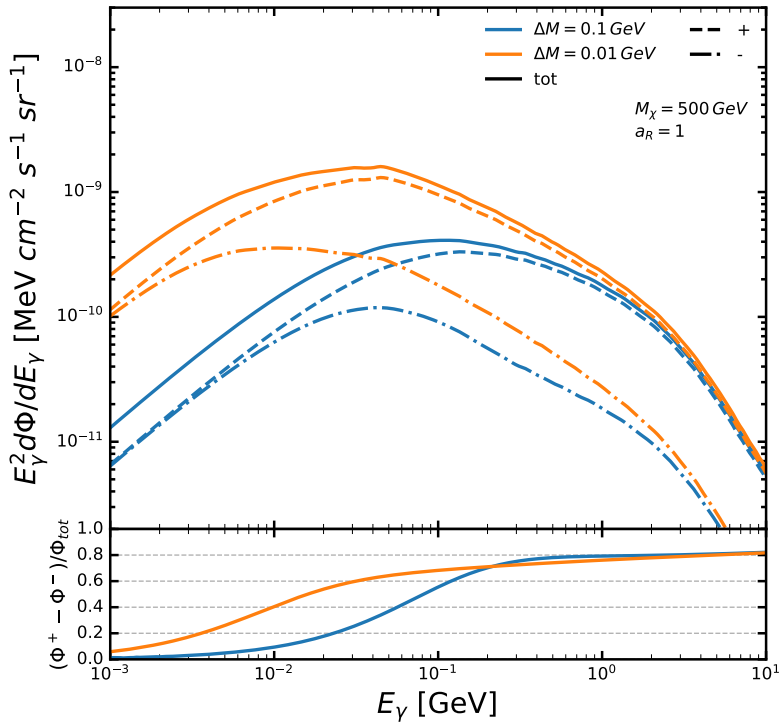

LIS spectrum

Prospects of detection for the GC

- Standard circular polarisation: synchrotron emission and curvature radiation
- Gamma-rays from the GC: ICS, bremsstrahlung and inelastic collisions of high energy CRs with the ambient medium
- $E_\gamma^2 \frac{d\phi_{\rm back}}{dE_\gamma} \sim 10^{-2} \ \frac{\rm MeV}{\rm cm^2 \ s \ sr}$

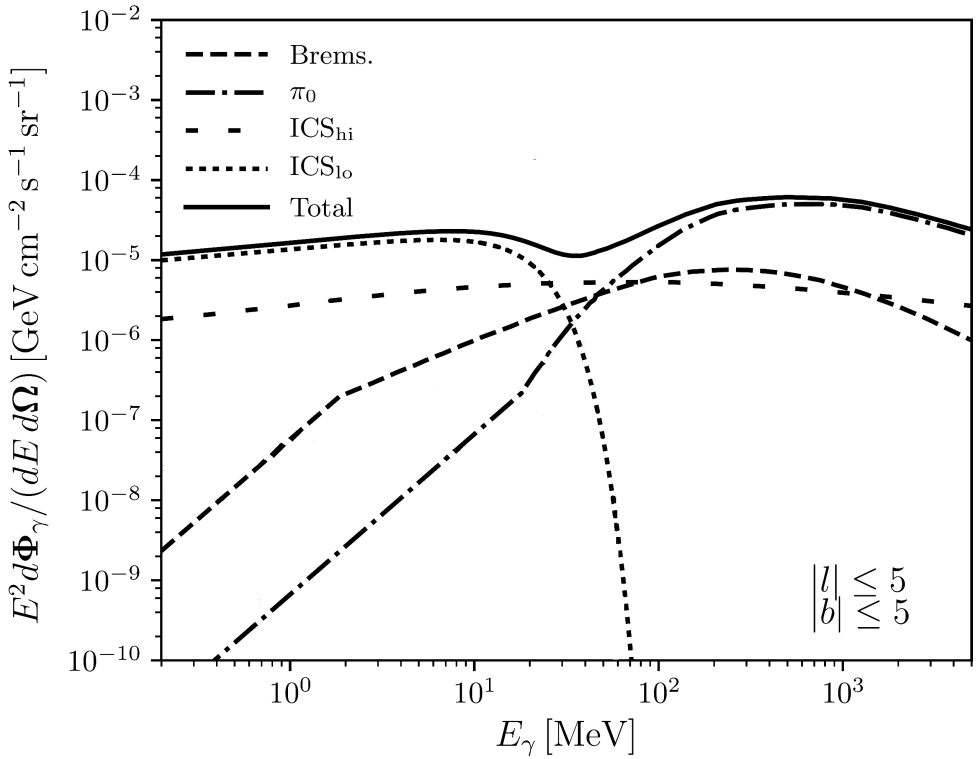

Adapted from *Bartels, Gaggero, Weniger, JCAP05 (2017) 001*

- $\frac{N_{\rm signal}}{\sqrt{N_{\rm back}}} \sim 3 \Rightarrow E_\gamma^2 \frac{d\Phi_{e\chi}}{dE_\gamma} \sim 10^{-5}$ MeV cm^{-2} s^{-1} sr^{-1}, $\Delta t \sim 10^8$ s (e-ASTROGAM)
- Detectable fluxes for $m_\chi \sim 5$ GeV
- Different source of electrons? $\Rightarrow$ AGN